Chapter 6

Dilute Absorption/Stripping Operations

In *absorption* (also called *gas absorption, gas scrubbing, and gas washing*), a gas mixture is contacted with a liquid (the *absorbent* or *solvent*) to selectively dissolve one or more components by mass transfer from the gas to the liquid. The components transferred to the liquid are referred to as *solutes* or *absorbate*. Absorption is used to separate gas mixtures; remove impurities, contaminants, pollutants, or catalyst poisons from a gas; or recover valuable chemicals. Thus, the species of interest in the gas mixture may be all components, only the component(s) not transferred, or only the component(s) transferred.

The opposite of absorption is *stripping* (also called *desorption*), wherein a liquid mixture is contacted with a gas to selectively remove components by mass transfer from the liquid to the gas phase. As discussed in Chapter 5, absorbers are frequently coupled with strippers to permit regeneration (or recovery) and recycling of the absorbent. Because stripping is not perfect, absorbent recycled to the absorber contains species present in the vapor entering the absorber. When water is used as the absorbent, it is more common to separate the absorbent from the solute by distillation rather than stripping.

6.0 INSTRUCTIONAL OBJECTIVES

After completing this chapter, you should be able to:

- Explain the difference between absorption and stripping.
- Explain the difference between physical and chemical absorption.
- Explain why absorbers are best operated at high pressure and low temperature, while strippers are best operated at low pressure and high temperature.
- Enumerate different types of industrial equipment for absorption and stripping and explain which are most popular.
- Explain how vapor and liquid streams flow from one tray to another in a trayed tower.
- Compare three different types of trays.
- Explain the difference between random and structured packings and cite examples of each.
- Explain the importance of the liquid distributor and redistributors in a packed column with respect to liquid flow.
- Derive the "operating-line equation," used in graphical methods, starting with a component material balance.
- Calculate the minimum MSA flow rate to achieve a specified recovery of a key component in a single-section, countercurrent cascade.
- Determine graphically, by stepping off stages, or algebraically, the required number of equilibrium stages in a countercurrent cascade to achieve a specified recovery of a key component, given an MSA flow rate greater than the minimum value.
- Define the overall stage efficiency and explain why efficiency values are relatively low for absorbers and at a moderate level for strippers.
- Make preliminary estimates of overall stage efficiency of absorbers and strippers.
- Explain why multiple liquid-flow passes are necessary in trayed columns of moderate to large column diameter.
- Define Murphree point and tray vapor efficiencies and their relationship to overall stage efficiency.
- Explain how experimental stage-efficiency data from a small laboratory Oldershaw column can be scaled up to a large-diameter column.
- Explain two mechanisms by which a trayed column can flood.
- Enumerate the contributions to pressure drop in a trayed column.
- Estimate column diameter and tray pressure drop for a trayed column.
- Estimate tray efficiency from correlations of mass-transfer coefficients using two-film theory.
- Estimate weeping, entrainment, and downcomer backup in a trayed column.

- For a packed column, define the "height equivalent to a theoretical (equilibrium) stage (plate)," HETP, and explain how it and the number of equilibrium stages differ from "height of a transfer unit," HTU, and "number of transfer units," NTU, respectively.
- Explain differences between "loading point" and "flooding point" in a packed column.
- Estimate packed height, packed-column diameter, and pressure drop across the packing.
- Estimate HTU from correlations of mass-transfer coefficients.
- Explain how the number of theoretical stages is computed for concentrated solutions in which equilibrium and operating lines are curved.

Industrial Example

A typical absorption operation is shown in Figure 6.1. The feed, which contains air (21% O_2, 78% N_2, and 1% Ar), water vapor, and acetone vapor, is the gas leaving a dryer where solid cellulose acetate fibers, wet with water and acetone, are dried. The purpose of the 30-tray (equivalent to 10 equilibrium stages) absorber is to remove the acetone by contacting the gas with a suitable absorbent, water. By using countercurrent flow of gas and liquid in a multiple-stage device, the material balance, shown in Figure 6.1, indicates that 99.5% of the acetone is absorbed. The gas leaving the absorber contains only 143 ppm (parts per million) by weight of acetone vapor and can be recycled to the dryer or exhausted to the atmosphere. Although the major component transferred between phases is acetone, the material balance indicates that small amounts of oxygen and nitrogen are also absorbed by the water solvent. Because water is present in both the feed gas and the absorbent, it can be both absorbed and stripped. As seen in Figure 6.1, the net effect is that water is stripped because more water appears in the exit gas than in the feed gas. The exit gas is almost saturated with water vapor and the exit liquid is almost saturated with air. The temperature of the absorbent decreases by 3°C to supply the energy of vaporization needed to strip the water, which in this example is greater than the energy of condensation liberated from the absorption of acetone.

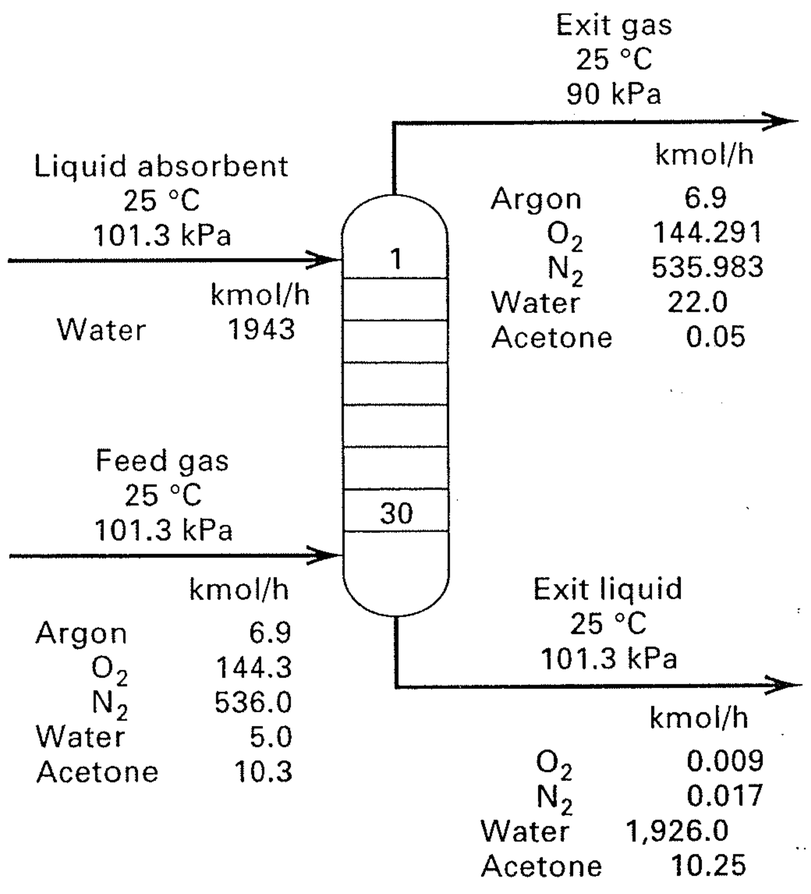

Figure 6.1 Typical absorption process.

As was shown in Figure 5.9, the fraction of a component absorbed in a countercurrent cascade depends on the number of equilibrium stages and the absorption factor, $A = L/(KV)$, for that component. For the conditions of Figure 6.1, using $L = 1943$ kmol/h and $V = 703$ kmol/h, estimated K-values and absorption factors, which range over many orders of magnitude, are

Component	$A = L/(KV)$	K-value
Water	89.2	0.031
Acetone	1.38	2.0
Oxygen	0.00006	45,000
Nitrogen	0.00003	90,000
Argon	0.00008	35,000

For acetone, the K-value is based on Eq. (4) of Table 2.3, the modified Raoult's law, $K = \gamma P^s/P$, with $\gamma = 6.7$ for a dilute solution of acetone in water at 25°C and 101.3 kPa. For oxygen and nitrogen, K-values are based on the use of Eq. (6) of Table 2.3, Henry's law, $K = H/P$, using constants from Figure 4.27 at 25°C. For water, the K-value is obtained from Eq. (3) of Table 2.3, Raoult's law, $K = P^s/P$, which applies because the mole fraction of water in the liquid phase is close to 1. For argon, the Henry's law constant at 25°C was obtained from the International Critical Tables [1].

Figure 5.9 shows that if the value of A is greater than 1, any degree of absorption can be achieved: the larger the value of A, the fewer the number of stages required to absorb a desired fraction of the solute. However, very large values of A can correspond to absorbent flow rates that are larger than necessary. From an economic standpoint, the value of A, for the main (key) species to be absorbed, should be in the range of 1.25 to 2.0, with 1.4 being a frequently recommended value. Thus, the above value of 1.38 for acetone is favorable.

For a given feed-gas flow rate and choice of absorbent, factors that influence the value of A are absorbent flow rate, temperature, and pressure. Because $A = L/(KV)$, the larger the absorbent flow rate is, the larger will be the value of A. The required absorbent flow rate can be reduced by reducing the K-value of the solute. Because the K-value for many solutes varies exponentially with temperature and is inversely proportional to pressure, this reduction can be achieved by

reducing the temperature and/or increasing the pressure. Increasing the pressure also serves to reduce the diameter of the equipment for a given gas throughput. However, temperature adjustment by feed-gas refrigeration and/or absorbent refrigeration, and/or adjustment of the feed-gas pressure by gas compression can be expensive. For these reasons, the absorber in Figure 6.1 operates at near-ambient conditions.

For a stripper, the stripping factor, $S = 1/A = KV/L$, is crucial. To reduce the required flow rate of stripping agent, operation of the stripper at a high temperature and/or a low pressure is desirable, with an optimum stripping factor in the vicinity of 1.4.

Absorption and stripping are technically mature separation operations. Design procedures are well developed and commercial processes are common. Table 6.1 lists representative, commercial absorption applications. In most cases, the solutes are contained in gaseous effluents from chemical reactors. Passage of strict environmental standards with respect to pollution by emission of noxious gases has greatly increased the use of gas absorbers in the past decade.

When water and hydrocarbon oils are used as absorbents, no significant chemical reactions occur between the absorbent and the solute, and the process is commonly referred to as *physical absorption*. When aqueous sodium hydroxide (a strong base) is used as the absorbent to dissolve an acid gas, absorption is accompanied by a rapid and irreversible neutralization reaction in the liquid phase and the process is referred to as *chemical absorption* or *reactive absorption*. More complex examples of chemical absorption are processes for absorbing CO_2 and H_2S with aqueous solutions of monoethanolamine (MEA) and diethanolamine (DEA), where a reversible chemical reaction takes place in the liquid phase. Chemical reactions can increase the rate of absorption, increase the absorption capacity of the solvent, increase selectivity to preferentially dissolve only certain components of the gas, and convert a hazardous chemical to a safe compound.

In this chapter, trayed and packed-column equipment for conducting absorption and stripping operations is discussed and fundamental *equilibrium-based* and *rate-based* (mass-transfer) models and calculation procedures, both graphical and algebraic, are presented for physical absorption and stripping of mainly dilute mixtures. The methods also apply to reactive absorption with irreversible and complete chemical reactions of the solute in the liquid phase. Calculations for concentrated mixtures and reactive absorption with reversible chemical reactions are best handled by computer-aided calculations, which are discussed in Chapters 10 and 11. An introduction to calculations for concentrated mixtures in packed columns is given in the last section of this chapter.

Table 6.1 Representative, Commercial Applications of Absorption

Solute	Absorbent	Type of Absorption
Acetone	Water	Physical
Acrylonitrile	Water	Physical
Ammonia	Water	Physical
Ethanol	Water	Physical
Formaldehyde	Water	Physical
Hydrochloric acid	Water	Physical
Hydrofluoric acid	Water	Physical
Sulfur dioxide	Water	Physical
Sulfur trioxide	Water	Physical
Benzene and toluene	Hydrocarbon oil	Physical
Butadiene	Hydrocarbon oil	Physical
Butanes and propane	Hydrocarbon oil	Physical
Naphthalene	Hydrocarbon oil	Physical
Carbon dioxide	Aq. NaOH	Irreversible chemical
Hydrochloric acid	Aq. NaOH	Irreversible chemical
Hydrocyanic acid	Aq. NaOH	Irreversible chemical
Hydrofluoric acid	Aq. NaOH	Irreversible chemical
Hydrogen sulfide	Aq. NaOH	Irreversible chemical
Chlorine	Water	Reversible chemical
Carbon monoxide	Aq. cuprous ammonium salts	Reversible chemical
CO_2 and H_2S	Aq. monoethanolamine (MEA) or diethanolamine (DEA)	Reversible chemical
CO_2 and H_2S	Diethyleneglycol (DEG) or triethyleneglycol (TEG)	Reversible chemical
Nitrogen oxides	Water	Reversible chemical

6.1 EQUIPMENT

Absorption and stripping are conducted mainly in trayed towers (plate columns) and packed columns, and less often in spray towers, bubble columns, and centrifugal contactors, as shown schematically in Figure 6.2. A trayed tower is a vertical, cylindrical pressure vessel in which vapor and liquid, which flow countercurrently, are contacted on a series of trays or plates, an example of which is shown in Figure 6.3. Liquid flows across each tray, over an outlet weir, and into a downcomer, which takes the liquid by gravity to the tray below. Gas flows upward through openings in each tray, bubbling through the liquid on the tray. When the openings are holes, any of the five two-phase-flow regimes shown in Figure 6.4, and considered in detail by Lockett [2], may occur. The most common and favored regime is the *froth regime,* in which the liquid phase is continuous and the gas passes through in the form of jets or a series of bubbles. The *spray regime,* in which the gas phase is continuous, occurs for low weir heights (low liquid depths) at high gas rates. For low gas rates, the *bubble regime* can occur, in which the liquid is fairly quiescent and bubbles rise in swarms. At high liquid rates, small gas bubbles may be undesirably emulsified. If bubble coalescence is hindered, an undesirable foam forms. Ideally, the liquid carries no vapor bubbles (*occlusion*) to the tray below, the vapor carries no liquid droplets (*entrainment*) to the tray above, and there is no *weeping* of liquid through the holes in the tray. With good contacting, equilibrium between the exiting vapor and liquid phases is approached on each tray.

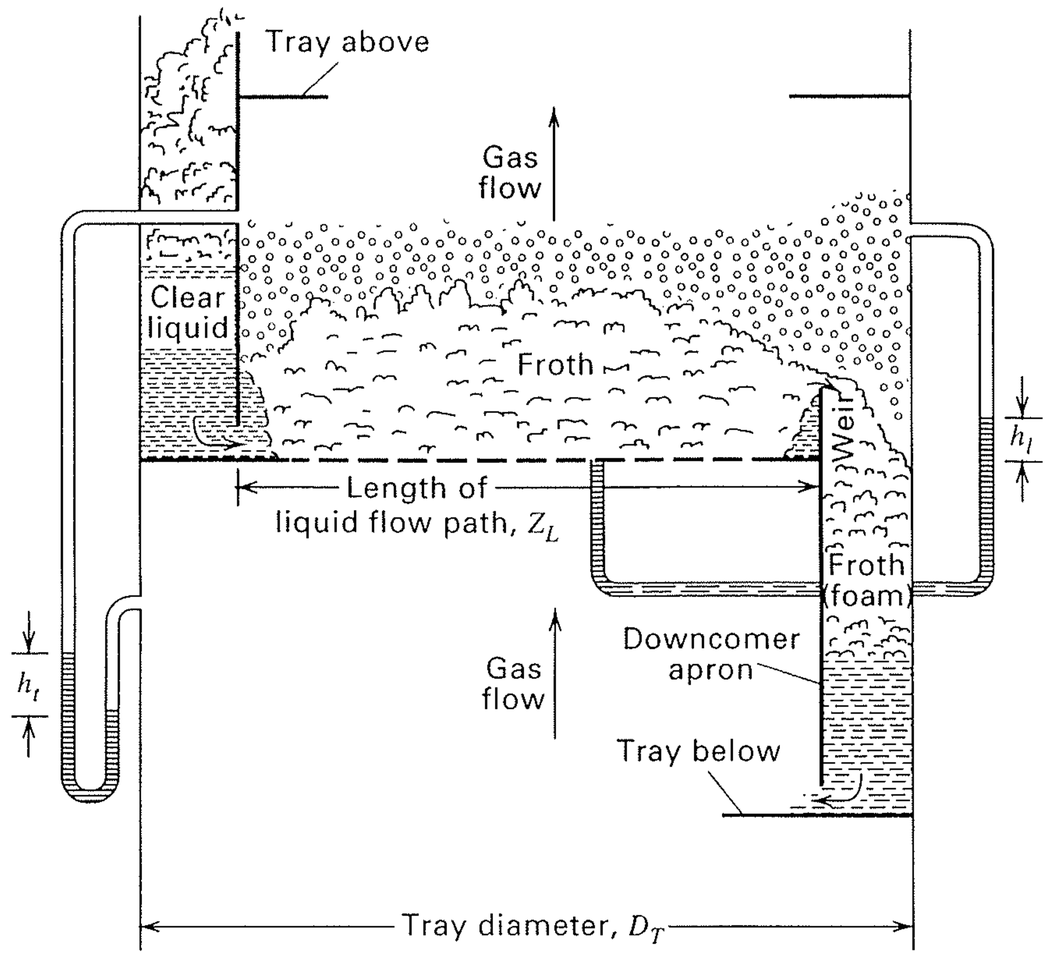

Figure 6.3 Details of a contacting tray in a trayed tower.
[Adapted from B.F. Smith, *Design of Equilibrium Stage Processes*, McGraw-Hill, New York (1963).]

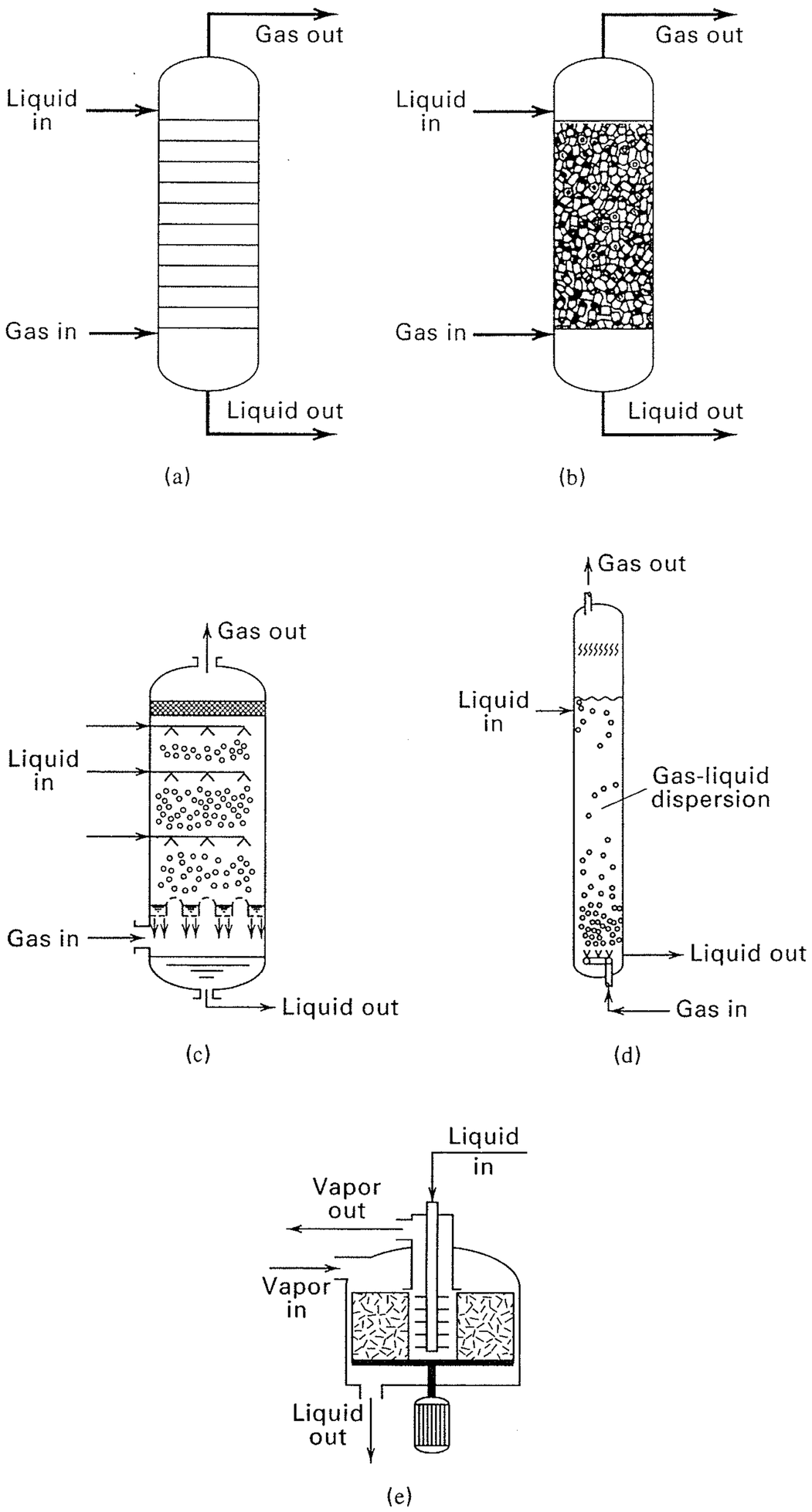

Figure 6.2 Industrial equipment for absorption and stripping: (a) trayed tower; (b) packed column; (c) spray tower; (d) bubble column; (e) centrifugal contactor.

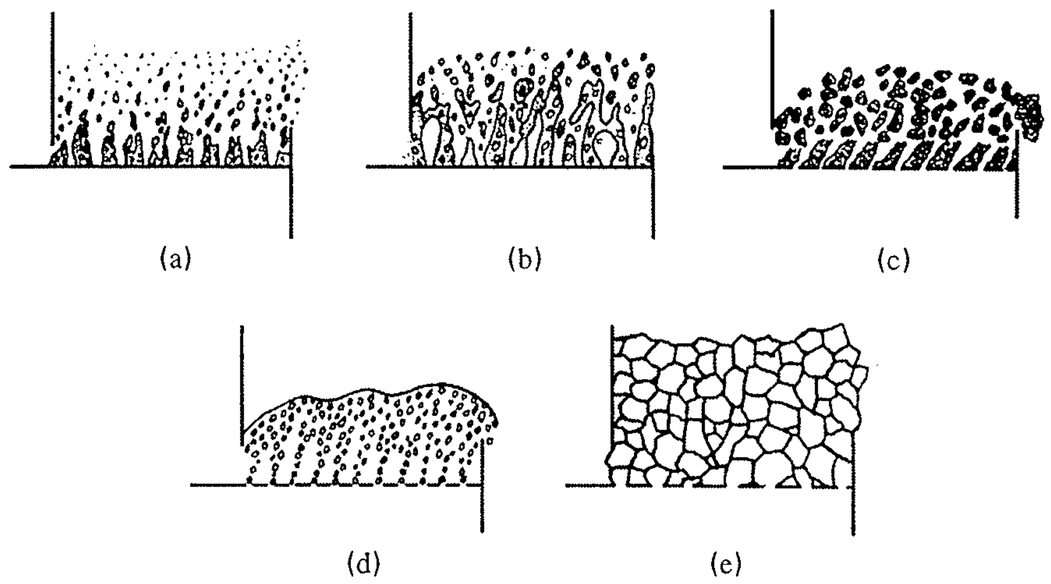

Figure 6.4 Possible vapor–liquid flow regimes for a contacting tray: (a) spray; (b) froth; (c) emulsion; (d) bubble; (e) cellular foam.
[Reproduced by permission from M.J. Lockett, *Distillation Tray Fundamentals,* Cambridge University Press, London (1986).]

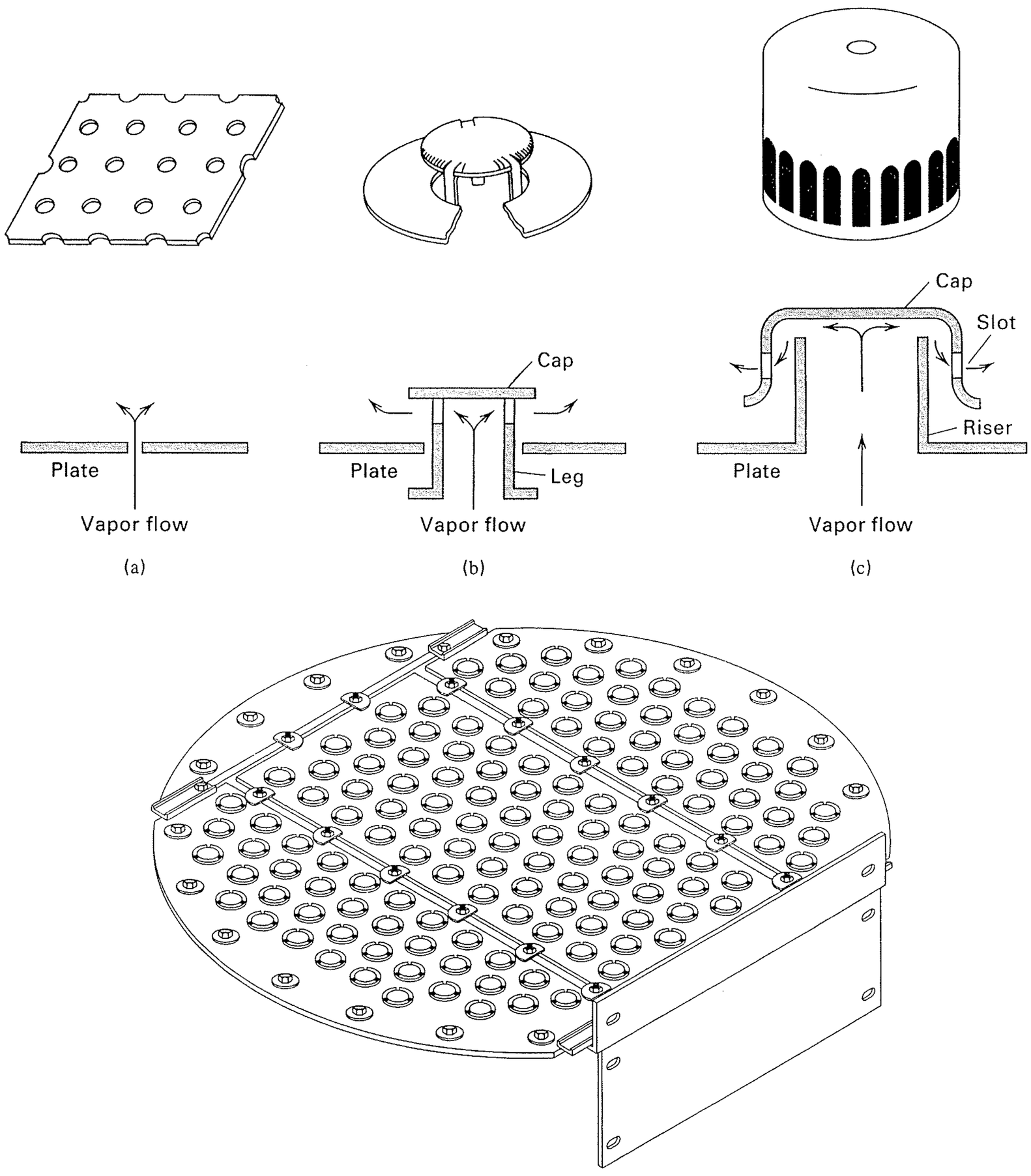

Figure 6.5 Three types of tray openings for passage of vapor up into liquid: (a) perforation; (b) valve cap; (c) bubble cap; (d) tray with valve caps.

As shown in Figure 6.5, openings in the tray for the passage of vapor are most commonly perforations, valves, and/or bubble caps. The simplest is perforations, usually $\frac{1}{8}$ to $\frac{1}{2}$ in. in diameter, used in a so-called *sieve tray* (also called a *perforated tray*). A *valve tray* has much larger openings, commonly from 1 to 2 in. in diameter. Each hole is fitted with a valve that consists of a cap, which overlaps the hole, with legs or a cage to limit the vertical rise while maintaining the horizontal location of the valve. With no vapor flow, each valve sits on the tray, over a hole. As the vapor rate is increased, the valve rises, providing a larger and larger peripheral opening for vapor to flow into the liquid to create a froth. A bubble-cap tray has bubble caps that consist of a fixed cap, 3 to 6 in. in diameter, mounted over and above a concentric riser of 2 to 3 in. in diameter. The cap has rectangular or triangular slots cut around its side. The vapor flows up through the tray opening into the riser, turns around, and passes out through the slots of the cap, into the liquid to form a froth. An 11-ft-diameter column might have trays with 50,000 $\frac{3}{16}$-in.-diameter perforations, or 1,000 2-in.-diameter valve caps, or 500 4-in.-diameter bubble caps.

As listed in Table 6.2, tray types are compared on the basis of cost, pressure drop, mass-transfer efficiency, vapor capacity, and flexibility in terms of turndown ratio (ratio of

Table 6.2 Comparison of Types of Trays

	Sieve Trays	Valve Trays	Bubble-Cap Trays
Relative cost	1.0	1.2	2.0
Pressure drop	Lowest	Intermediate	Highest
Efficiency	Lowest	Highest	Highest
Vapor capacity	Highest	Highest	Lowest
Typical turndown ratio	2	4	5

maximum to minimum vapor capacity). At the limiting vapor capacity, *flooding* of the column occurs because of excessive entrainment of liquid droplets in the vapor causing the liquid flow rate to exceed the capacity of the downcomer and, thus, go back up the column. At low vapor rates, weeping of liquid through the tray openings or vapor pulsation becomes excessive. Because of their low relative cost, sieve trays are preferred unless flexibility is required, in which case valve trays are best. Bubble-cap trays, which exist in many pre-1950 installations, are rarely specified for new installations, but may be preferred when the amount of liquid holdup on a tray must be controlled to provide adequate residence time for a chemical reaction or when weeping must be prevented.

A *packed column,* shown in detail in Figure 6.6, is a vertical, cylindrical pressure vessel containing one or more sections of a packing material over whose surface the liquid flows downward by gravity, as a film or as droplets between packing elements. Vapor flows upward through the wetted packing, contacting the liquid. The sections of packing are contained between a lower gas-injection support plate, which holds the packing, and an upper grid or mesh hold-down plate, which prevents packing movement. A *liquid distributor,* placed above the hold-down plate, ensures uniform distribution of liquid over the cross-sectional area of the column as it enters the packed section. If the depth of packing is more than about 20 ft, liquid channeling may occur, causing the liquid to flow down the column mainly near the wall, and gas to flow mainly up the center of the column, thus greatly reducing the extent of vapor–liquid contact. In that case, a liquid *redistributor* should be installed.

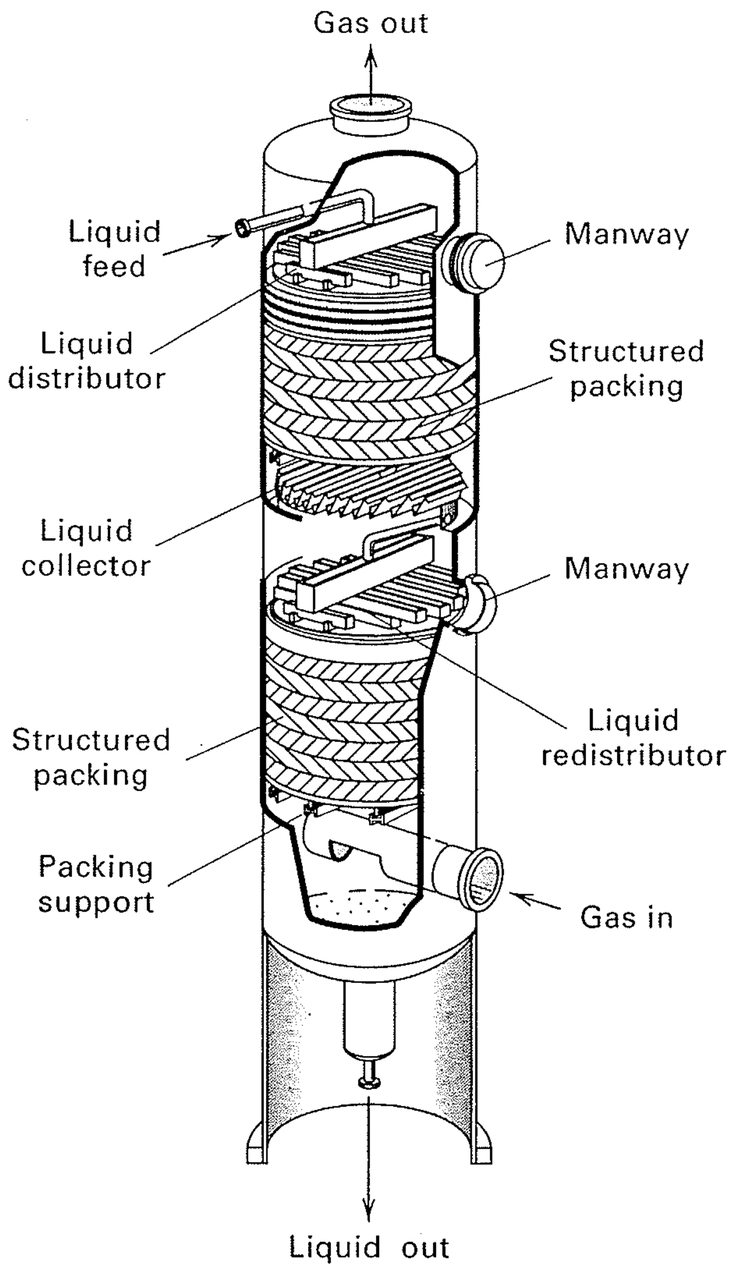

Figure 6.6 Details of internals used in a packed column.

Commercial packing materials include *random* (dumped) packings, some of which are shown in Figure 6.7a, and *structured* (also called arranged, ordered, or stacked packings), some of which are shown in Figure 6.7b. Among the random packings, which are poured into the column, are the old (1895–1950) ceramic Raschig rings and Berl saddles, which are seldom specified for new installations. They have been largely replaced by metal and plastic Pall rings, metal Bialecki rings, and ceramic Intalox saddles, which provide more surface area for mass transfer, a higher flow capacity, and a lower pressure drop. More recently, through-flow packings of a lattice-work design have been developed. These packings, which include metal Intalox IMTP; metal, plastic, and ceramic Cascade Mini-Rings; metal Levapak; metal, plastic, and ceramic Hiflow rings; metal tri-packs; and plastic Nor Pac rings, exhibit even lower pressure drop per unit height of packing and even higher mass-transfer rates per unit volume of packing. Accordingly, they are called "high-efficiency" random packings. Most random packings are available in nominal diameters, ranging from 1 in. to 3.5 in. As packing size increases, mass-transfer efficiency and pressure drop may decrease. Therefore, for a given column diameter an optimal packing size exists that represents a compromise between these two factors, since low pressure drop and high mass-transfer rates are both desirable. However, to minimize channeling of liquid, the nominal diameter of the packing should be less than one-eighth of the column diameter. Most recently, a "fourth generation" of random packings, including VSP rings, Fleximax, and Raschig super-rings, has been developed, which features a very open undulating geometry that promotes even wetting, but with recurrent turbulence promotion. The result is lower pressure drop, but sustained mass-transfer efficiency that may not decrease noticeably with increasing column diameter and may permit a larger depth of packing before a liquid redistributor is necessary. Metal packings are usually preferred because of their superior strength and good wettability. Ceramic packings, which have superior wettability but inferior strength, are used only to resist corrosion at elevated temperatures, where plastics would fail. Plastic packings, usually of polypropylene, are inexpensive and have sufficient strength, but may experience poor wettability, particularly at low liquid rates.

Representative structured packings include the older corrugated sheets of metal gauze, such as Sulzer BX, Montz A, Gempak 4BG, and Intalox High-Performance Wire Gauze Packing. Newer and less-expensive structured packings, which are fabricated from sheet metal and plastics and may or may not be perforated, embossed, or surface roughened, include metal and plastic Mellapak 250Y, metal Flexipac, metal and plastic Gempak 4A, metal Montz B1, and metal Intalox High-Performance Structured Packing. Structured

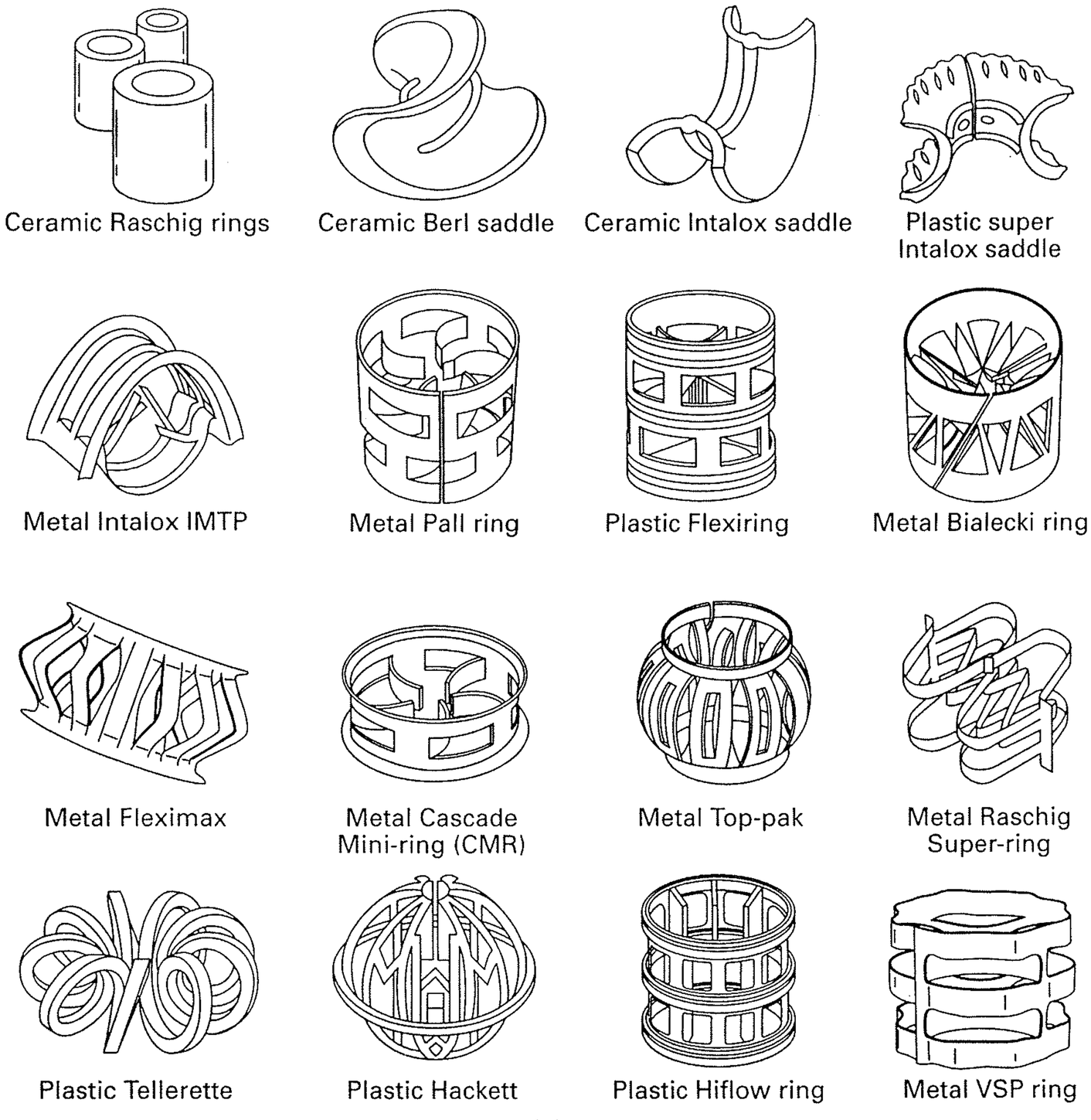

Figure 6.7 Typical materials used in a packed column: (a) random packing materials; (*continued*)

packings come with different size openings between adjacent corrugated layers and are stacked in the column. Although structured packings are considerably more expensive per unit volume than random packings, structured packings exhibit far less pressure drop per theoretical stage and have higher efficiency and capacity.

As shown in Table 6.3, packings are usually compared on the basis of the same factors used to compare tray types. However, the differences between random and structured packings are much greater than the differences among the three types of trays listed in Table 6.2.

Table 6.3 Comparison of Types of Packing

	Random		
	Raschig Rings and Saddles	"Through Flow"	Structured
Relative cost	Low	Moderate	High
Pressure drop	Moderate	Low	Very low
Efficiency	Moderate	High	Very high
Vapor capacity	Fairly high	High	High
Typical turndown ratio	2	2	2

If only one or two theoretical stages are required, only a very low pressure drop is allowed, and the solute is very soluble in the liquid phase, the use of a *spray tower* may be advantageous. As shown in Figure 6.2, a spray tower consists of a vertical, cylindrical vessel filled with gas into which liquid is sprayed. A *bubble column,* also shown in Figure 6.2, consists of a vertical, cylindrical vessel partially filled with liquid into which the vapor is bubbled. Vapor pressure drop is high, and only one or two theoretical stages can be achieved. Such a device has a low vapor throughput and should not be considered unless the solute has a very low solubility in the liquid and/or a slow chemical reaction takes place in the liquid phase, thus requiring an appreciable residence time. A novel device is the *centrifugal contactor,* one example of which, as shown in Figure 6.2, consists of a stationary, ringed housing, intermeshed with a ringed rotating section. The liquid phase is fed near the center of the packing, from which it is caused to flow outward by centrifugal force. The vapor phase flows inward by a pressure driving force. Very high mass-transfer rates can be achieved with only moderately high rotation rates. It is possible to obtain the equivalent of several equilibrium stages in a very compact unit. This type of contact is favored when headroom for a trayed tower or packed column is not available or when a short residence time is desired.

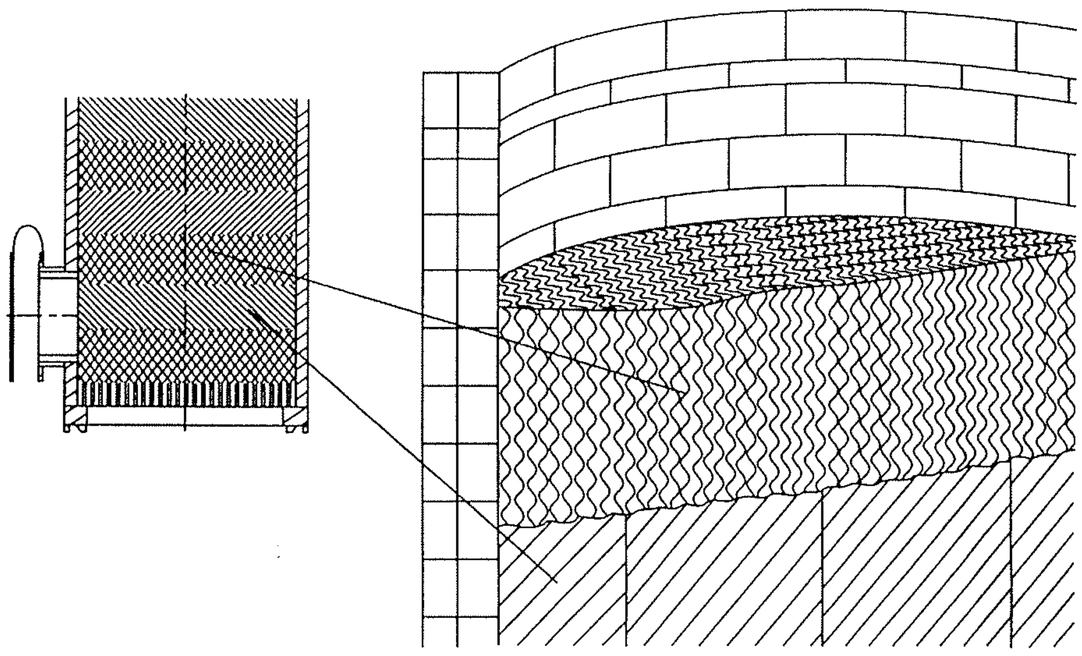

Flexiceramic

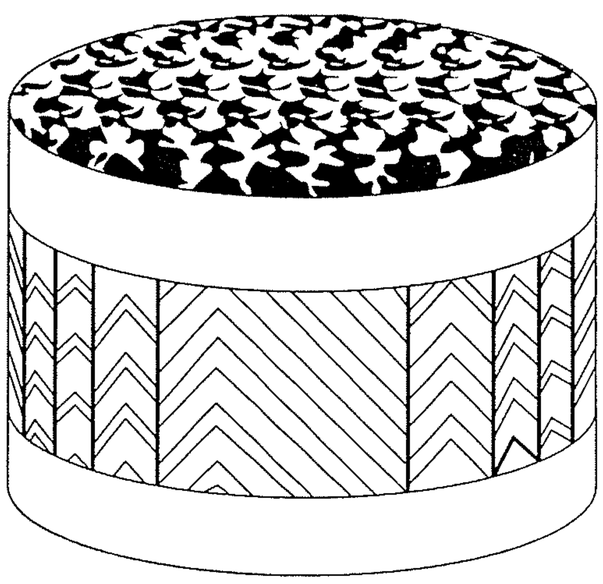

Mellapak

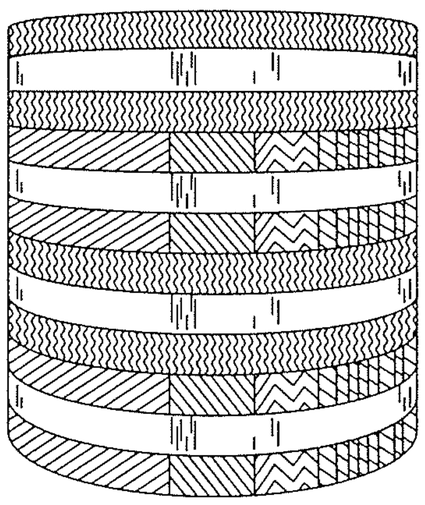

Flexipac

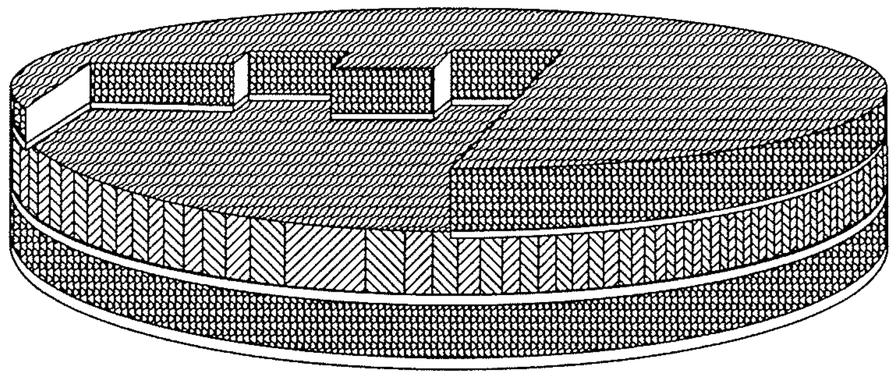

Montz

(b)

Figure 6.7 (*Continued*) (b) structured packing materials.

In most applications, the choice of contacting device is between a trayed tower and a packed column. The latter, using dumped packings, is almost always favored when a column diameter of less than 2 ft and a packed height of not more than 20 ft are sufficient. In addition, packed columns should be considered for corrosive services where ceramic or plastic materials are preferred over metals, in services where foaming may be severe if trays are used, and when pressure drop must be low, as in vacuum or near-ambient-pressure operations. Otherwise, trayed towers, which can be designed and scaled up more reliably, are preferred. Although structured packings are quite expensive, they may be the best choice for a new installation when pressure drop must be very low or for replacing existing trays (retrofitting) when a higher capacity or degree of separation is required in an existing column. Trayed towers are preferred when liquid velocities are low, while columns with random packings are best for high-liquid velocities. The use of structured packings should be avoided at high-pressures (> 200 psia) and high-liquid flow rates (> 10 gpm/ft^2), Kister [33]. In general, a continuous, turbulent liquid flow is desirable if mass transfer is limiting in the liquid phase, while a continuous, turbulent gas flow is desirable if mass transfer is limiting in the gas phase.

6.2 GENERAL DESIGN CONSIDERATIONS

Design or analysis of an absorber (or stripper) requires consideration of a number of factors, including:

1. Entering gas (liquid) flow rate, composition, temperature, and pressure
2. Desired degree of recovery of one or more solutes
3. Choice of absorbent (stripping agent)
4. Operating pressure and temperature, and allowable gas pressure drop

5. Minimum absorbent (stripping agent) flow rate and actual absorbent (stripping agent) flow rate as a multiple of the minimum rate needed to make the separation
6. Number of equilibrium stages and stage efficiency
7. Heat effects and need for cooling (heating)
8. Type of absorber (stripper) equipment
9. Height of absorber (stripper)
10. Diameter of absorber (stripper)

The ideal absorbent should (a) have a high solubility for the solute(s) to minimize the need for absorbent, (b) have a low volatility to reduce the loss of absorbent and facilitate separation of absorbent from solute(s), (c) be stable to maximize absorbent life and reduce absorbent makeup requirement, (d) be noncorrosive to permit use of common materials of construction, (e) have a low viscosity to provide low pressure drop and high mass- and heat-transfer rates, (f) be nonfoaming when contacted with the gas so as to make it unnecessary to increase absorber dimensions, (g) be nontoxic and nonflammable to facilitate its safe use, and (h) be available, if possible, within the process, to make it unnecessary to provide an absorbent from external sources, or be inexpensive. As already indicated at the beginning of this chapter, the most widely used absorbents are water, hydrocarbon oils, and aqueous solutions of acids and bases. The most common stripping agents are steam, air, inert gases, and hydrocarbon gases.

In general, operating pressure should be high and temperature low for an absorber, to minimize stage requirements and/or absorbent flow rate and to lower the equipment volume required to accommodate the gas flow. Unfortunately, both compression and refrigeration of a gas are expensive. Therefore, most absorbers are operated at feed-gas pressure, which may be greater than ambient pressure, and ambient temperature, which can be achieved by cooling the feed gas and absorbent with cooling water, unless one or both streams already exist at a subambient temperature. Operating pressure should be low and temperature high for a stripper to minimize stage requirements or stripping agent flow rate. However, because maintenance of a vacuum is expensive, strippers are commonly operated at a pressure just above ambient. A high temperature can be used, but it should not be so high as to cause undesirable chemical reactions. Of course, operating temperature and pressure must be compatible with the necessary phase conditions of the streams being contacted. For example, an absorber should not be operated at a pressure and/or temperature that would condense the feed gas, and a stripper should not be operated at a pressure and/or temperature that would vaporize the feed liquid. The possibility of such conditions occurring can be checked by bubble-point and dew-point calculations, discussed in Chapter 4.

For given feed-gas (liquid) flow rate, extent of solute absorption (stripping), operating pressure and temperature, and absorbent (stripping agent) composition, a minimum absorbent (stripping agent) flow rate exists that corresponds to an infinite number of countercurrent equilibrium contacts between the gas and liquid phases. In every design problem involving flow rates of the absorbent (stripping agent) and number of stages, a trade-off exists between the number of equilibrium stages and the absorbent (stripping agent) flow rate at rates greater than the minimum value. Graphical and analytical methods for computing the minimum flow rate and this trade-off are developed in the following sections for a mixture that is dilute in the solute(s). For this essentially isothermal case, the energy balance can be ignored. As discussed in Chapters 10 and 11, computer-aided methods are best used for concentrated mixtures, where multicomponent phase-equilibrium and mass-transfer effects can become complicated and it is necessary to consider the energy balance.

6.3 GRAPHICAL EQUILIBRIUM-STAGE METHOD FOR TRAYED TOWERS

Consider the countercurrent-flow, trayed tower for absorption (or stripping) operating under isobaric, isothermal, continuous, steady-state flow conditions shown in Figure 6.8. For convenience, the stages are numbered from top to bottom for the absorber and from bottom to top for the stripper. Phase equilibrium is assumed to be achieved at each of the N trays between the vapor and liquid streams leaving the tray. That is, each tray is treated as an equilibrium stage. Assume that the only component transferred from one phase to the

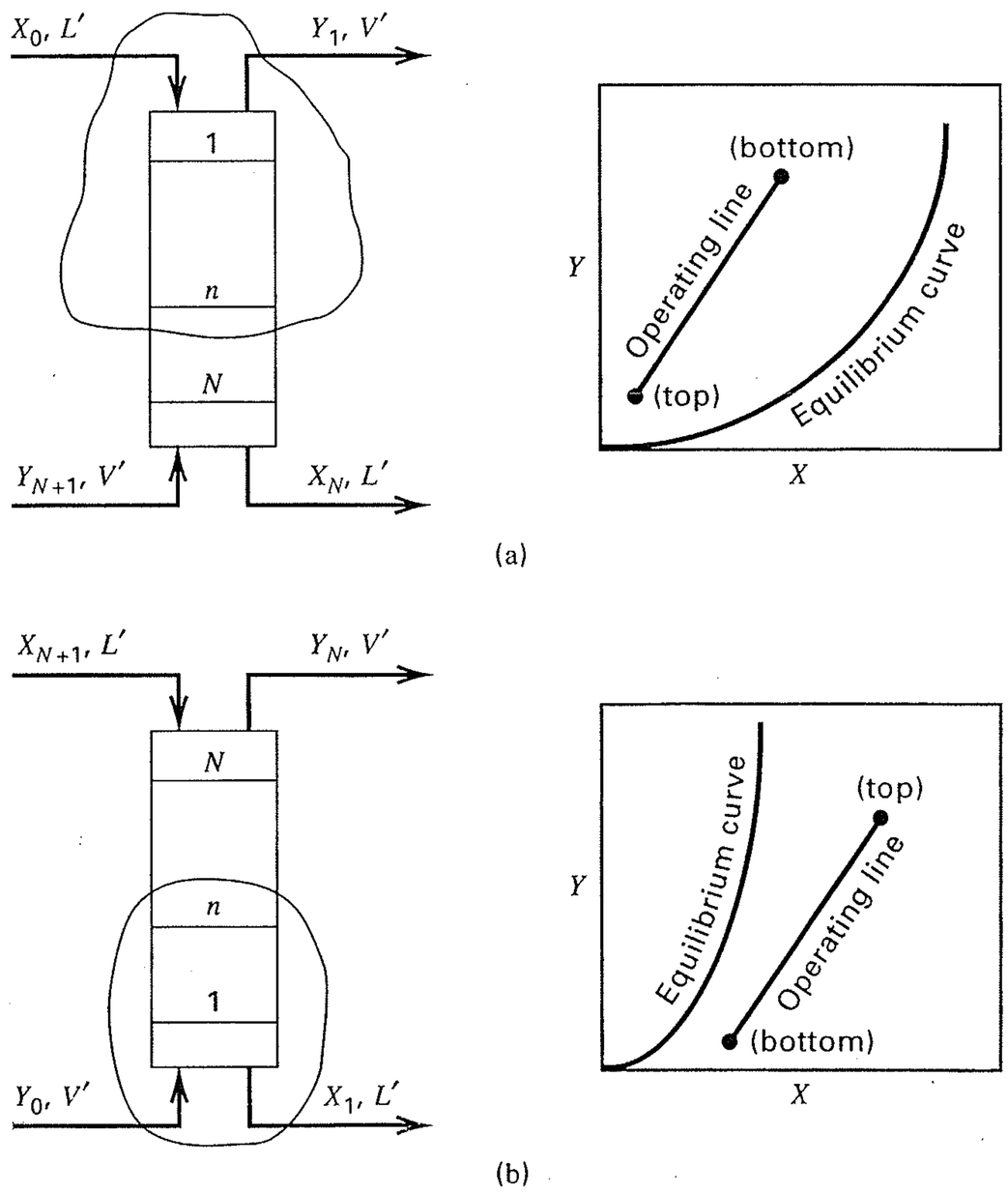

Figure 6.8 Continuous, steady-state operation in a countercurrent cascade with equilibrium stages: (a) absorber; (b) stripper.

other is the solute. For application to an absorber, let:

L' = molar flow rate of solute-free absorbent

V' = molar flow rate of solute-free gas (carrier gas)

X = mole ratio of solute to solute-free absorbent in the liquid

Y = mole ratio of solute to solute-free gas in the vapor

Note that with these definitions, values of L' and V' remain constant through the tower, assuming no vaporization of absorbent into carrier gas or absorption of carrier gas by liquid. For the solute at any equilibrium stage, n, the K-value is given in terms of X and Y as:

$$K_n = \frac{y_n}{x_n} = \frac{Y_n/(1+Y_n)}{X_n/(1+X_n)} \tag{6-1}$$

where $Y = y/(1-y)$ and $X = x/(1-x)$.

For the fixed temperature and pressure and a series of values of x, equilibrium values of y in the presence of the solute-free absorbent and solute-free gas are estimated by methods discussed in Chapter 2. From these values, an equilibrium curve of Y as a function of X is calculated and plotted, as shown in Figure 6.8. In general, this curve will not be a straight line, but it will pass through the origin. If the solute undergoes, in the liquid phase, a complete irreversible conversion by chemical reaction, to a nonvolatile solute, the equilibrium curve will be a straight line of zero slope passing through the origin.

At either end of the towers shown in Figure 6.8, entering and leaving streams and solute mole ratios are paired. For the absorber, the pairs are (X_0, L' and Y_1, V') at the top and (X_N, L' and Y_{N+1}, V') at the bottom; for the stripper, (X_{N+1}, L' and Y_N, V') at the top and (X_1, L' and Y_0, V') at the bottom. These terminal pairs can be related to intermediate pairs of passing streams by the following solute material balances for the envelopes shown in Figure 6.8. The balances are written around one end of the tower and an arbitrary intermediate equilibrium stage, n.

For the absorber,

$$X_0 L' + Y_{n+1} V' = X_n L' + Y_1 V' \tag{6-2}$$

or, solving for Y_{n+1},

$$Y_{n+1} = X_n(L'/V') + Y_1 - X_0(L'/V') \tag{6-3}$$

For the stripper,

$$X_{n+1} L' + Y_0 V' = X_1 L' + Y_n V' \tag{6-4}$$

or, solving for Y_n,

$$Y_n = X_{n+1}(L'/V') + Y_0 - X_1(L'/V') \tag{6-5}$$

Equations (6-3) and (6-5), which are called *operating-line equations,* are plotted in Figure 6.8. The terminal points of these lines represent the conditions at the top and bottom of the towers. For the absorber, the operating line is above the equilibrium line because, for a given solute concentration in the liquid, the solute concentration in the gas is always greater than the equilibrium value, thus providing the driving force for mass transfer of solute from the gas to the liquid. For the stripper, the operating line lies below the equilibrium line for the opposite reason. For the coordinate systems in Figure 6.8, the operating lines are straight with a slope of L'/V'.

For an absorber, the terminal point of the operating line at the top of the tower is fixed at X_0 by the amount of solute, if any, in the entering absorbent, and the specified degree of absorption of the solute, which fixes the value of Y_1 in the leaving gas. The terminal point of the operating line at the bottom of the tower depends on Y_{N+1} and the slope of the operating line and, thus, the flow rate, L', of solute-free absorbent.

Minimum Absorbent Flow Rate

Operating lines for four different absorbent flow rates are shown in Figure 6.9, where each operating line passes through the terminal point, (Y_1, X_0), at the top of the column, and corresponds to a different liquid absorbent rate and corresponding slope, L'/V'. To achieve the desired value of Y_1 for given Y_{N+1}, X_0, and V', the solute-free absorbent flow rate L', must lie in the range of ∞ (operating line 1) to L'_{min} (operating line 4). The value of the solute concentration in the outlet liquid, X_N, depends on L' by a material balance on

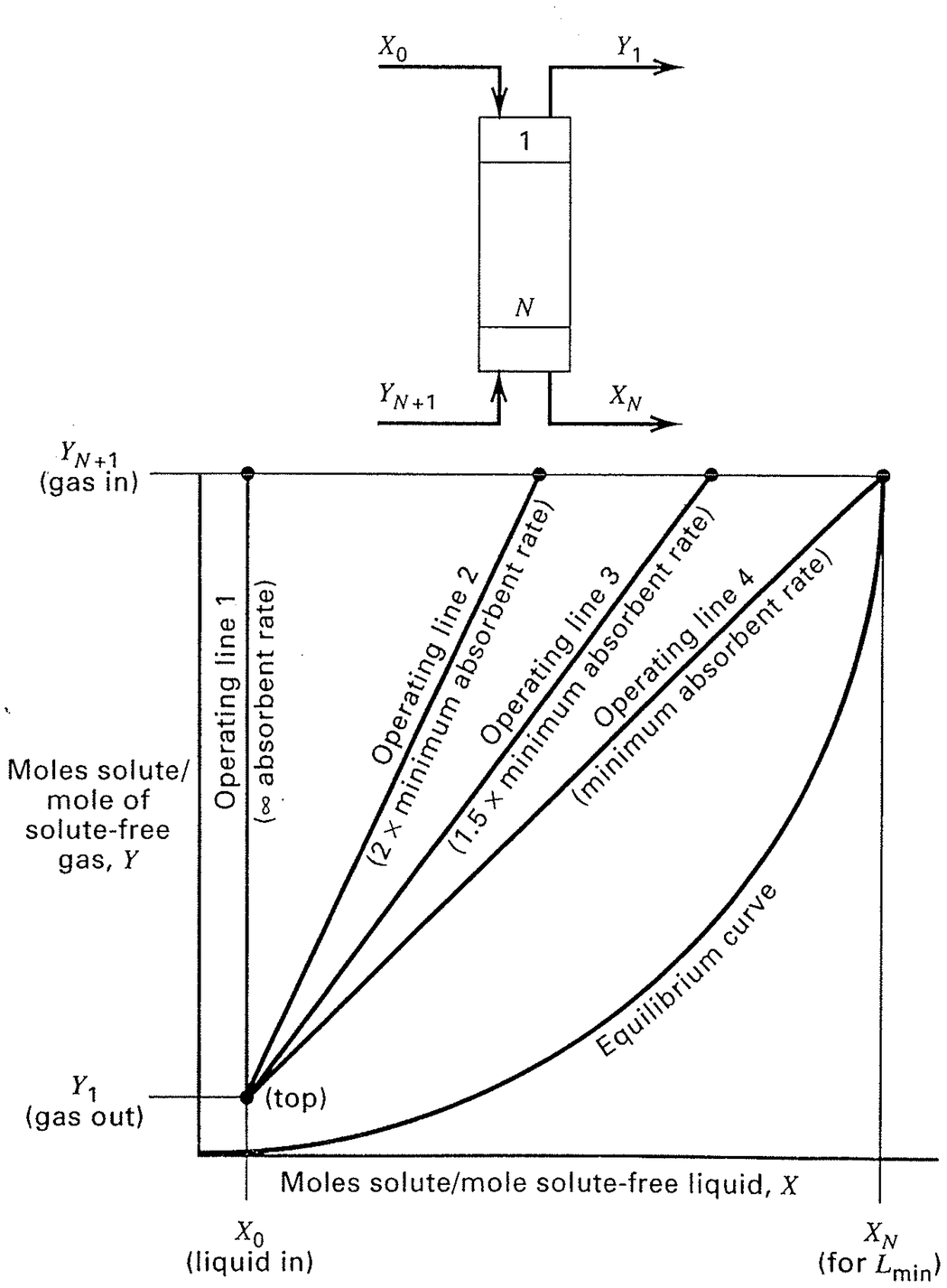

Figure 6.9 Operating lines for an absorber.

the solute for the entire absorber. From (6-2), for $n = N$,

$$X_0 L' + Y_{N+1} V' = X_N L' + Y_1 V' \tag{6-6}$$

or

$$L' = \frac{V'(Y_{N+1} - Y_1)}{(X_N - X_0)} \tag{6-7}$$

Note that the operating line can terminate at the equilibrium line, as for operating line 4, but cannot cross it because that would be a violation of the second law of thermodynamics.

The value of L'_{min} corresponds to a value of X_N (leaving the bottom of the tower) in equilibrium with Y_{N+1}, the solute concentration in the feed gas. It takes an infinite number of stages for this equilibrium to be achieved. An expression for L'_{min} of an absorber can be derived from (6-7) as follows.

For stage N, (6-1) becomes, for the minimum absorbent rate,

$$K_N = \frac{Y_{N+1}/(1 + Y_{N+1})}{X_N/(1 + X_N)} \tag{6-8}$$

Solving (6-8) for X_N and substituting the result into (6-7) gives

$$L'_{\text{min}} = \frac{V'(Y_{N+1} - Y_1)}{\{Y_{N+1}/[Y_{N+1}(K_N - 1) + K_N]\} - X_0} \tag{6-9}$$

For dilute-solute conditions, where $Y \approx y$ and $X \approx x$, (6-9) approaches

$$L'_{\text{min}} = V' \left(\frac{y_{N+1} - y_1}{\dfrac{y_{N+1}}{K_N} - x_0} \right) \tag{6-10}$$

Furthermore, if the entering liquid contains no solute, that is, $X_0 \approx 0$, (6-10) approaches

$$L'_{\text{min}} = V' K_N \text{ (fraction of solute absorbed)} \tag{6-11}$$

This equation is reasonable because it would be expected that L'_{min} would increase with increasing V', K-value, and fraction of solute absorbed.

The selection of the actual operating absorbent flow rate is based on some multiple of L'_{min}, typically from 1.1 to 2. A value of 1.5 corresponds closely to the value of 1.4 for the optimal absorption factor mentioned earlier. In Figure 6.9, operating lines 2 and 3 correspond to 2.0 and 1.5 times L'_{min}, respectively. As the operating line moves from 1 to 4, the number of required equilibrium stages, N, increases from zero to infinity. Thus, a trade-off exists between L' and N, and an optimal value of L' exists.

A similar derivation of V'_{min}, for the stripper of Figure 6.8, results in an expression analogous to (6-11):

$$V'_{\text{min}} = \frac{L'}{K_N} \text{ (fraction of solute stripped)} \tag{6-12}$$

Number of Equilibrium Stages

As shown in Figure 6.10a, the operating line relates the solute concentration in the vapor passing upward between two stages to the solute concentration in the liquid passing downward between the same two stages. Figure 6.10b illustrates that the equilibrium curve relates the solute concentration in the vapor leaving an equilibrium stage to the solute concentration in the liquid leaving the same stage. This makes it possible, in the case of an absorber, to start from the top of the tower (at the bottom of the Y–X diagram) and move to the bottom of the tower (at the top of the Y–X diagram) by constructing a staircase alternating between the operating line and the equilibrium curve, as shown in Figure 6.11a. The number of equilibrium stages required for a particular absorbent flow rate corresponding to the slope of the operating line, which in Figure 6.11a is for $(L'/V') = 1.5(L'_{\text{min}}/V')$, is stepped off by moving up the staircase, starting from the point (Y_1, X_0), on the operating line and moving horizontally to the right to the point (Y_1, X_1) on the equilibrium curve. From there, a vertical move is made to the point (Y_2, X_1) on the operating line. Proceeding in this manner, the staircase is climbed until the terminal point (Y_{N+1}, X_N) on the operating line is reached. As shown in Figure 6.11a, the stages are counted at the points of the staircase on the equilibrium curve. As the slope (L'/V') is increased, fewer equilibrium stages are required. As (L'/V') is decreased, more stages are required until (L'_{min}/V') is reached, at which the operating line and equilibrium curve intersect at a so-called *pinch point,* for which an infinite number of stages is required. Operating line 4 in Figure 6.9 has a pinch point at Y_{N+1}, X_N. If (L'/V') is reduced below (L'_{min}/V'), the specified extent of absorption of the solute cannot be achieved.

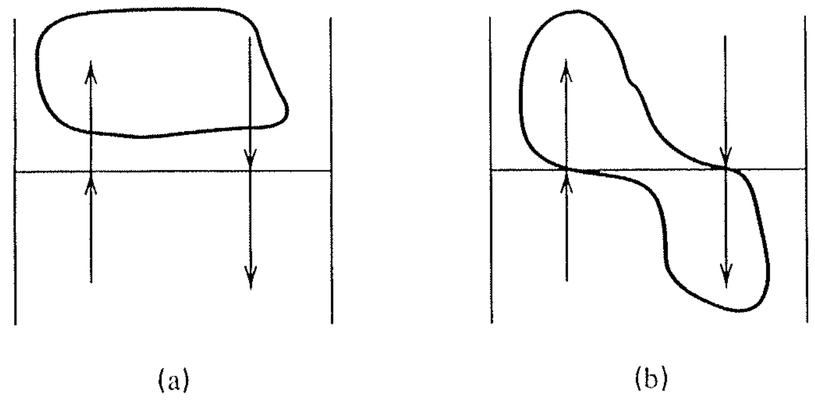

(a) (b)

Figure 6.10 Vapor–liquid stream relationships: (a) operating line (passing streams); (b) equilibrium curve (leaving streams).

The number of equilibrium stages required for stripping a solute is determined in a manner similar to that for absorption. An illustration is shown in Figure 6.11b, which refers to Figure 6.8b. For given specifications of Y_0, X_{N+1}, and the extent of stripping of the solute, which corresponds to a value of X_1, V'_{min} is determined from the slope of the operating line that passes through the points (Y_0, X_1), and (Y_N, X_{N+1}) on the equilibrium curve. The operating line in Figure 6.11b is for $V' = 1.5V'_{\text{min}}$ or a slope of $(L'/V') = (L'/V'_{\text{min}})/1.5$.

In Figure 6.11, the number of equilibrium stages for the absorber and stripper is exactly three each. These integer results are coincidental. Ordinarily, the result is some fraction above an integer number of stages, as is the case in the following example. In practice, the result is usually rounded to the next highest integer.

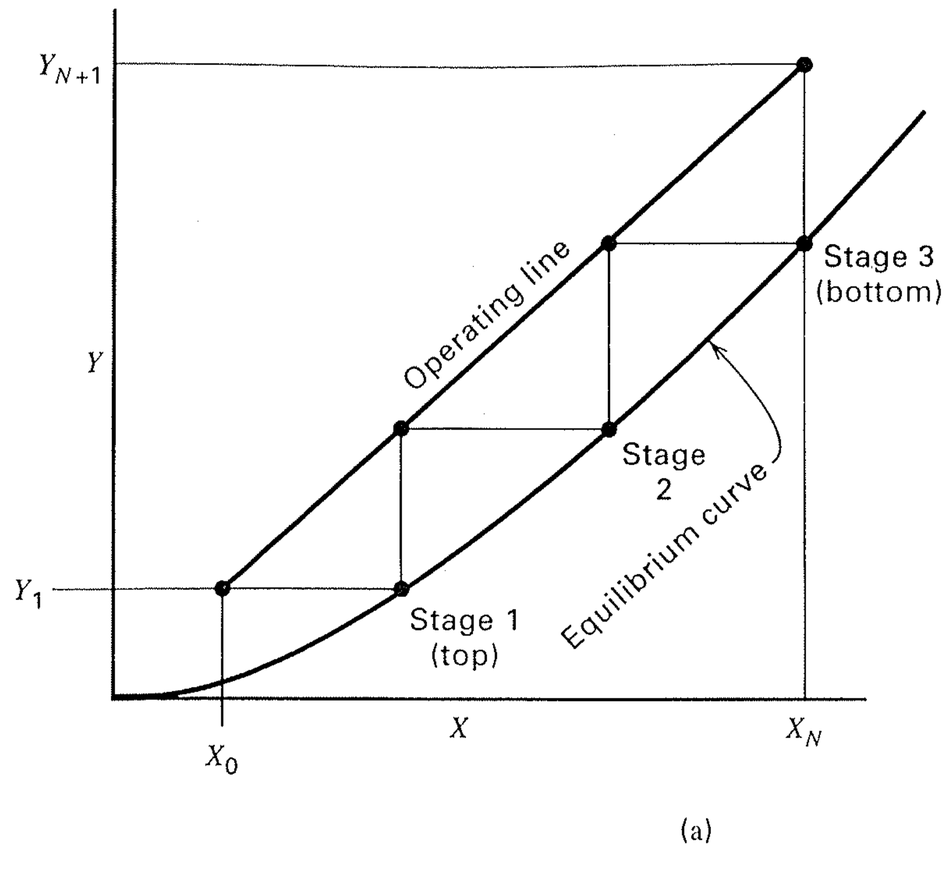

(a)

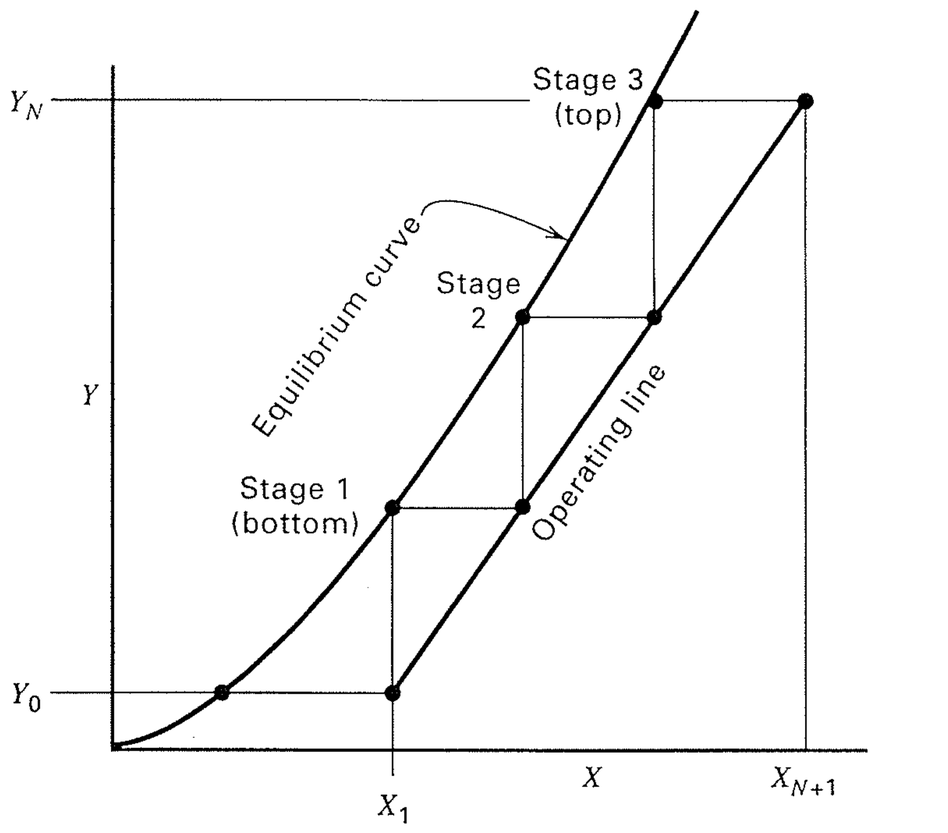

(b)

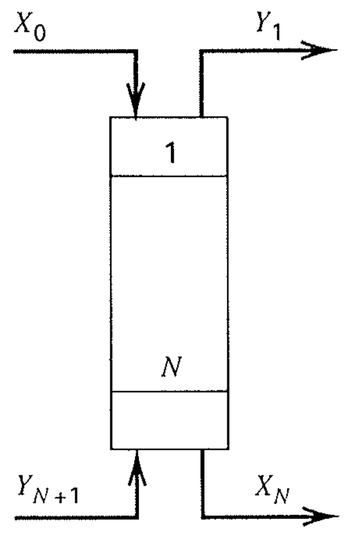

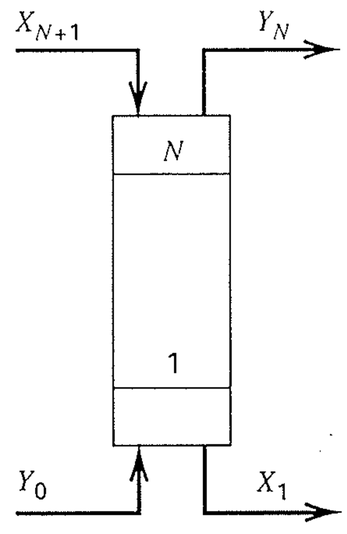

Figure 6.11 Graphical determination of the number of equilibrium stages for (a) absorber and (b) stripper.

EXAMPLE 6.1

When molasses is fermented to produce a liquor containing ethyl alcohol, a CO_2-rich vapor containing a small amount of ethyl alcohol is evolved. The alcohol can be recovered by absorption with water in a sieve-tray tower. For the following conditions, determine the number of equilibrium stages required for countercurrent flow of liquid and gas, assuming isothermal, isobaric conditions in the tower and neglecting mass transfer of all components except ethyl alcohol.

Entering gas:

180 kmol/h; 98% CO_2, 2% ethyl alcohol; 30°C, 110 kPa

Entering liquid absorbent:

100% water; 30°C, 110 kPa

Required recovery (absorption) of ethyl alcohol: 97%

SOLUTION

From Section 5.7 for a single-section, countercurrent cascade, the number of degrees of freedom is $2N + 2C + 5$. All stages operate adiabatically at a pressure of approximately 1 atm, taking $2N$ degrees of freedom. The entering gas is completely specified, taking $C + 2$ degrees of freedom. The entering liquid flow rate is not specified; thus, only $C + 1$ degrees of freedom are taken by the entering liquid. The recovery of ethyl alcohol takes one additional degree of freedom. Thus, the total number of degrees of freedom taken by the problem specification is $2N + 2C + 4$. This leaves one additional specification to be made, which in this example can be the entering liquid flow rate at, say, 1.5 times the minimum value.

The above application of the degrees of freedom analysis from Chapter 5 has assumed the use of an energy balance for each stage. The energy balances are assumed to result in the assumed isothermal operation at 30°C.

Assume that the exiting absorbent will be dilute in ethyl alcohol, whose K-value is determined from a modified Raoult's law, $K = \gamma P^s / P$. The vapor pressure of ethyl alcohol at 30°C is 10.5 kPa. At infinite dilution in water at 30°C, the liquid-phase activity coefficient of ethyl alcohol is taken as 6. Therefore, $K = (6)(10.5)/110 = 0.57$. The minimum solute-free absorbent rate is given by (6-11), where the solute-free gas rate, V', is $(0.98)(180) = 176.4$ kmol/h. Thus,

$$L'_{\min} = (176.4)(0.57)(0.97) = 97.5 \text{ kmol/h}$$

The actual solute-free absorbent rate, at 50% above the minimum rate, is

$$L' = 1.5(97.5) = 146.2 \text{ kmol/h}$$

The amount of ethyl alcohol transferred from the gas to the liquid is 97% of the amount of alcohol in the entering gas or

$$(0.97)(0.02)(180) = 3.49 \text{ kmol/h}$$

The amount of ethyl alcohol remaining in the exiting gas is

$$(1.00 - 0.97)(0.02)(180) = 0.11 \text{ kmol/h}$$

We now compute the alcohol mole ratios at both ends of the operating line as follows, referring to Figure 6.8a:

$$\text{top} \begin{cases} X_0 = 0, & Y_1 = \dfrac{0.11}{176.4} = 0.0006 \end{cases}$$

$$\text{bottom} \begin{cases} Y_{N+1} = \dfrac{0.11 + 3.49}{176.4} = 0.0204, & X_N = \dfrac{3.49}{146.2} = 0.0239 \end{cases}$$

The equation for the operating line from (6-3) with $X_0 = 0$ is

$$Y_{N+1} = \left(\frac{146.2}{176.4}\right) X_N + 0.0006 = 0.829 X_N + 0.0006 \qquad (1)$$

It is clear that we are dealing with a dilute system. The equilibrium curve for ethyl alcohol can be determined from (6-1) using the value of $K = 0.57$ computed above. From (6-1),

$$0.57 = \frac{Y/(1+Y)}{X/(1+X)}$$

Solving for Y, we obtain

$$Y = \frac{0.57X}{1 + 0.43X} \qquad (2)$$

To cover the entire column, the necessary range of X for a plot of Y vs X is 0 to almost 0.025. From the Y–X equation, (2),

Y	X
0.00000	0.000
0.00284	0.005
0.00569	0.010
0.00850	0.015
0.01130	0.020
0.01410	0.025

For this dilute system in ethyl alcohol, the maximum error in Y is 1.0% if Y is taken simply as $Y = KX = 0.57X$.

The equilibrium curve, which is almost straight in this example, and a straight operating line drawn through the terminal points (Y_1, X_0) and (Y_{N+1}, X_N) is given in Figure 6.12. The determination of points for the operating line and the equilibrium curve, as well as the plot of the points, is conveniently done with a spreadsheet program on a computer using Eqs. (1) and (2). The theoretical stages are stepped off as shown starting from the top stage (Y_1, X_0) located near the lower left corner of Figure 6.12. The required number of theoretical stages for 97% absorption of ethyl alcohol is just slightly more than six. Accordingly, it is best to provide seven theoretical stages.

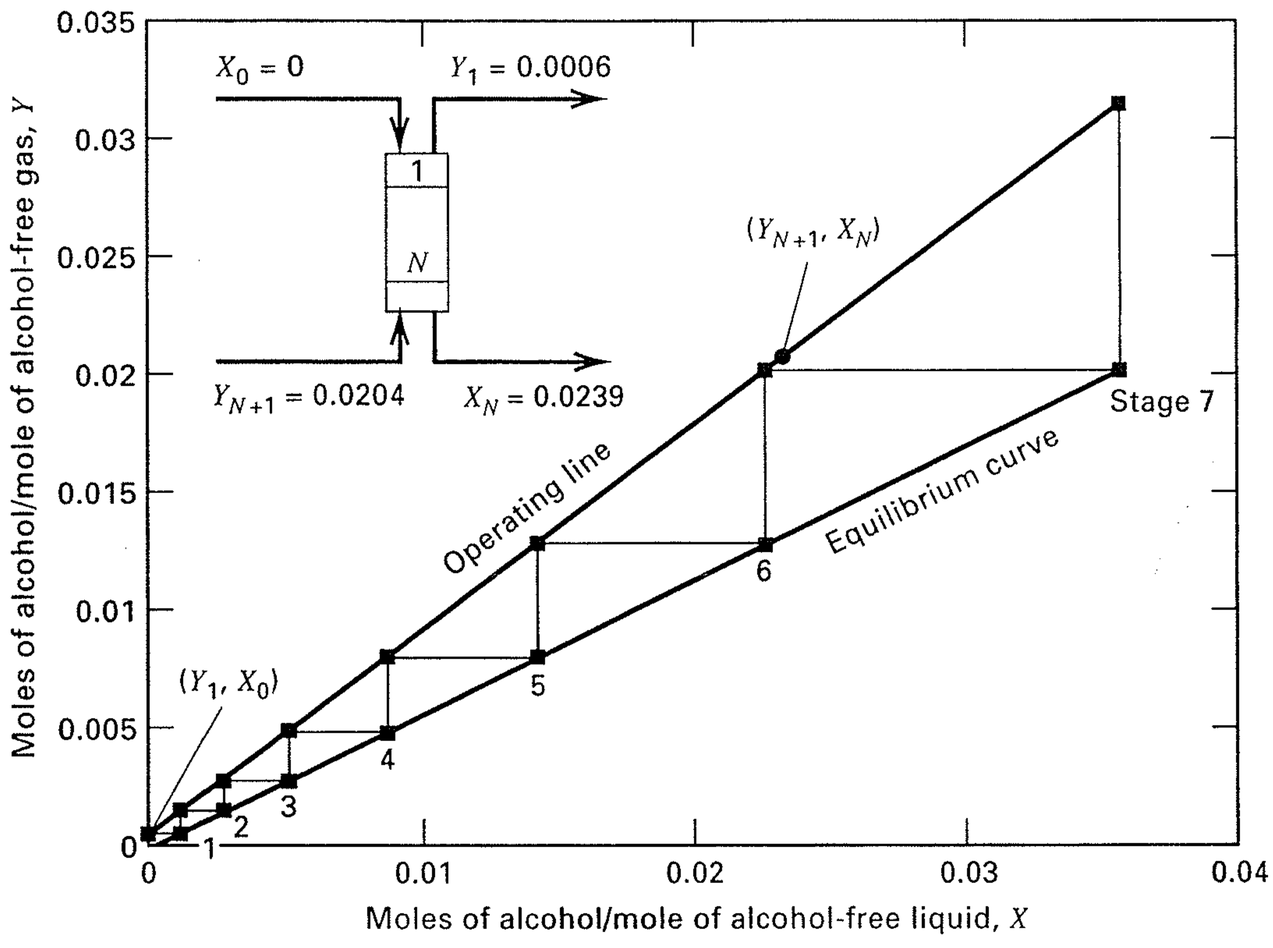

Figure 6.12 Graphical determination of number of equilibrium stages for an absorber.

6.4 ALGEBRAIC METHOD FOR DETERMINING THE NUMBER OF EQUILIBRIUM STAGES

Graphical methods for determining equilibrium stages have great educational value because a fairly complex multistage problem can be readily followed and understood. Furthermore, one can quickly gain visual insight into the phenomena involved. However, the application of a graphical method can become very tedious when (1) the problem specification fixes the number of stages rather than the percent recovery of solute, (2) when more than one solute is being absorbed or stripped, (3) when the best operating conditions of temperature and pressure are to be determined so that the location of the equilibrium curve is unknown, and/or (4) if very low or very high concentrations force the graphical construction to the corners of the diagram so that multiple y–x diagrams of varying sizes and dimensions are needed.

Then, the application of an algebraic method may be preferred.

The Kremser method for single-section cascades, as developed in Section 5.4, is ideal for absorption and stripping of dilute mixtures. For example, (5-48) and (5-50) can be written in terms of the fraction of solute absorbed or stripped as

$$\text{Fraction of a solute, } i, \text{ absorbed} = \frac{A_i^{N+1} - A_i}{A_i^{N+1} - 1} \quad (6\text{-}13)$$

and

$$\text{Fraction of a solute, } i, \text{ stripped} = \frac{S_i^{N+1} - S_i}{S_i^{N+1} - 1} \quad (6\text{-}14)$$

where the solute absorption and stripping factors are, respectively,

$$A_i = L/(K_i V) \quad (6\text{-}15)$$

$$S_i = K_i V/L \quad (6\text{-}16)$$

Values of L and V in moles per unit time may be taken as entering values. Values of K_i depend mainly on temperature, pressure, and liquid-phase composition. Methods for estimating K-values are discussed in detail in Chapter 2. At near-ambient pressure, for dilute mixtures, some common expressions are

$$K_i = P_i^s/P \qquad \text{(Raoult's law)} \quad (6\text{-}17)$$

$$K_i = \gamma_{iL}^{\infty} P_i^s/P \qquad \text{(modified Raoult's law)} \quad (6\text{-}18)$$

$$K_i = H_i/P \qquad \text{(Henry's law)} \quad (6\text{-}19)$$

$$K_i = P_i^s/x_i^* P \qquad \text{(solubility)} \quad (6\text{-}20)$$

The first expression applies for ideal solutions involving solutes at subcritical temperatures. The second expression is useful for moderately nonideal solutions when activity coefficients are known at infinite dilution. For solutes at supercritical temperatures, the use of Henry's law may be preferable. For sparingly soluble solutes at subcritical temperatures, the fourth expression is preferred when solubility data in mole fractions, x_i^*, are available. This expression is derived by considering a three-phase system consisting of an ideal-vapor-containing solute, carrier vapor, and solvent; a pure or near-pure solute as liquid (1); and the solvent liquid (2) with dissolved solute. In that case, for solute, i, at equilibrium between the two liquid phases,

$$x_i^{(1)} \gamma_{iL}^{(1)} = x_i^{(2)} \gamma_{iL}^{(2)}$$

But,

$$x_i^{(1)} \approx 1, \quad \gamma_{iL}^{(1)} \approx 1, \quad x_i^{(2)} = x_i^*$$

Therefore,

$$\gamma_{iL}^{(2)} \approx 1/x_i^*$$

and from (6-18),

$$K_i^{(2)} = \gamma_{iL}^{(2)} P_i^s/P = P_i^s/(x_i^* P)$$

The advantage of (6-13) and (6-14) is that they can be solved directly for the percent absorption or stripping of a solute when the number of theoretical stages, N, and the absorption or stripping factor are known.

EXAMPLE 6.2

As discussed by Okoniewski [3], volatile organic compounds (VOCs) can be stripped from wastewater by air. Such compounds are to be stripped at 70°F and 15 psia from 500 gpm of wastewater with 3,400 scfm of air (standard conditions of 60°F and 1 atm) in an existing tower containing 20 plates. A chemical analysis of the wastewater shows three organic chemicals in the amounts shown in the following table. Included are necessary thermodynamic properties from the 1966 *Technical Data Book–Petroleum Refining* of the American Petroleum Institute. For all three organic compounds, the wastewater concentrations can be shown to be below the solubility values.

Organic Compound	Concentration in the Wastewater, mg/L	Solubility in Water at 70°F, mole fraction	Vapor Pressure at 70°F, psia
Benzene	150	0.00040	1.53
Toluene	50	0.00012	0.449
Ethylbenzene	20	0.000035	0.149

It is desirable that 99.9% of the total VOCs be stripped, but the plate efficiency of the tower is uncertain, with an estimated range of 5% to 20%, corresponding to one to four theoretical stages for the 20-plate tower. Calculate and plot the percent stripping of each of the three organic compounds for one, two, three, and four theoretical stages. Under what conditions can we expect to achieve the desired degree of stripping? What should be done with the exiting air?

SOLUTION

Because the wastewater is dilute in the VOCs, the Kremser equation may be applied independently to each of the three organic chemicals. We will ignore the absorption of air by the water and the stripping of water by the air. The stripping factor for each compound is given by $S_i = K_i V/L$, where V and L will be taken at entering conditions. The K-value may be computed from a modified Raoult's law, $K_i = \gamma_{iL} P_i^s/P$, where for a compound that is only slightly soluble, take $\gamma_{iL} = 1/x_i^*$, where x_i^* is the solubility in mole fraction. Thus, from (6-20), $K_i = P_i^s/x_i^* P$

$V = 3{,}400(60)/(379 \text{ scf/lbmol})$ or 538 lbmol/h

$L = 500(60)(8.33 \text{ lb/gal})/(18.02 \text{ lb/lbmol})$ or 13,870 lbmol/h

The corresponding K-values and stripping factors are

Component	K at 70°F, 15 psia	S
Benzene	255	9.89
Toluene	249	9.66
Ethylbenzene	284	11.02

From (6-14),

$$\text{Fraction stripped} = \frac{S^{N+1} - S}{S^{N+1} - 1}$$

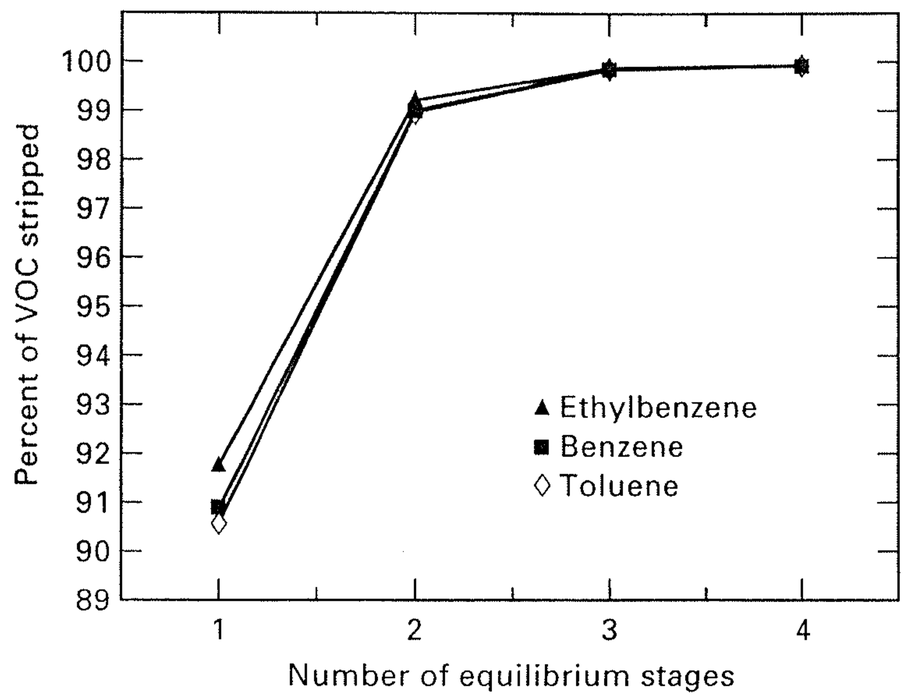

Figure 6.13 Results of Example 6.2 for stripping of VOCs from water with air.

The calculations when carried out with a spreadsheet computer program give the following results:

	Percent Stripped			
Component	1 Stage	2 Stages	3 Stages	4 Stages
Benzene	90.82	99.08	99.91	99.99
Toluene	90.62	99.04	99.90	99.99
Ethylbenzene	91.68	99.25	99.93	99.99

The results are quite sensitive to the number of theoretical stages as shown in Figure 6.13. To achieve 99.9% removal of the total VOCs, three theoretical stages are needed, corresponding to the necessity for a 15% stage efficiency in the existing 20-tray tower.

It is best to process the exiting air to remove or destroy the VOCs, particularly the benzene, which is a carcinogen [4]. The amount of benzene stripped is

$$(500 \text{ gpm})(60 \text{ min/h})(3.785 \text{ liters/gal})(150 \text{ mg/liters}) = 17{,}030{,}000 \text{ mg/h} \quad \text{or} \quad 37.5 \text{ lb/h}$$

If benzene is valued at \$0.30/lb, the annual value is approximately \$100,000. It is doubtful that this would justify a recovery technique, such as carbon adsorption. It is perhaps preferable to destroy the VOCs by incineration. For example, the air can be sent to a utility boiler, a waste-heat boiler, or a catalytic incinerator. It is also to be noted that the amount of air was arbitrarily given as 3,400 scfm. To complete the design procedure, various air rates should be investigated. It will also be necessary to verify by methods given later in this chapter that, at the chosen air flow rates, no flooding or weeping will occur in the column.

6.5 STAGE EFFICIENCY

Graphical and algebraic methods for determining stage requirements for absorption and stripping assume equilibrium with respect to both heat and mass transfer at each stage. Thus, the number of *equilibrium stages* (*theoretical stages, ideal stages,* or *ideal plates*) is determined or specified when using those methods. Except when temperature changes significantly from stage to stage, the assumption that vapor and liquid phases leaving a stage are at the same temperature is often reasonable. The assumption of equilibrium with respect to mass transfer, however, is not often reasonable and, for streams leaving a stage, vapor-phase mole fractions are not related to liquid-phase mole fractions simply by thermodynamic K-values. To determine the actual number of plates, the number of equilibrium stages must be adjusted with a *stage efficiency* (*plate efficiency* or *tray efficiency*).

Stage efficiency concepts are applicable to devices in which the phases are contacted and then separated, that is, when discrete stages can be identified. This is not the case for packed columns or continuous-contact devices. For these, the efficiency is imbedded into an equipment- and system-dependent parameter, an example of which is the HETP (height of packing equivalent to a theoretical plate).

The simplest approach for staged columns, in preliminary design studies and in the evaluation of the performance of an existing column, is to apply an overall stage (or column) efficiency, defined by Lewis [5] as

$$E_o = N_t / N_a \tag{6-21}$$

where E_o is the fractional overall stage efficiency, usually less than 1.0; N_t is the calculated number of equilibrium (theoretical) stages; and N_a is the actual number of contacting trays or plates (usually greater than N_t) required. Based on the results of extensive research conducted over a period of more than 60 years, the overall stage efficiency has been found to be a complex function of the

1. Geometry and design of the contacting trays
2. Flow rates and flow paths of vapor and liquid streams
3. Compositions and properties of vapor and liquid streams

For well-designed trays and for flow rates near the capacity limit, E_o depends mainly on the physical properties of the vapor and liquid streams.

Values of E_o can be predicted by any of the following four methods:

1. Comparison with performance data from industrial columns for the same or similar systems
2. Use of empirical efficiency models derived from data on industrial columns
3. Use of semitheoretical models based on mass- and heat-transfer rates
4. Scale-up from data obtained with laboratory or pilot-plant columns

These methods, which are discussed in some detail in the following four subsections, are applied to other vapor–liquid separation operations, such as distillation, as well as to absorption and stripping. Suggested correlations of mass-transfer coefficients for trayed towers are deferred to Section 6.6, following the discussion of tray capacity.

Table 6.4 Performance Data for Absorbers and Strippers in Hydrocarbon Service

Service	Type of Tray	Column Diameter, ft	No. of Trays	Tray Spacing, in.	Average Pressure, psia	Average Temp., °F	Molar Average Liquid Viscosity, cP	Overall Stage Efficiency, %
Absorption of butane	Bubble cap	4	24	18	260	120	0.48	36
Absorption of butane	Bubble cap	5	16	30	254	132	0.31	50
Absorption of butane	Bubble cap	4	16	24	94	117	1.41	10.4
Steam stripping of kerosene	Bubble cap	5	4	30	68	448	0.205	57
Steam stripping of gas oil	Bubble cap	5	6	30	60	507	0.250	49

Source: H.G. Drickamer and J.R. Bradford [6].

Performance Data

Performance data obtained from industrial absorption and stripping columns equipped with trays generally include gas- and liquid-feed and product flow rates and compositions, average column pressure and temperature or pressures and temperatures at the bottom and top of the column, number of actual trays, N_a, column diameter, and type of tray with, perhaps, some details of the tray design. From these data, particularly if the system is dilute with respect to the solute(s), the graphical or algebraic methods, described in Sections 6.3 and 6.4, respectively, can be used to estimate the number of equilibrium stages, N_t, required. Then (6-21) can be applied to determine the overall stage efficiency, E_o. Values of E_o for absorbers and strippers are typically low, often less than 50%.

Table 6.4 presents performance data, from a study by Drickamer and Bradford [6], for five industrial hydrocarbon absorption and stripping operations using columns with bubble-cap trays. For the three absorbers, the stage efficiencies are based on the absorption of *n*-butane as the key component. For the two strippers, both of which use steam as the stripping agent, the key component is not given, but is probably *n*-heptane. Although the data cover a wide range of average pressure and temperature, the overall stage efficiencies, which cover a wide range of 10.4% to 57%, appear to depend primarily on the molar average liquid viscosity, a key factor for the rate of mass transfer in the liquid phase.

The gas feed to a hydrocarbon absorber contains a range of light hydrocarbons, each of which is absorbed to a different extent based on its *K*-value, as illustrated in Example 5.3. The data of Jackson and Sherwood [7] for a 9-ft-diameter hydrocarbon absorber equipped with 19 bubble-cap trays on 30-in. tray spacing and operating at 92 psia and 60°F, as analyzed by O'Connell [8] and summarized in Table 6.5, show that each component being absorbed has a different overall stage efficiency, which appears to increase with decreasing *K*-value (increasing solubility in the liquid absorbent). For

Table 6.5 Effect of Species on Overall Stage Efficiency in a 9-ft-Diameter Industrial Absorber Using Bubble-Cap Trays

Component	Overall Stage Efficiency, %
Ethylene	10.3
Ethane	14.9
Propylene	25.5
Propane	26.8
Butylene	33.8

Source: H.E. O'Connell [8].

the same molar-average liquid viscosity (1.90 cps), the overall stage efficiency is seen to vary from as low as 10.3% for ethylene, the most-volatile species considered, to 33.8% for butylene (presumably *n*-butene), the least-volatile species considered.

An even more dramatic effect of the species solubility in the absorbent on the overall stage efficiency is seen in Table 6.6, from a study by Walter and Sherwood [9] using small laboratory, bubble-cap tray columns ranging in size from 2 to 18 in. in diameter. Stage efficiencies vary over a very wide range from 0.65% to 69%. Comparing the data for the water absorption of ammonia (a very soluble gas) and carbon dioxide (a slightly soluble gas), it is clear that the solubility of the gas (i.e., the *K*-value) has a large effect on stage efficiency. Thus, low stage efficiency can occur when the liquid viscosity is high and/or the gas solubility is low (high *K*-value); high stage efficiency can occur when the liquid viscosity is low and the gas solubility is high (low *K*-value).

Empirical Correlations

Using 20 sets of performance data from industrial hydrocarbon absorbers and strippers, including the data in Table 6.4, Drickamer and Bradford [6] correlated the overall stage efficiency of the key component absorbed or stripped with just

Table 6.6 Performance Data for Absorption in Laboratory Bubble-Cap Tray Columns

Service	Column Diameter, in.	No. of Trays	Tray Spacing, in.	Average Pressure, psia	Average Temp., °F	Overall Stage Efficiency, %
Absorption of ammonia in water	18	1	—	14.7	57	69
Absorption of isobutylene in heavy naphtha	2	1	—	66	78.8	36.4
Absorption of propylene in gas oil	2	1	—	66	118.4	13.1
Absorption of propylene in gas lube oil	2	1	—	66	105.8	4.7
Absorption of carbon dioxide in water	18	1	—	14.7	50.4	2.0
Desorption of carbon dioxide from 43.7 wt% aqueous glycerol	5	4	11	14.7	77	0.65

Source: J.F. Walter and T.K. Sherwood [9].

the molar-average viscosity of the rich oil (liquid leaving an absorber or liquid entering a stripper) at the average tower temperature over a viscosity range of 0.19 to 1.58 cP. The empirical equation,

$$E_o = 19.2 - 57.8 \log \mu_L, \quad 0.2 < \mu_L < 1.6 \text{ cP} \quad (6\text{-}22)$$

where E_o is in percent and μ is in centipoise, fits the data with average- and maximum-percent deviations of 10.3% and 41%, respectively. A plot of the Drickamer and Bradford correlation, compared to performance data, is given in Figure 6.14. Equation (6-22) should not be used for absorption into nonhydrocarbon liquids and is restricted to the listed range of the liquid viscosity data used to develop the correlation.

Mass-transfer theory indicates that when the volatility of species being absorbed or stripped covers a wide range, the relative importance of liquid-phase and gas-phase mass-transfer resistances can shift. Thus, O'Connell [8] found that the Drickamer-Bradford correlation, (6-22), was inadequate for absorbers and strippers when applied to species covering a wide range of volatility or K-values. This additional effect is indicated clearly in the performance data of Tables 6.5 and 6.6, where liquid viscosity alone cannot correlate the data. O'Connell obtained a more general correlation by using a parameter that included not only the liquid viscosity but also the liquid density and the Henry's law constant of the species being absorbed or stripped. Edmister [10] and Lockhart and Leggett [11] suggested slight modifications to the O'Connell correlation to permit its use with K-values (instead of Henry's-law constants). An O'Connell-type plot of overall stage efficiency for absorption or stripping in bubble-cap tray columns is given in Figure 6.15.

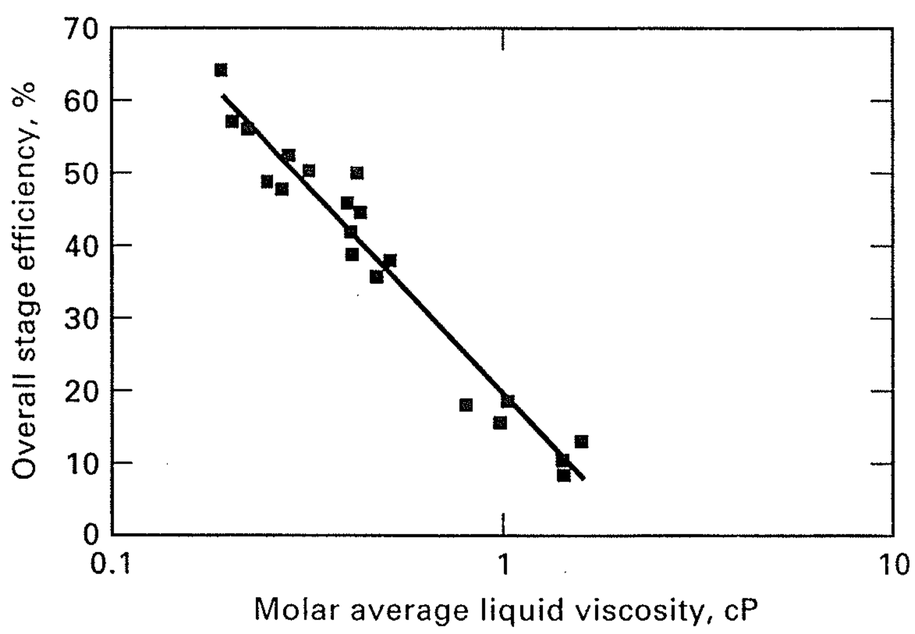

Figure 6.14 Drickamer and Bradford correlation for plate efficiency of hydrocarbon absorbers and strippers.

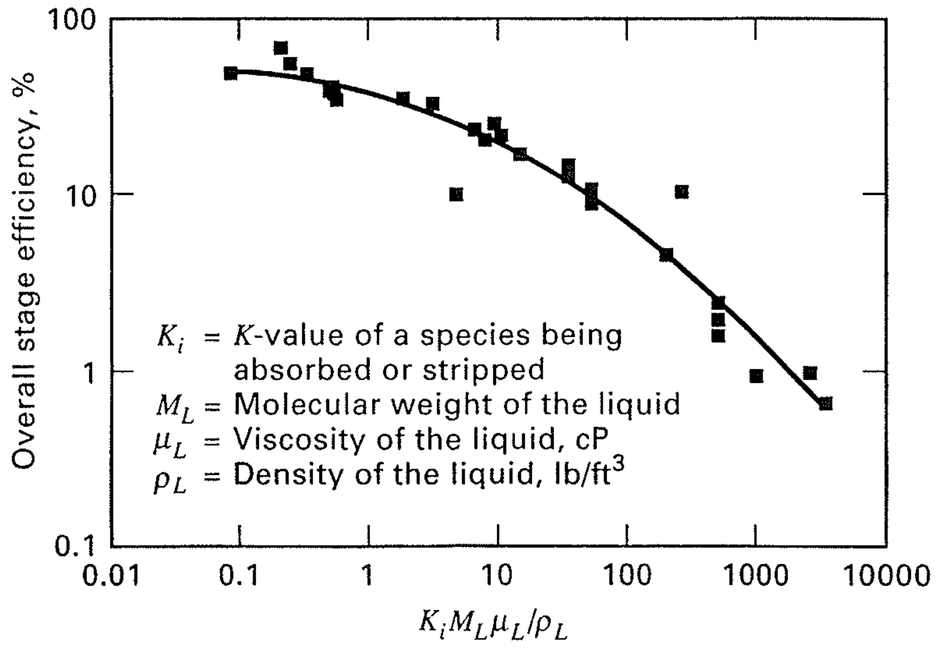

Figure 6.15 O'Connell correlation for plate efficiency of absorbers and strippers.

The correlating parameter, suggested by Edmister, is $K_i M_L \mu_L / \rho_L$, where:

K_i = K-value of species being absorbed or stripped
M_L = molecular weight of the liquid, lb/lbmol
μ_L = viscosity of the liquid, cP
ρ_L = density of the liquid, lb/ft^3

Thus, the correlating parameter has the units of cP-ft^3/lbmol. A reasonable fit to the 33 data points used by O'Connell is given by the empirical equation

$$\log E_o = 1.597 - 0.199 \log\left(\frac{K M_L \mu_L}{\rho_L}\right) - 0.0896\left[\log\left(\frac{K M_L \mu_L}{\rho_L}\right)\right]^2 \quad (6\text{-}23)$$

The average and maximum deviations of (6-23) for the 33 data points of Figure 6.15 are 16.3% and 157%, respectively. More than 50% of the data points, including points for the highest- and lowest-observed efficiencies, are predicted to within 10%.

The 33 data points in Figure 6.15 cover a wide range of conditions:

Column diameter:	2 in. to 9 ft
Average pressure:	14.7 to 485 psia
Average temperature:	60 to 138°F
Liquid viscosity:	0.22 to 21.5 cP
Overall stage efficiency:	0.65 to 69%

Absorbents include both hydrocarbons and water. For the absorption or stripping of more than one species, because of the effect of species K-value, different stage efficiencies are predicted, as observed from performance data of the type shown in Table 6.5. The inclusion of the K-value also permits the correlation to be used for aqueous systems where the solute may exhibit a very wide range of solubility (e.g., ammonia versus carbon dioxide) as included in Table 6.6. In using Figure 6.15 or Eq. (6-23), the K-value and absorbent properties are best evaluated at the end of the tower where the liquid phase is richest in solute(s). Prudent designs use the lowest predicted efficiency.

Most of the data used to develop the correlation of Figure 6.15 are for columns having a liquid flow path across the active tray area of from 2 to 3 ft. Theory and experimental data show that higher efficiencies are achieved for longer flow paths. For short liquid flow paths, the liquid flowing across the tray is usually completely mixed. For longer flow paths, the equivalent of two or more completely mixed, successive liquid zones may be present. The result is a greater average driving force for mass transfer and, thus, a higher efficiency—perhaps greater than 100%. For example, a column with a 10-ft liquid flow path may have an efficiency as much as 25% greater than that predicted by (6-23). However, at high liquid rates, long liquid-path lengths are

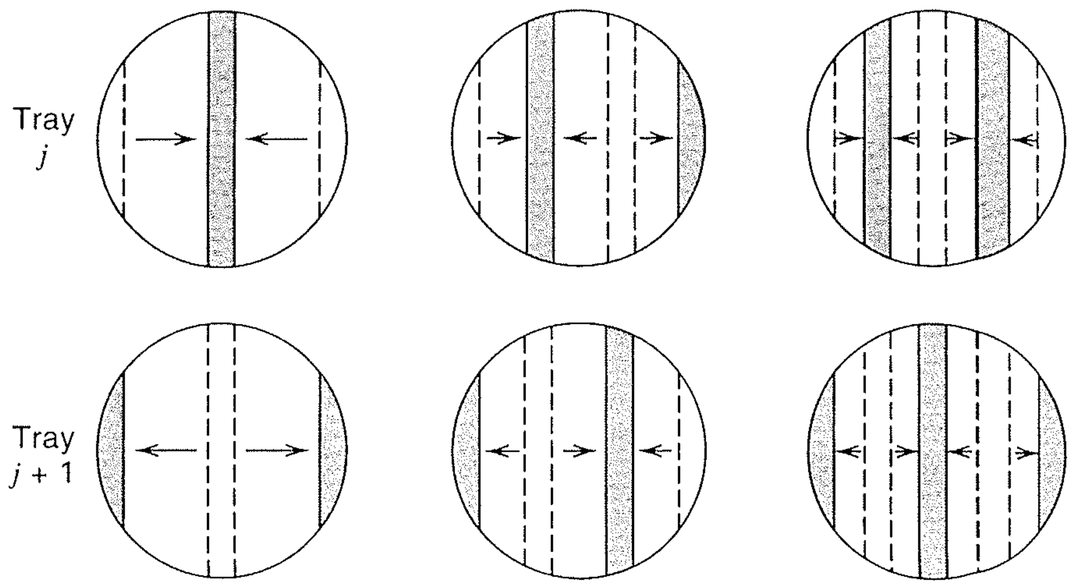

(a)

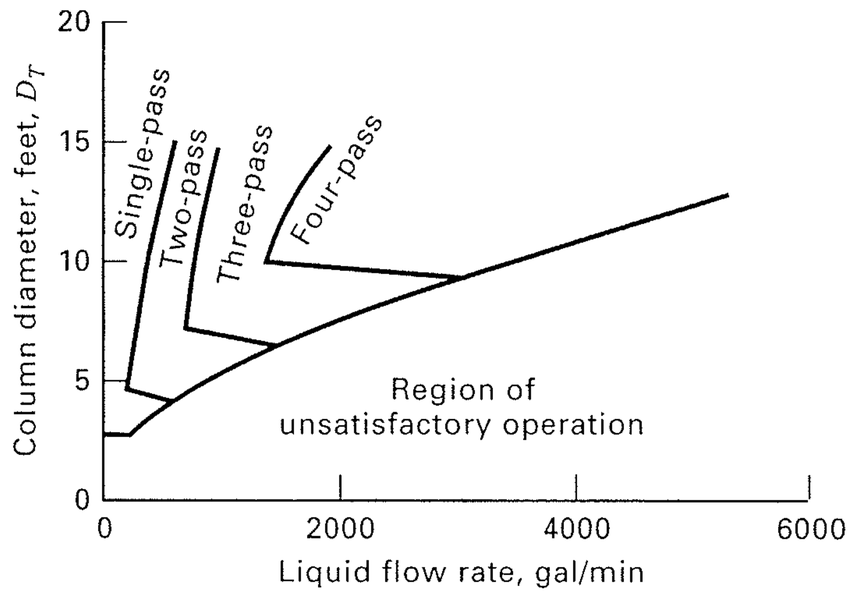

(b)

Figure 6.16 Estimation of number of required liquid flow passes. (a) Multipass trays: (1) two-pass; (2) three-pass; (3) four-pass. (b) Flow pass selection.
(Derived from *Koch Flexitray Design Manual, Bulletin 960*, Koch Engineering Co., Inc., Wichita, KA, 1960.)

undesirable because they lead to excessive hydraulic gradients. When the effective height of a liquid on a tray is appreciably higher on the inflow side than at the overflow weir, vapor may prefer to enter the tray in the latter region, leading to nonuniform bubbling action. Multipass trays, as shown in Figure 6.16a, are used to prevent excessive liquid gradients. Estimation of the desired number of flow paths can be made with Figure 6.16b, where, e.g., a 10-foot-diameter column with a liquid flow rate of 1000 gpm should use a three-pass tray.

Based on estimates of the number of actual trays and tray spacing, the height of a column between the top tray and the bottom tray is computed. By adding another 4 ft above the top tray for removal of entrained liquid and 10 ft below the bottom tray for bottoms surge capacity, the total column height is estimated. If the height is greater than 212 ft (equivalent to 100 trays on 24-in. spacing), two or more columns arranged in series may be preferable to a single column. Perhaps the tallest column in the world, located at the Shell Chemical Company complex in Deer Park, Texas, stands 338 ft tall [*Chem. Eng.*, **84** (26), 84 (1977)].

EXAMPLE 6.3

Performance data, given below, for a bubble-cap tray absorber located in a Texas petroleum refinery, were reported by Drickamer and Bradford [6]. Based on these data, back-calculate the overall stage efficiency for *n*-butane and compare the result with both the Drickamer–Bradford and O'Connell correlations. Lean oil and rich gas enter the tower; rich oil and lean gas leave the tower.

Performance Data

Number of plates	16
Plate spacing, in.	24
Tower diameter, ft	4
Tower pressure, psig	79
Lean oil temperature, °F	102
Rich oil temperature, °F	126
Rich gas temperature, °F	108
Lean gas temperature, °F	108
Lean oil rate, lbmol/h	368
Rich oil rate, lbmol/h	525.4
Rich gas rate, lbmol/h	946
Lean gas rate, lbmol/h	786.9
Lean oil molecular weight	250
Lean oil viscosity at 116°F, cP	1.4
Lean oil gravity, °API	21

Stream Compositions, Mol%

Component	Rich Gas	Lean Gas	Rich Oil	Lean Oil
C_1	47.30	55.90	1.33	
C_2	8.80	9.80	1.16	
$C_3^=$	5.20	5.14	1.66	
C_3	22.60	21.65	8.19	
$C_4^=$	3.80	2.34	3.33	
nC_4	7.40	4.45	6.66	
nC_5	3.00	0.72	4.01	
nC_6	1.90		3.42	
Oil absorbent			70.24	100
Totals	100.00	100.00	100.00	100

SOLUTION

Before computing the overall stage efficiency for *n*-butane, it is worthwhile to check the consistency of the plant data by examining the overall material balance and the material balance for each component. From the above stream compositions, it is apparent that the compositions have been normalized to total 100%.

The overall material balance is

$$\text{Total flow into tower} = 368 + 946 = 1{,}314 \text{ lbmol/h}$$

$$\text{Total flow from tower} = 525.4 + 786.9 = 1{,}312.3 \text{ lbmol/h}$$

These two totals agree to within 0.13%. This is excellent agreement.

The component material balance for the oil absorbent is

$$\text{Total oil in} = 368 \text{ lbmol/h}$$

$$\text{Total oil out} = (0.7024)(525.4) = 369 \text{ lbmol/h}$$

These two totals agree to within 0.3%. Again, this is excellent agreement.

Component material balances for other hydrocarbons from spreadsheet calculations are as follows.

	lbmol/h			
Component	**Lean Gas**	**Rich Oil**	**Total Out**	**Total In**
C_1	439.9	7.0	446.9	447.5
C_2	77.1	6.1	83.2	83.2
$C_3^=$	40.4	8.7	49.1	49.2
C_3	170.4	43.0	213.4	213.8
$C_4^=$	18.4	17.5	35.9	35.9
nC_4	35.0	35.0	70.0	70.0
nC_5	5.7	21.1	26.8	28.4
nC_6	0.0	18.0	18.0	18.0
	786.9	156.4	943.3	946.0

Again, we see excellent agreement. The largest difference is 6% for pentanes. Plant data are not always so consistent.

For the back-calculation of stage efficiency from the performance data, the Kremser equation is applied to compute the number of equilibrium stages required for the measured absorption of *n*-butane.

$$\text{Fraction of } nC_4 \text{ absorbed} = \frac{35}{70} = 0.50$$

From (6-13), $$0.50 = \frac{A^{N+1} - A}{A^{N+1} - 1}$$

where A = absorption factor $= \dfrac{L}{KV}$

Because L and V vary greatly through the column, let

$$L = \text{average liquid rate} = \frac{368 + 525.4}{2} = 446.7 \text{ lbmol/h}$$

and let

$$V = \text{average vapor rate} = \frac{946 + 786.9}{2} = 866.5 \text{ lbmol/h}$$

Assume average tower temperature = the average of inlet and outlet temperatures = (102 + 126 + 108 + 108)/4 = 111°F. Also assume that the viscosity of the lean oil at 116°F equals the viscosity of the rich oil at 111°F. Therefore, $\mu = 1.4$ cP.

Assume the ambient pressure is 14.7 psia. Then

$$\text{Tower pressure} = 79 + 14.7 = 93.7 \text{ psia}$$

From Figure 2.8, at 93.7 psia and 111°F, $K_{nC_4} = 0.7$. Thus,

$$A = \frac{446.7}{(0.7)(866.5)} = 0.736$$

Therefore, $$0.50 = \frac{0.736^{N+1} - 0.736}{0.736^{N+1} - 1}$$

Solving, $$N = N_t = 1.45$$

From the performance data, $N_a = 16$

From (6-21), $$E_o = \frac{1.45}{16} = 0.091 \quad \text{or} \quad 9.1\%$$

Equation (6-22) is applicable to *n*-butane, because that component is absorbed to the extent of about 50% and thus can be considered one of the key components. Other possible key components are butenes and *n*-pentane.

From (6-22), $$E_o = 19.2 - 57.8 \log(1.4) = 10.8\%$$

To estimate the stage efficiency from the O'Connell correlation, use the following properties for the rich oil at 126°F, 93.7 psia, and 30 mol% light hydrocarbons/70 mol% of 250-MW oil, as obtained from a simulation program.

$$K = 0.77 \text{ for } n\text{-butane}$$
$$M_L = 195$$
$$\mu_L = 0.9 \text{ cP}$$
$$\rho_L = 44.1 \text{ lb/ft}^3$$

Therefore, $$\frac{K M_L \mu_L}{\rho_L} = \frac{0.77(195)(0.9)}{(44.1)} = 3.1$$

From (6-23),

$$\log E_o = 1.597 - 0.199 \log(3.1) - 0.0896[\log(3.1)]^2 = 1.48$$
$$E_o = 10^{1.48} = 30.2$$

For this hydrocarbon absorber, the Drickamer and Bradford correlation (10.8%) gives better agreement than the O'Connell correlation (30.2%) with the plant performance data (9.1%).

Semitheoretical Models

A third method for predicting the overall stage efficiency involves the application of a semitheoretical tray model based on mass- and heat-transfer rates. With this model, the fractional approach to equilibrium, called the *plate* or *tray efficiency,* is estimated for each component in the mixture for each tray in the column. These efficiency values are then utilized to determine conditions for each tray, or averaged for the column to obtain the overall plate efficiency.

Tray efficiency models, in order of increasing complexity, have been proposed by Holland [12], Murphree [13], Hausen [14], and Standart [15]. All four models are based on the assumption that vapor and liquid streams entering each tray are of uniform compositions. The *Murphree vapor efficiency,* which is the oldest and most widely used, is derived with the additional assumptions of (1) complete mixing of the liquid flowing across the tray such that the liquid is of a uniform concentration, equal to the composition of the liquid leaving the tray and entering the next tray below, and (2) plug flow of the vapor passing up through the liquid, as indicated in Figure 6.17 for tray n. Considering species i, let

n = rate of mass transfer for absorption from the gas to the liquid

K_G = overall gas mass-transfer coefficient based on a partial-pressure driving force

a = vapor–liquid interfacial area per volume of combined gas and liquid holdup (froth or dispersion) on the tray,

A_b = active bubbling area of the tray (total cross-sectional area minus liquid down-comer areas)

Z_f = height of combined gas and liquid holdup on the tray

P = total absolute pressure

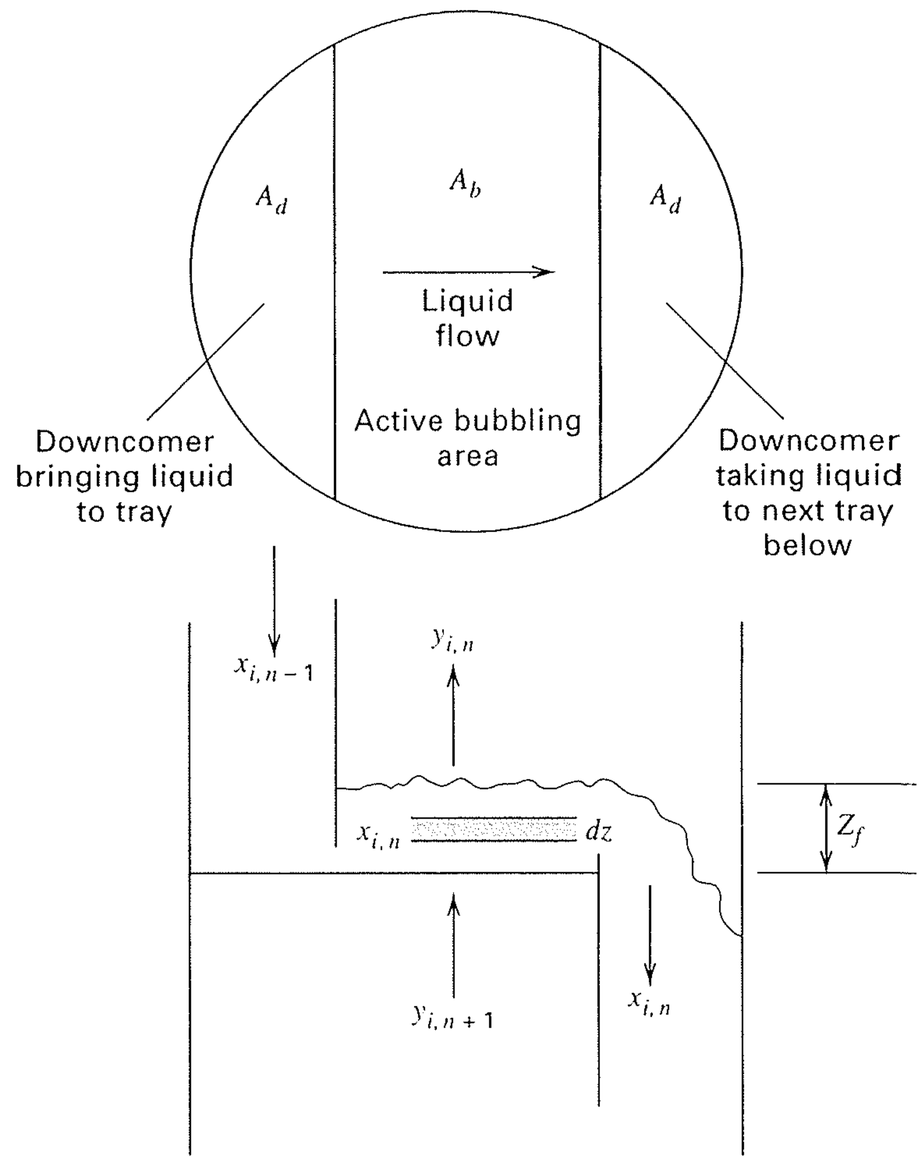

Figure 6.17 Schematic top and side views of tray for derivation of Murphree vapor-tray efficiency.

y_i = mole fraction of i in the vapor rising up through the liquid

y_i^* = vapor mole fraction of i in equilibrium with the completely mixed liquid on the tray

Then the differential rate of mass transfer for a differential height of holdup on tray n, numbered down from the top, is

$$dn_i = K_G a (y_i - y_i^*) P A_b \, dZ \qquad (6\text{-}24)$$

where K_G takes into account both gas- and liquid-phase resistances to mass transfer. By material balance, assuming a negligible change in V across the stage,

$$dn_i = -V \, dy_i \qquad (6\text{-}25)$$

where V = molar gas flow rate up through the liquid on the tray.

Combining (6-24) and (6-25) to eliminate dn_i, separating variables, and converting to integral form,

$$A_b \int_0^{Z_f} \frac{K_G a P}{V} dZ = \int_{y_{i,n+1}}^{y_{i,n}} \frac{dy_i}{y_{i,n}^* - y_i} = N_{OG} \qquad (6\text{-}26)$$

where a second subscript involving the tray number, n, has been added to the mole fraction of the vapor phase. The vapor enters tray n at $y_{i,n+1}$ and exits at $y_{i,n}$. This equation defines

N_{OG} = number of overall gas-phase mass-transfer units

Values of K_G, a, P, and V may vary somewhat as the gas flows up through the liquid on the tray, but if they as well as

y_i^* are taken to be constant, (6-26) can be integrated to give

$$N_{OG} = \frac{K_G a P Z_f}{(V/A_b)} = \ln\left(\frac{y_{i,n+1} - y_{i,n}^*}{y_{i,n} - y_{i,n}^*}\right) \qquad (6\text{-}27)$$

A rearrangement of (6-27) in terms of the fractional approach of y_i to equilibrium defines the Murphree vapor efficiency as

$$E_{MV} = \frac{y_{i,n+1} - y_{i,n}}{y_{i,n+1} - y_{i,n}^*} = 1 - e^{-N_{OG}} \qquad (6\text{-}28)$$

or

$$N_{OG} = -\ln(1 - E_{MV}) \qquad (6\text{-}29)$$

Suppose that measurements give

$$y_i \text{ entering tray } n = y_{i,n+1} = 0.64$$

$$y_i \text{ leaving tray } n = y_{i,n} = 0.61$$

and, from thermodynamics or phase equilibrium data, y_i^* in equilibrium with x_i on and leaving tray $n = 0.60$.

Then, from (6-28),

$$E_{MV} = (0.64 - 0.61)/(0.64 - 0.60) = 0.75$$

or a 75% approach to equilibrium. From (6-29),

$$N_{OG} = -\ln(1 - 0.75) = 1.386$$

When $N_{OG} = 1$, $E_{MV} = 1 - e^{-1} = 0.632$.

The derivation of the Murphree vapor efficiency does not consider the exiting stream temperatures. However, it is implied that the completely mixed liquid phase is at its bubble-point temperature so that the equilibrium vapor phase mole fraction, $y_{i,n}^*$, can be computed.

For multicomponent mixtures, values of E_{MV} are component-dependent and can vary from tray to tray; but at each tray it can be shown that the number of independent values of E_{MV} is one less than the number of components. The dependent value of E_{MV} is determined by forcing $\sum y_i = 1$. It is thus possible that a negative value of E_{MV} can result for a component in a multicomponent mixture. Such negative efficiencies are possible because of mass-transfer coupling among concentration gradients in a multicomponent mixture, which is discussed in Chapter 12. However, for a binary mixture, values of E_{MV} are always positive and identical for the two components.

Only if liquid travel distance across a tray is small will the liquid on a tray approach the complete-mixing assumption used to derive (6-27). To handle the more general case of incomplete liquid mixing, a *Murphree vapor-point efficiency* is defined by assuming that liquid composition varies with distance of travel across a tray, but is uniform in the vertical direction. Thus, for species i on tray n, at any horizontal distance from the downcomer that directs liquid onto tray n, as shown in Figure 6.18,

$$E_{OV} = \frac{y_{i,n+1} - y_i}{y_{i,n+1} - y_i^*} \qquad (6\text{-}30)$$

Because x_i varies across a tray, y_i^* and y_i also vary. However, the exiting vapor is then assumed to mix completely to give a uniform $y_{i,n}$ before entering the tray above. Because E_{OV} is

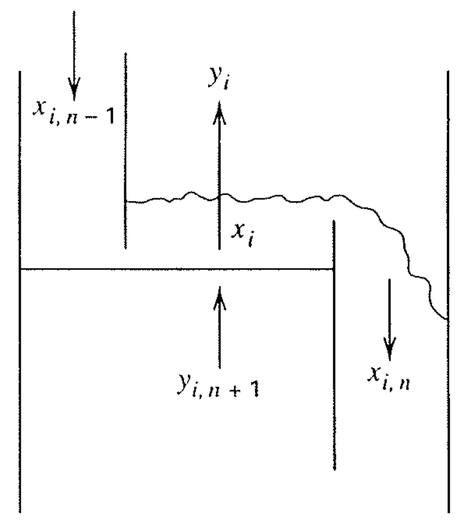

Figure 6.18 Schematic of tray for Murphree vapor-point efficiency.

a more fundamental quantity than E_{MV}, E_{OV} serves as the basis for semitheoretical estimates of tray efficiency and overall column efficiency.

Lewis [16] integrated E_{OV} over a tray for several cases. For complete mixing of liquid on a tray to give a uniform composition, $x_{i,n}$, it is obvious that

$$E_{OV} = E_{MV} \qquad (6\text{-}31)$$

For plug flow of liquid across a tray with no longitudinal diffusion (no mixing of liquid in the horizontal direction), Lewis derived

$$E_{MV} = \frac{1}{\lambda}(e^{\lambda E_{OV}} - 1) \qquad (6\text{-}32)$$

with

$$\lambda = mV/L \qquad (6\text{-}33)$$

where V and L are gas and liquid molar flow rates, respectively, and $m = dy/dx$ = slope of the equilibrium line for a species, using the expression $y = mx + b$. If b is taken as zero, then m is the K-value, and for the key component, k, being absorbed,

$$\lambda = K_k V/L = 1/A_k$$

If A_k, the key-component absorption factor, is given the typical value of 1.4, $\lambda = 0.71$. Suppose the measured or predicted point efficiency is $E_{OV} = 0.25$. From (6-32),

$$E_{MV} = 1.4(e^{0.71(0.25)} - 1) = 0.27$$

which is only 9% higher than E_{OV}. However, if $E_{OV} = 0.9$, E_{MV} is 1.25, which is significantly higher and equivalent to more than a theoretical stage. This surprising result is due to the concentration gradient in the liquid across the length of travel on the tray, which allows the vapor to contact a liquid having an average concentration of species k that can be appreciably lower than that in the liquid leaving the tray.

Equations (6-31) and (6-32) represent extremes between complete mixing and no mixing of the liquid phase, respectively. A more realistic, but considerably more complex model that accounts for partial liquid mixing on the tray, as developed by Gerster et al. [17], is

$$\frac{E_{MV}}{E_{OV}} = \frac{1 - e^{-(\eta + N_{Pe})}}{(\eta + N_{Pe})\{1 + [(\eta + N_{Pe})/\eta]\}} + \frac{e^{\eta} - 1}{\eta\{1 + [\eta/(\eta + N_{Pe})]\}} \qquad (6\text{-}34)$$

where

$$\eta = \frac{N_{\text{Pe}}}{2}\left[\left(1 + \frac{4\lambda E_{OV}}{N_{\text{Pe}}}\right)^{1/2} - 1\right] \tag{6-35}$$

The dimensionless Peclet number, N_{Pe}, which serves as a partial-mixing parameter, is defined by

$$N_{\text{Pe}} = Z_L^2/D_E\theta_L = Z_L u/D_E \tag{6-36}$$

where Z_L is the length of liquid flow path across the tray as shown in Figure 6.3, D_E is the eddy diffusion coefficient in the direction of liquid flow, θ_L is the average liquid residence time on the tray, and $u = Z_L/\theta_L$ is the mean liquid velocity across the tray. Equation (6-34) is plotted in Figure 6.19 for wide ranges of N_{Pe} and λE_{OV}. When $N_{\text{Pe}} = 0$, (6-31) holds; when $N_{\text{Pe}} = \infty$, (6-32) holds.

From (6-36), the Peclet number can be viewed as the ratio of the mean liquid bulk velocity to the eddy-diffusion velocity. When N_{Pe} is small, eddy diffusion is important and the liquid approaches a well-mixed condition. When N_{Pe} is large, bulk flow predominates and the liquid approaches plug flow. Experimental measurements of D_E in bubble-cap and sieve-plate columns [18–21] cover a range of 0.02 to 0.20 ft^2/s. Values of u/D_E typically range from 3 to 15 ft^{-1}. Based on the second form of (6-36), N_{Pe} increases directly with increasing Z_L and, therefore, column diameter. A typical value of N_{Pe} for a 2-ft-diameter column is 10; for a 6-ft-diameter column, N_{Pe} might be 30. For N_{Pe} values of this magnitude, Figure 6.19 shows that values of E_{MV} can be significantly larger than E_{OV} for large values of λ.

Lewis [16] showed that when the equilibrium and operating lines are straight, but not necessarily parallel, the overall stage efficiency, defined by (6-21), is related to the Murphree vapor efficiency by

$$E_o = \frac{\log[1 + E_{MV}(\lambda - 1)]}{\log \lambda} \tag{6-37}$$

When the two lines are not only straight but parallel, such that $\lambda = 1$, (6-37) becomes $E_o = E_{MV}$. Also, when $E_{MV} = 1$, then $E_o = 1$ regardless of the value of λ.

Scale-up from Laboratory Data

When vapor–liquid equilibrium data for a system are unavailable or not well known, and particularly if the system forms a highly nonideal liquid solution with possible formation of azeotropes, tray requirements are best estimated, and the feasibility of achieving the desired degree of separation verified, by conducting laboratory tests. A particularly useful apparatus is a small glass or metal sieve-plate column with center-to-side downcomers developed by Oldershaw [22]

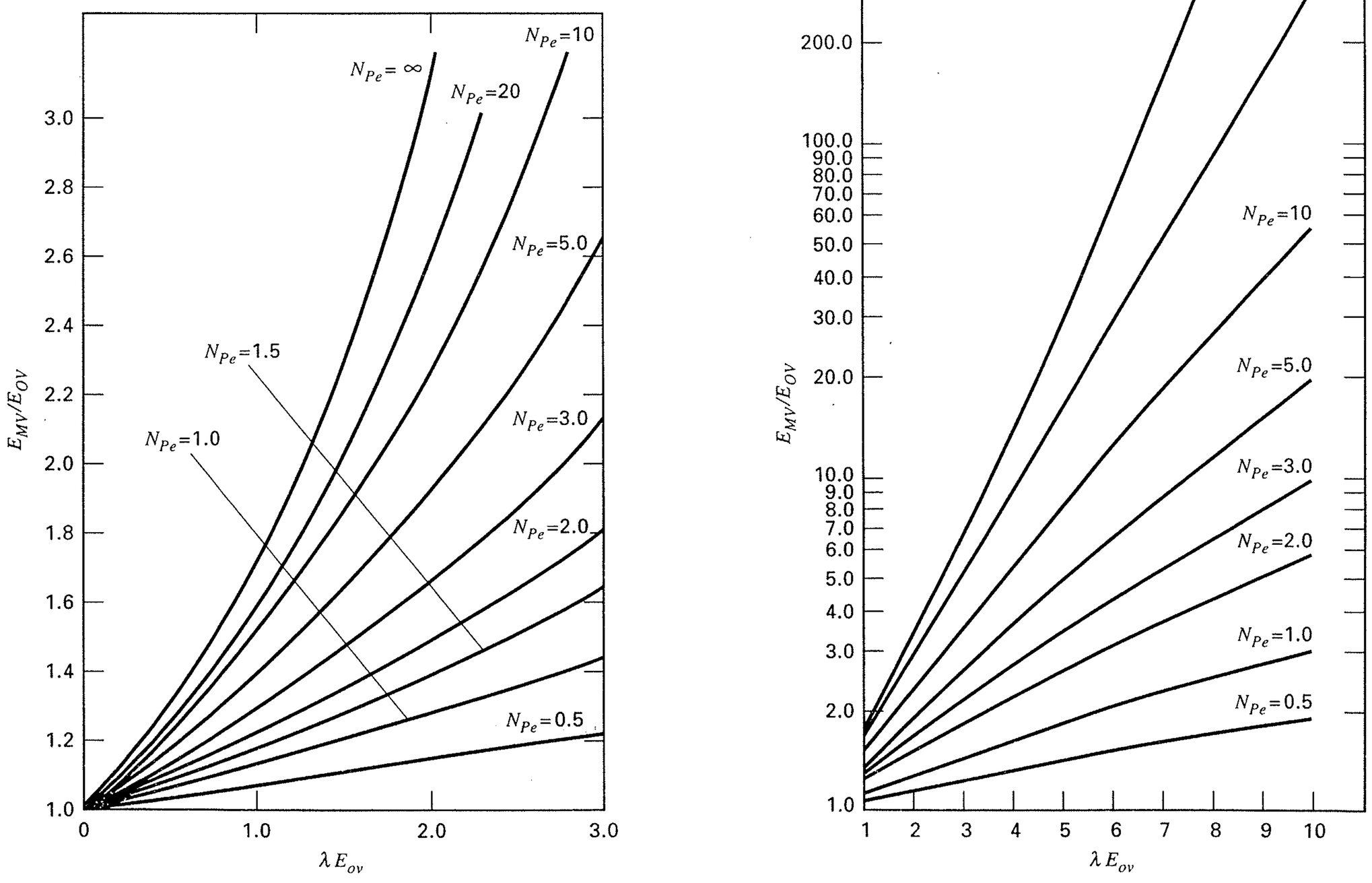

Figure 6.19 Effect of longitudinal mixing on Murphree vapor tray efficiency.

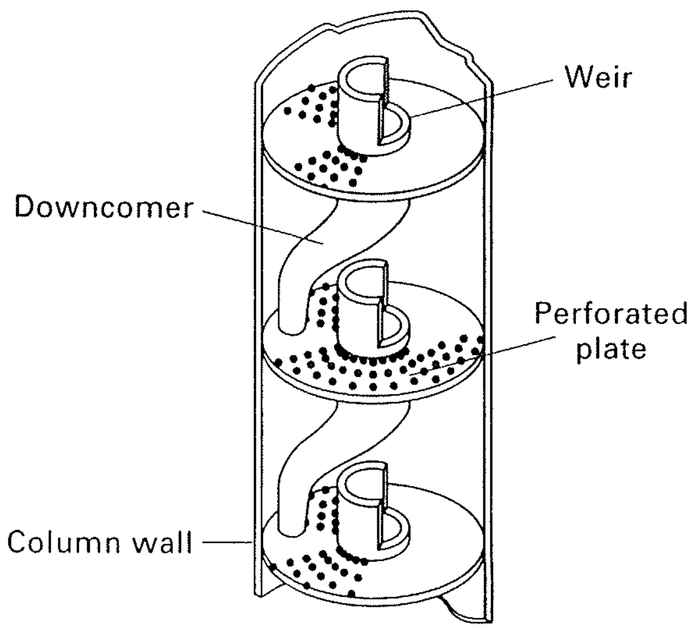

Figure 6.20 Oldershaw column.

and shown schematically in Figure 6.20. Oldershaw columns are typically 1 to 2 in. in diameter and can be assembled with almost any number of sieve plates, usually containing 0.035- to 0.043-in. holes with a hole area of approximately 10%. A detailed study by Fair, Null, and Bolles [23] showed that overall plate efficiencies of Oldershaw columns operated over a pressure range of 3 to 165 psia are in conservative agreement with distillation data obtained from sieve-tray, pilot-plant and industrial-size columns ranging in size from 18 in. to 4 ft in diameter when operated in the range of 40% to 90% of flooding. It may be assumed that similar agreement might be realized for absorption and stripping.

It is believed that the small-diameter Oldershaw column achieves essentially complete mixing of liquid on each tray, thus permitting the measurement of a point efficiency. As discussed above, somewhat larger efficiencies may be observed in much-larger-diameter columns due to incomplete liquid mixing, which results in a higher Murphree tray efficiency and, therefore, higher overall plate efficiency.

Fair et al. [23] recommend the following conservative scale-up procedure for the Oldershaw column:

1. Determine the flooding point.
2. Establish operation at about 60% of flooding (but 40 to 90% seems acceptable).
3. Run the system to find a combination of plates and flow rates that gives the desired degree of separation.
4. Assume that the commercial column will require the same number of plates for the same ratio of liquid to vapor molar flow rates.

If reliable vapor–liquid equilibrium data are available, they can be used with the Oldershaw data to determine the overall column efficiency, E_o. Then (6-37) and (6-34) can be used to estimate the average point efficiency. For the commercial-size column, the Murphree vapor efficiency can be determined from the Oldershaw column point efficiency using (6-34), which takes into account incomplete liquid mixing. In general, the tray efficiency of the commercial column, depending on the length of the liquid flow path, will be higher than for the Oldershaw column at the same percentage of flooding.

EXAMPLE 6.4

Assume that the column diameter for the absorption operation of Example 6.1 is 3 ft. If the overall stage efficiency, E_o, is 30% for the absorption of ethyl alcohol, estimate the average Murphree vapor efficiency, E_{MV}, and the possible range of the Murphree vapor-point efficiency, E_{OV}.

SOLUTION

For Example 6.1, the system is dilute in ethyl alcohol, the main component undergoing mass transfer. Therefore, the equilibrium and operating lines are essentially straight, and (6-37) can be applied. From the data of Example 6.1, $\lambda = KV/L = 0.57(180)/151.5 = 0.68$.

Solving (6-37) for E_{MV}, using $E_o = 0.30$,

$$E_{MV} = (\lambda^{E_o} - 1)/(\lambda - 1) = (0.68^{0.30} - 1)/(0.68 - 1) = 0.34$$

For a 3-ft-diameter column, the degree of liquid mixing probably lies intermediate between complete mixing and plug flow. From (6-31) for the former case, $E_{OV} = E_{MV} = 0.34$. From a rearrangement of (6-32) for the latter case, $E_{OV} = \ln(1 + \lambda E_{MV})/\lambda = \ln[1 + 0.68(0.34)]/0.68 = 0.31$. Therefore, E_{OV} lies in the range of 31% to 34%, probably closer to 34% for complete mixing. However, the differences between E_o, E_{MV}, and E_{OV} for this example are almost negligible.

6.6 TRAY DIAMETER, PRESSURE DROP, AND MASS TRANSFER

In the trayed tower shown in Figure 6.21, vapor flows vertically upward, contacting liquid in crossflow on each tray. When trays are designed properly, a stable operation is achieved wherein (1) vapor flows only through the perforations or open regions of the tray between the downcomers, (2) liquid flows from tray to tray only by means of the downcomers, (3) liquid neither weeps through the tray perforations nor is carried by the vapor as entrainment to the tray above, and (4) vapor is neither carried (occluded) down by the liquid in the downcomer to the tray below nor allowed to bubble up through the liquid in the downcomer. Tray design includes the determination of tray diameter and the division of the tray cross-sectional area, A, as shown in Figure 6.21, into active vapor bubbling area, A_a, and liquid downcomer area, A_d. With the tray diameter fixed, vapor pressure drop and mass-transfer coefficients can be estimated.

Tray Diameter

For a given liquid flow rate, as shown in Figure 6.22 for a sieve-tray column, a maximum vapor flow rate exists beyond which incipient column flooding occurs because of backup of liquid in the downcomer. This condition, if sustained, leads to carryout of liquid with the overhead vapor leaving the column. *Downcomer flooding* takes place when, in the absence of entrainment, liquid backup is caused by downcomers of inadequate cross-sectional area, A_d, to carry

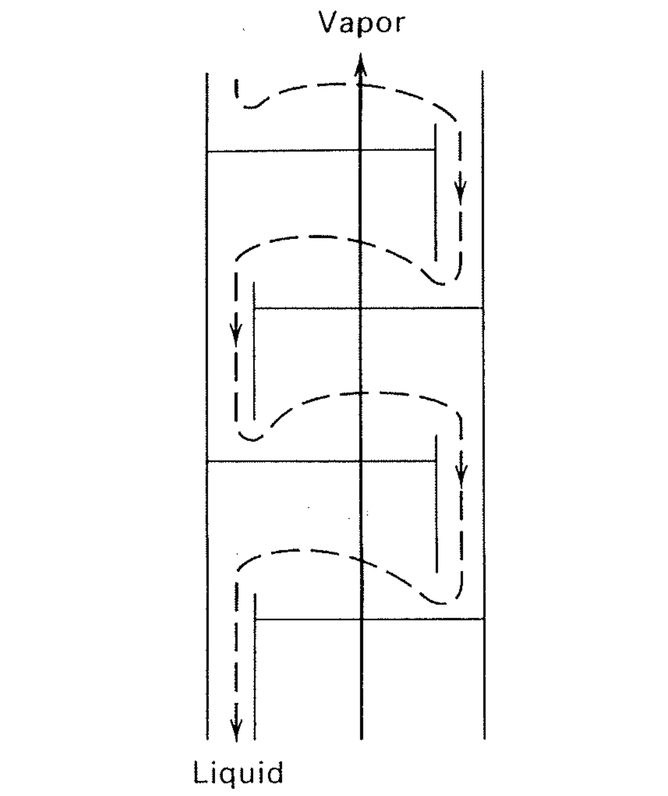

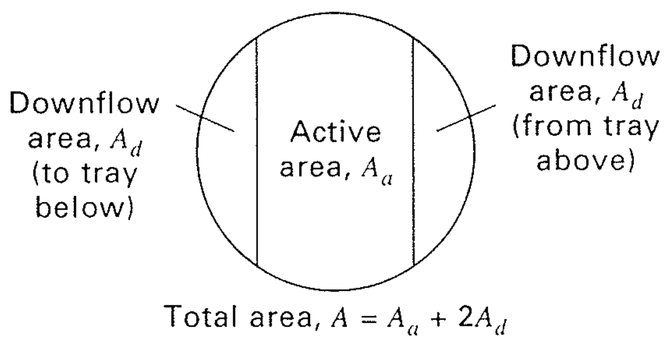

Figure 6.21 Vapor and liquid flow through a trayed tower.

the liquid flow. It rarely occurs if downcomer cross-sectional area is at least 10% of total column cross-sectional area and if tray spacing is at least 24 in. The usual design limit is *entrainment flooding,* which is caused by excessive carry-up of liquid, at the rate e, by vapor entrainment to the tray above. At incipient flooding, $(e + L) \gg L$ and downcomer cross-sectional area is inadequate for the excessive liquid load $(e + L)$. Tray diameter is determined as follows to avoid entrainment flooding.

Entrainment of liquid is due to carry-up of suspended droplets by rising vapor or to throw-up of liquid particles by vapor jets formed at tray perforations, valves, or bubble-cap slots. Souders and Brown [24] successfully correlated

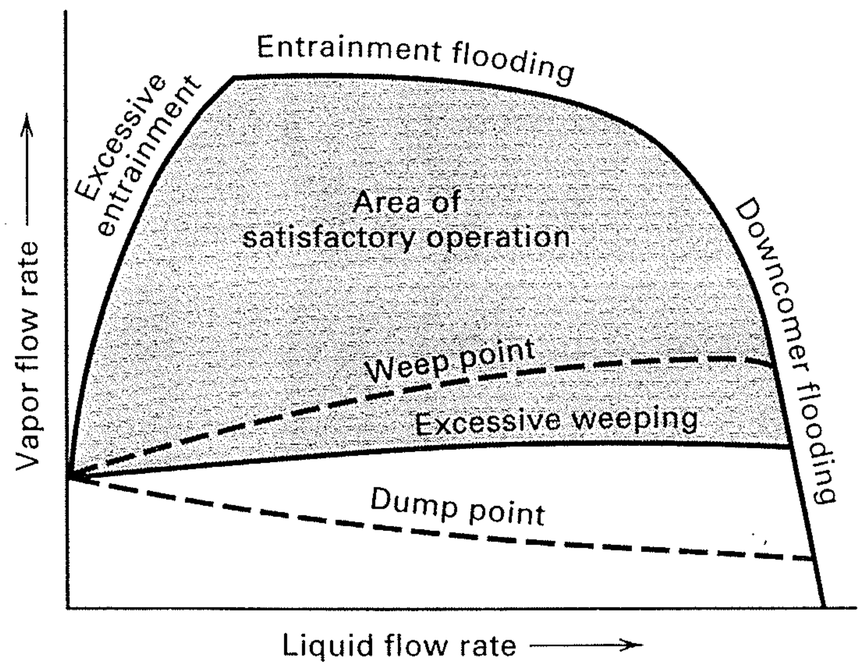

Figure 6.22 Limits of stable operation in a trayed tower.
[Reproduced by permission from H.Z. Kister, *Distillation Design,* McGraw-Hill, New York (1992).]

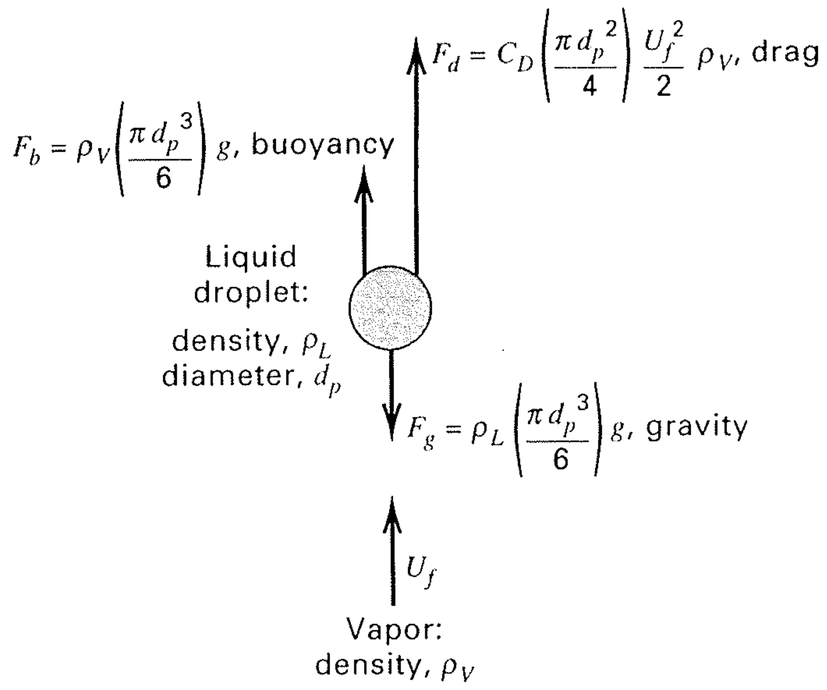

Figure 6.23 Forces acting on a suspended liquid droplet.

entrainment flooding data for 10 commercial trayed columns by assuming that carry-up of suspended droplets controls entrainment. At low vapor velocity, a droplet settles out; at high vapor velocity, it is entrained. At flooding or incipient entrainment velocity, U_f, the droplet is suspended such that the vector sum of the gravitational, buoyant, and drag forces acting on the droplet, as shown in Figure 6.23, are zero. Thus,

$$\sum F = 0 = F_g - F_b - F_d \tag{6-38}$$

In terms of droplet diameter, d_p, terms on the right-hand side of (16-38) become, respectively,

$$\rho_L\left(\frac{\pi d_p^3}{6}\right)g - \rho_V\left(\frac{\pi d_p^3}{6}\right)g - C_D\left(\frac{\pi d_p^2}{4}\right)\frac{U_f^2}{2}\rho_V = 0 \tag{6-39}$$

where C_D is the drag coefficient. Solving for flooding velocity,

$$U_f = C\left(\frac{\rho_L - \rho_V}{\rho_V}\right)^{1/2} \tag{6-40}$$

where C = capacity parameter of Souders and Brown. According to the above theory,

$$C = \left(\frac{4d_p g}{3C_D}\right)^{1/2} \tag{6-41}$$

Parameter C can be calculated from (6-41) if the droplet diameter d_p is known. In practice, however, d_p is distributed over a wide range and C is treated as an empirical parameter determined using experimental data obtained from operating equipment. Souders and Brown considered all the important variables that could influence the value of C and obtained a correlation for commercial-size columns with bubble-cap trays. Data covered column pressures from 10 mmHg to 465 psia, plate spacings from 12 to 30 in., and liquid surface tensions from 9 to 60 dyne/cm. In accordance with (6-41), the value of C increases with increasing surface tension, which increases d_p. Also, C increases with increasing tray spacing, since this allows more time for agglomeration to a larger d_p.

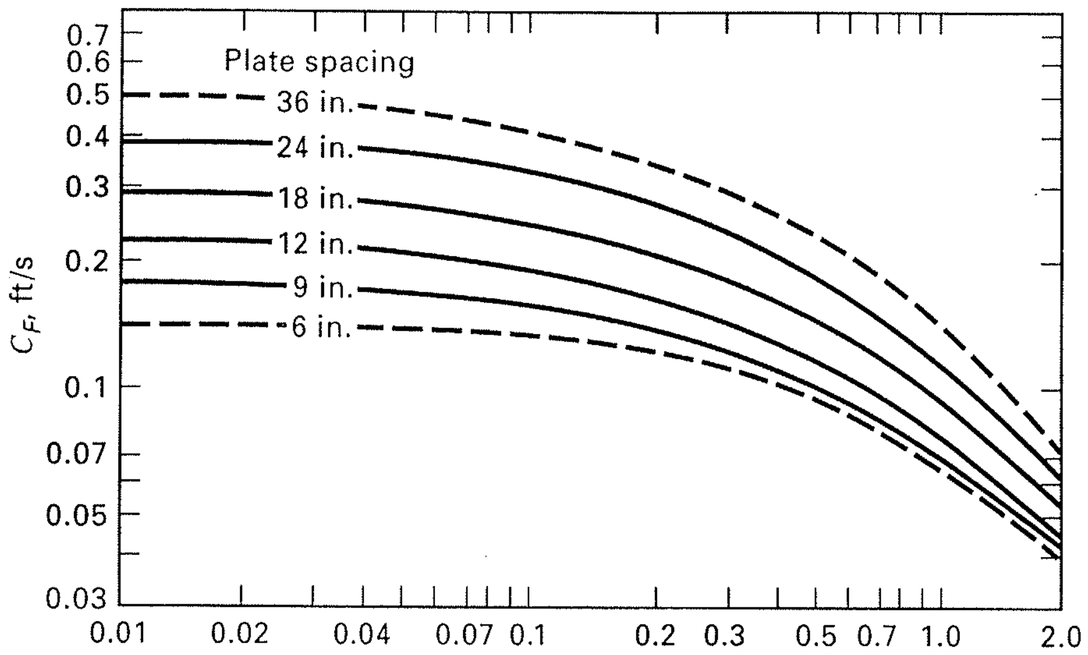

Figure 6.24 Entrainment flooding capacity in a trayed tower.

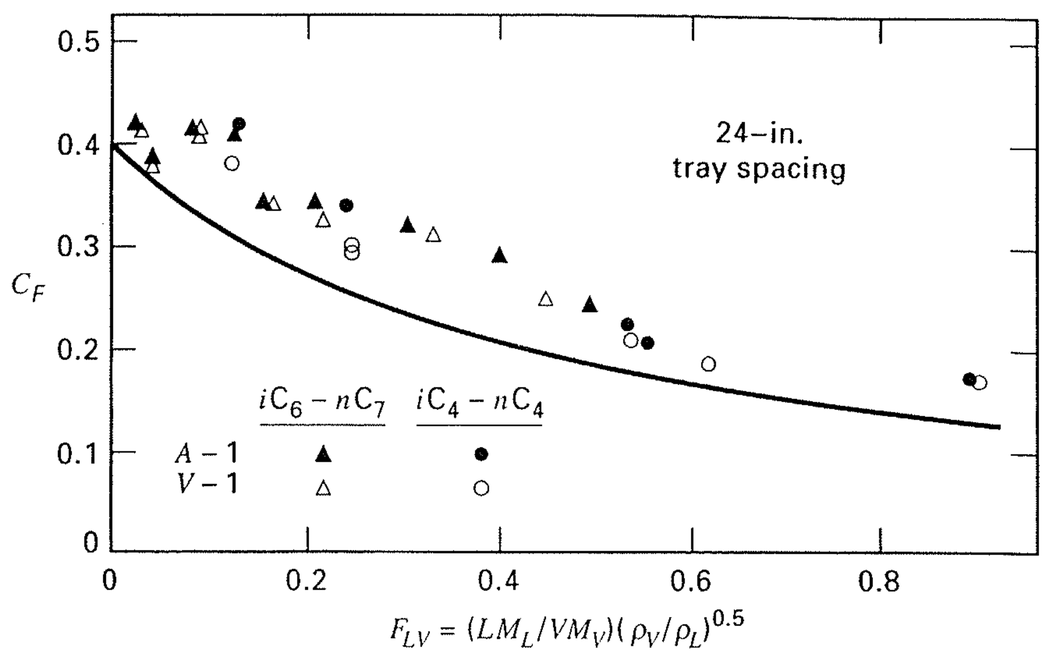

Figure 6.25 Comparison of flooding correlation with data for valve trays.

Using additional commercial operating data, Fair [25] produced the more general correlation of Figure 6.24, which is applicable to columns with bubble cap and sieve trays. Whereas Souders and Brown base the vapor velocity on the entire column cross-sectional area, Fair utilizes a net vapor flow area equal to the total inside column cross-sectional area minus the area blocked off by the downcomer, that is, $A - A_d$ in Figure 6.21. The value of C_F in Figure 6.24 depends on tray spacing and the abscissa ratio $F_{LV} = (LM_L/VM_V)(\rho_V/\rho_L)^{0.5}$ (where flow rates are in molar units), which is a kinetic energy ratio first used by Sherwood, Shipley, and Holloway [26] to correlate packed-column flooding data. The value of C in (6-41) is obtained from Figure 6.24 by correcting C_F for surface tension, foaming tendency, and the ratio of vapor hole area A_h to tray active area A_a, according to the empirical relationship

$$C = F_{ST} F_F F_{HA} C_F \tag{6-42}$$

where

F_{ST} = surface tension factor = $(\sigma/20)^{0.2}$

F_F = foaming factor

F_{HA} = 1.0 for $A_h/A_a \geq 0.10$ and $5(A_h/A_a) + 0.5$ for $0.06 \leq A_h/A_a \leq 0.1$

σ = liquid surface tension, dyne/cm

For nonfoaming systems, $F_F = 1.0$; for many absorbers, F_F may be 0.75 or even less. The quantity A_h is the area open to the vapor as it penetrates into the liquid on a tray. It is the total cap slot area for bubble-cap trays and the perforated area for sieve trays.

Figure 6.24 appears to be conservative for valve trays. This is shown in Figure 6.25, where entrainment-flooding data of Fractionation Research, Inc. (FRI) [27,28], for a 4-ft-diameter column equipped with Glitsch type A-1 and V-1 valve trays on 24-in. spacing are compared to the correlation in Figure 6.24. For valve trays, the slot area A_h is taken as the full valve opening through which vapor enters the frothy liquid on the tray at a 90° angle with the axis of the column.

Column diameter D_T is based on a fraction, f, of flooding velocity U_f, which is calculated from (6-40), using C from (6-42), based on C_F from Figure 6.24. By the continuity equation from fluid mechanics (flow rate = velocity × flow area × density), the molar vapor flow rate is related to the flooding velocity by

$$V = (fU_f)(A - A_d)\frac{\rho_V}{M_V} \tag{6-43}$$

where A = total column cross-sectional area = $\pi D_T^2/4$. Thus,

$$D_T = \left[\frac{4VM_V}{fU_f\pi(1 - A_d/A)\rho_V}\right]^{0.5} \tag{6-44}$$

Typically, the fraction of flooding, f, is taken as 0.80.

Oliver [29] suggests that A_d/A be estimated from F_{LV} in Figure 6.24 by

$$\frac{A_d}{A} = \begin{cases} 0.1, & F_{LV} \leq 0.1 \\ 0.1 + \dfrac{(F_{LV} - 0.1)}{9}, & 0.1 \leq F_{LV} \leq 1.0 \\ 0.2, & F_{LV} \geq 1.0 \end{cases}$$

Column diameter is calculated at both the top and bottom of the column, with the larger of the two diameters used for the entire column unless the two diameters differ appreciably. Because of the need for internal access to columns with trays, a packed column, discussed later in this chapter, is generally used if the calculated diameter from (6-44) is less than 2 ft.

Tray spacing must be specified to compute column diameter using Figure 6.24. As spacing is increased, column height is increased but column diameter is reduced. A spacing of 24 in., which provides ease of maintenance, is optimal for a wide range of conditions; however, a smaller spacing may be desirable for small-diameter columns with a large number of stages; and larger spacing is frequently used for large-diameter columns with a small number of stages.

As shown in Figure 6.22, a minimum vapor rate exists below which liquid weeps (dumps) through tray perforations or risers instead of flowing completely across the active area

and into the downcomer. Below this minimum, the degree of contacting of liquid with vapor is reduced, causing tray efficiency to decline. The ratio of the vapor rate at flooding to the minimum vapor rate is the *turndown ratio,* which is approximately 8 for bubble-cap trays, 5 for valve trays, but only about 2 for sieve trays.

When vapor and liquid flow rates change appreciably from tray to tray, column diameter, tray spacing, or hole area can be varied to reduce column cost and ensure stable operation at high tray efficiency. Variation of tray spacing is particularly applicable to columns with sieve trays because of their low turndown ratio.

High-Capacity Trays

Since the 1990s, a number of high-capacity trays have been introduced and installed in hundreds of columns. By various changes to the conventional tray design shown in Figure 6.3, capacity increases of more than 20% of that predicted by Figure 6.24 have been achieved with both perforated trays and valve trays. These changes, which are discussed in some detail by Sloley [71], have included:

1. Sloping or stepping of the downcomer to make the downcomer area smaller at the bottom than at the top so as to increase the active flow area.
2. Vapor flow through that portion of the tray located beneath the downcomer, in addition to the normal active flow area.
3. Use of staggered, louvered downcomer floor plates to impart a horizontal velocity to the liquid exiting the downcomer, thus enhancing the ability to allow vapor flow beneath the downcomer.
4. Elimination of vapor impingement from adjacent valves, in valve trays, by using bi-directional fixed valves.
5. Use of multiple-downcomer trays that provide very long outlet weirs leading to low crest heights and lower froth heights. The downcomers terminate in the active vapor space of the tray below.
6. Directional slotting of sieve trays to impart a horizontal component to the up-flowing vapor, enhance plug flow of liquid across the tray, and eliminate dead areas.

Regardless of the tray design, as shown by Stupin and Kister [72], an ultimate capacity, independent of tray spacing, exists for a countercurrent-flow, vapor–liquid contactor, in which the superficial vapor velocity in the column exceeds the settling velocity of large liquid droplets. Their correlation, based on FRI data, uses the following form of (6-40):

$$U_{S,ult} = C_{S,ult}\left(\frac{\rho_L - \rho_V}{\rho_V}\right)^{1/2} \tag{6-45}$$

where $U_{S,ult}$ is the superficial vapor velocity in m/s based on the column cross-sectional area. The ultimate capacity parameter, $C_{S,ult}$ in m/s, is independent of the superficial liquid velocity, L_S in m/s, below a critical value; but above that value it decreases with increasing L_S. It is given by the smaller of C_1 and C_2, both in m/s, where

$$C_1 = 0.445(1 - F)\left(\frac{\sigma}{\rho_L - \rho_V}\right)^{0.25} - 1.4L_S \tag{6-46}$$

$$C_2 = 0.356(1 - F)\left(\frac{\sigma}{\rho_L - \rho_V}\right)^{0.25} \tag{6-47}$$

where

$$F = \frac{1}{\left[1 + 1.4\left(\dfrac{\rho_L - \rho_V}{\rho_V}\right)^{1/2}\right]} \tag{6-48}$$

ρ is in kg/m^3 and σ is the surface tension in dynes/cm.

EXAMPLE 6.5

(a) Estimate the required tray diameter for the absorber of Example 6.1, assuming a tray spacing of 24 in., a foaming factor of $F_F = 0.90$, a fraction flooding of $f = 0.80$, and a surface tension of $\sigma = 70$ dynes/cm. (b) Estimate the ultimate superficial vapor velocity.

SOLUTION

Because tower conditions are almost the same at the top and bottom, the calculation of column diameter is made only at the bottom, where the gas rate is highest. From Example 6.1,

$$T = 30°C \quad P = 110 \text{ kPa}$$

$$V = 180 \text{ kmol/h}, \quad L = 151.5 + 3.5 = 155.0 \text{ kmol/h}$$

$$M_V = 0.98(44) + 0.02(46) = 44.0,$$

$$M_L = \frac{151.5(18) + 3.5(46)}{155} = 18.6$$

$$\rho_V = \frac{PM}{RT} = \frac{(110)(44)}{(8.314)(303)} = 1.92 \text{ kg/m}^3,$$

$$\rho_L = (0.986)(1{,}000) = 986 \text{ kg/m}^3$$

$$F_{LV} = \frac{(155)(18.6)}{(180)(44.0)}\left(\frac{1.92}{986}\right)^{0.5} = 0.016$$

(a) For tray spacing = 24 in., from Figure 6.24, $C_F = 0.39$ ft/s,

$$F_{ST} = \left(\frac{\sigma}{20}\right)^{0.2} = \left(\frac{70}{20}\right)^{0.2} = 1.285, \quad F_F = 0.90$$

Because $F_{LV} < 0.1$, $A_d/A = 0.1$ and $F_{HA} = 1.0$. Then, from (6-42),

$$C = 1.285(0.90)(1.0)(0.39) = 0.45 \text{ ft/s}$$

From (6-40),

$$U_f = 0.45\left(\frac{986 - 1.92}{1.92}\right)^{0.5} = 10.2 \text{ ft/s}$$

From (6-44), using SI units and time in seconds,

$$D_T = \left[\frac{4(180/3{,}600)(44.0)}{(0.80)(10.2/3.28)(3.14)(1-0.1)(1.92)}\right]^{0.5}$$
$$= 0.81 \text{ m} = 2.65 \text{ ft}$$

(b) From (6-48),

$$F = \frac{1}{\left[1 + 1.4\left(\frac{986-1.92}{1.92}\right)^{1/2}\right]} = 0.0306$$

From (6-47),

$$C_2 = 0.356(1-0.0306)\left(\frac{70}{986-1.92}\right)^{0.25}$$
$$= 0.178 \text{ m/s} = 0.584 \text{ ft/s}$$

If C_2 is the smaller value of C_1 and C_2, then from (6-45),

$$U_{S,ult} = 0.178\left(\frac{986-1.92}{1.92}\right)^{1/2} = 4.03 \text{ m/s} = 13.22 \text{ ft/s}$$

To apply (6-46) to compute C_1, the value of L_S is required. This value is related as follows to the value of the superficial vapor velocity, U_S.

$$L_S = U_S\frac{\rho_V L M_L}{\rho_L V M_V} = U_S\frac{(1.92)(155)(18.6)}{(986)(180)(44.0)} = 0.000709\, U_S$$

With this expression for L_S, (6-46) becomes

$$C_1 = 0.445(1-0.0306)\left(\frac{70}{986-1.92}\right)^{0.25} - 1.4(0.000709)\, U_S$$
$$= 0.223 - 0.000993\, U_S, \text{ m/s}$$

If C_1 is the smaller, then, using (6-45),

$$U_{S,ult} = (0.223 - 0.000993\, U_{S,ult})\left(\frac{986-1.92}{1.92}\right)^{1/2}$$
$$= 5.05 - 0.0225\, U_{S,ult}$$

Solving, $U_{S,ult} = 4.94$ m/s, which gives $C_1 = 0.223 - 0.000993(4.94) = 0.218$ m/s. Thus, C_2 is the smaller value and $U_{S,ult} = 4.03$ m/s $= 13.22$ ft/s. This ultimate velocity is 30% higher than the flooding velocity computed in part (a).

Tray Vapor Pressure Drop

Typical tray pressure drop for flow of vapor in a tower is from 0.05 to 0.15 psi/tray. Referring to Figure 6.3, pressure drop (head loss) for a sieve tray is due to friction for vapor flow through the tray perforations, holdup of the liquid on the tray, and a loss due to surface tension:

$$h_t = h_d + h_l + h_\sigma \tag{6-49}$$

where

h_t = total pressure drop/tray, in. of liquid
h_d = dry tray pressure drop, in. of liquid
h_l = equivalent head of clear liquid on tray, in. of liquid
h_σ = pressure drop due to surface tension, in. of liquid

The dry sieve-tray pressure drop is given by a modified orifice equation, applied to the holes in the tray,

$$h_d = 0.186\left(\frac{u_o^2}{C_o^2}\right)\left(\frac{\rho_V}{\rho_L}\right) \tag{6-50}$$

where u_o = hole velocity (ft/s) and C_o depends on the percent hole area and the ratio of tray thickness to hole diameter. For a typical 0.078-in.-thick tray with $\frac{3}{16}$-in.-diameter holes and a percent hole area (based on the cross-sectional area of the tower) of 10%, C_o may be taken as 0.73. Otherwise, C_o lies between about 0.65 and 0.85.

The equivalent height of clear liquid holdup on a tray depends on weir height, liquid and vapor densities and flow rates, and downcomer weir length, as given by the following empirical expression developed from experimental data by Bennett, Agrawal, and Cook [30]:

$$h_l = \phi_e\left[h_w + C_l\left(\frac{q_L}{L_w\phi_e}\right)^{2/3}\right] \tag{6-51}$$

where

h_w = weir height, in.
ϕ_e = effective relative froth density (height of clear liquid/froth height) $= \exp(-4.257\, K_s^{0.91})$ (6-52)

K_s = capacity parameter, ft/s $= U_a\left(\frac{\rho_V}{\rho_L - \rho_V}\right)^{1/2}$ (6-53)

U_a = superficial vapor velocity based on active bubbling area,
$A_a = (A - 2A_d)$, of the tray, ft/s,
L_w = weir length, in.
q_L = liquid flow rate across tray, gal/min
$C_l = 0.362 + 0.317\exp(-3.5h_w)$ (6-54)

The second term in (6-51) is related to the Francis weir equation for a straight segmental weir, taking into account the froth nature of the liquid flow over the weir. For $A_d/A = 0.1$, $L_w = 73\%$ of the tower diameter.

As the gas emerges from the tray perforations, the bubbles must overcome surface tension. The pressure drop due to surface tension is given by the difference between the pressure inside the bubble and that of the liquid, according to the theoretical relation

$$h_\sigma = \frac{6\sigma}{g\rho_L D_{B(\max)}} \tag{6-55}$$

where, except for tray perforations much smaller than $\frac{3}{16}$-in. in diameter, $D_{B(\max)}$, the maximum bubble size, may be taken as the perforation diameter, D_H.

Methods for estimating vapor pressure drop for bubble-cap trays and valve trays are given by Smith [31] and Klein [32], respectively, and are discussed by Kister [33] and Lockett [34].

EXAMPLE 6.6

Estimate the tray vapor pressure drop for the absorber of Example 6.1, assuming use of sieve trays with a tray diameter of 1 m, a weir height of 2 in., and a hole diameter of $\frac{3}{16}$ in.

SOLUTION

From Example 6.5,

$$\rho_V = 1.92 \text{ kg/m}^3 \quad \rho_L = 986 \text{ kg/m}^3$$

At the bottom of the tower, vapor velocity based on the total cross-sectional area of the tower is

$$\frac{(180/3{,}600)(44)}{(1.92)[3.14(1)^2/4]} = 1.46 \text{ m/s}$$

For a 10% hole area, based on the total cross-sectional area of the tower,

$$u_o = \frac{1.46}{0.10} = 14.6 \text{ m/s} \quad \text{or} \quad 47.9 \text{ ft/s}$$

Using the above densities, (6-50) gives

$$h_d = 0.186\left(\frac{47.9^2}{0.73^2}\right)\left(\frac{1.92}{986}\right) = 1.56 \text{ in. of liquid}$$

Take weir length as 73% of tower diameter, with $A_d/A = 0.10$. Then

$$L_w = 0.73(1) = 0.73 \text{ m} \quad \text{or} \quad 28.7 \text{ in.}$$

$$\text{Liquid flow rate in gpm} = \frac{(155/60)(18.6)}{986(0.003785)} = 12.9 \text{ gpm}$$

with $\quad A_d/A = 0.1 \quad A_a/A = (A - 2A_d)/A = 0.8$

Therefore, $U_a = 1.46/0.8 = 1.83 \text{ m/s} = 5.99 \text{ ft/s}$

From (6-53),

$$K_s = 5.99[1.92/(986 - 1.92)]^{0.5} = 0.265 \text{ ft/s}$$

From (6-52),

$$\phi_e = \exp[-4.257(0.265)^{0.91}] = 0.28$$

From (6-54),

$$C_l = 0.362 + 0.317\exp[-3.5(2)] = 0.362$$

From (6-51),

$$h_l = 0.28[2 + 0.362(12.9/28.7/0.28)^{2/3}]$$
$$= 0.28(2 + 0.50) = 0.70 \text{ in.}$$

From (6-55), in metric units, using $D_{B(\max)} = D_H = \frac{3}{16}$ in. = 0.00476 m,

$$\sigma = 70 \text{ dynes/cm} = 0.07 \text{ N/m} = 0.07 \text{ kg/s}^2,$$
$$g = 9.8 \text{ m/s}^2, \text{ and } \rho_L = 986 \text{ kg/m}^3$$
$$h_\sigma = \frac{6(0.07)}{9.8(986)(0.00476)} = 0.00913 \text{ m} = 0.36 \text{ in.}$$

From (6-45), the total tray head loss is $h_t = 1.56 + 0.70 + 0.36 = 2.62$ in.

For $\rho_L = 986 \text{ kg/m}^3 = 0.0356 \text{ lb/in}^3$,

tray vapor pressure drop $= h_t\rho_L = 2.62(0.0356) = 0.093$ psi/tray

Mass-Transfer Coefficients and Transfer Units

Following the determination of tower diameter and major details of the tray layout, an estimate of the Murphree vapor point efficiency, defined by (6-30), can be made using empirical correlations for mass-transfer coefficients, based on experimental data. For a vertical path for vapor flow up through the froth from a point on the bubbling area of the tray, (6-29) applies to the Murphree vapor-point efficiency:

$$N_{OG} = -\ln(1 - E_{OV}) \tag{6-56}$$

where

$$N_{OG} = \frac{K_G a P Z_f}{(V/A_b)} \tag{6-57}$$

The overall, volumetric mass-transfer coefficient, $K_G a$, is related to the individual volumetric mass-transfer coefficients by the sum of the mass-transfer resistances, which from equations in Section 3.7 can be shown to be

$$\frac{1}{K_G a} = \frac{1}{k_G a} + \frac{(KPM_L/\rho_L)}{k_L a} \tag{6-58}$$

where the two terms on the right-hand side are the gas- and liquid-phase resistances, respectively, and the symbols k_p for the gas and k_c for the liquid used in Chapter 3 have been replaced by k_G and k_L, respectively. In terms of individual transfer units, defined by

$$N_G = \frac{k_G a P Z_f}{(V/A_b)} \tag{6-59}$$

and

$$N_L = \frac{k_L a \rho_L Z_f}{M_L(L/A_b)} \tag{6-60}$$

we obtain from (6-57) and (6-58)

$$\frac{1}{N_{OG}} = \frac{1}{N_G} + \frac{(KV/L)}{N_L} \tag{6-61}$$

Important empirical mass-transfer correlations have been published by the AIChE [35] for bubble-cap trays, Chan and Fair [36, 37] for sieve trays, and Scheffe and Weiland [38] for one type of valve tray (Glitsch V-1). These correlations have been developed in terms of N_L, N_G, k_L, k_G, a, and N_{Sh} for either the gas or liquid phase. In this section, we present only correlations for sieve trays, as given for binary systems by Chan and Fair [36], who used a correlation for the liquid phase based on the work of Foss and Gerster [39] as reported by the AIChE [40], and who developed a correlation for the vapor phase from a fairly extensive experimental data bank of 143 points for towers 2.5 to 4.0 ft in diameter, operating at pressures from 100 mmHg to 400 psia.

Experimental data for sieve trays have validated the assumed direct dependence of mass transfer on the interfacial area between the gas and liquid phases, and on the residence times in the froth of the gas and liquid phases. Accordingly,

Chan and Fair give the following modifications of (6-59) and (6-60):

$$N_G = k_G \bar{a} \bar{t}_G \tag{6-62}$$

$$N_L = k_L \bar{a} \bar{t}_L \tag{6-63}$$

where $\bar{a}$ is the interfacial area per unit volume of equivalent clear liquid, $\bar{t}_G$ is the average residence time of the gas in the froth, and $\bar{t}_L$ is the average residence time of the liquid in the froth.

Average residence times are estimated from the following dimensionally consistent, theoretical continuity equations, using (6-51) for the equivalent head of clear liquid on the tray and (6-52) for the effective relative density of the froth:

$$\bar{t}_L = \frac{h_l A_a}{q_L} \tag{6-64}$$

and

$$\bar{t}_G = \frac{(1 - \phi_e) h_l}{(\phi_e U_a)} \tag{6-65}$$

where $(1 - \phi_e)h_l/\phi_e$ is the equivalent height of vapor holdup in the froth, and the residence times are usually computed in seconds.

Empirical expressions for $k_G \bar{a}$ and $k_L \bar{a}$ in units of s^{-1} are

$$k_G \bar{a} = \frac{1{,}030 D_V^{0.5} (f - 0.842 f^2)}{(h_l)^{0.5}} \tag{6-66}$$

and

$$k_L \bar{a} = 78.8 D_L^{0.5} (F + 0.425) \tag{6-67}$$

where the variables and their units are

D_V, D_L = diffusion coefficients, cm^2/s

h_l = clear liquid height, cm

$f = U_a/U_f$, fractional approach to flooding

$F = F$-factor $= U_a \rho_V^{0.5}$, $(kg/m)^{0.5}/s$

From (6-66), it is seen that an important factor influencing the value of $k_G \bar{a}$ is the fractional approach to flooding, $f = U_a/U_f$. This effect is shown in Figure 6.26, where (6-66) is compared to experimental data. At gas rates corresponding to a fractional approach to flooding of greater than 0.60, the mass-transfer factor decreases with increasing value of f. This may be due to entrainment, which is discussed in the next sub-section. On an entrainment-free basis, the curve in Figure 6.26 might be expected to at least remain at its peak value for conditions above $f = 0.60$.

From (6-67), it is seen that the F-factor is an important consideration for liquid-phase mass transfer. Experimental data that support this are shown in Figure 6.27, where $k_L \bar{a}$ depends strongly on F but is almost independent of liquid flow rate and weir height. The Murphree vapor-point efficiency model of (6-56), (6-61), (6-64), (6-65), (6-66), and (6-67) correlates the 143 points of the Chan and Fair [36] data bank with an average absolute deviation of 6.27%. Lockett [34] pointed out that (6-67) implies that $k_L \bar{a}$ depends on tray spacing, which seems unreasonable.

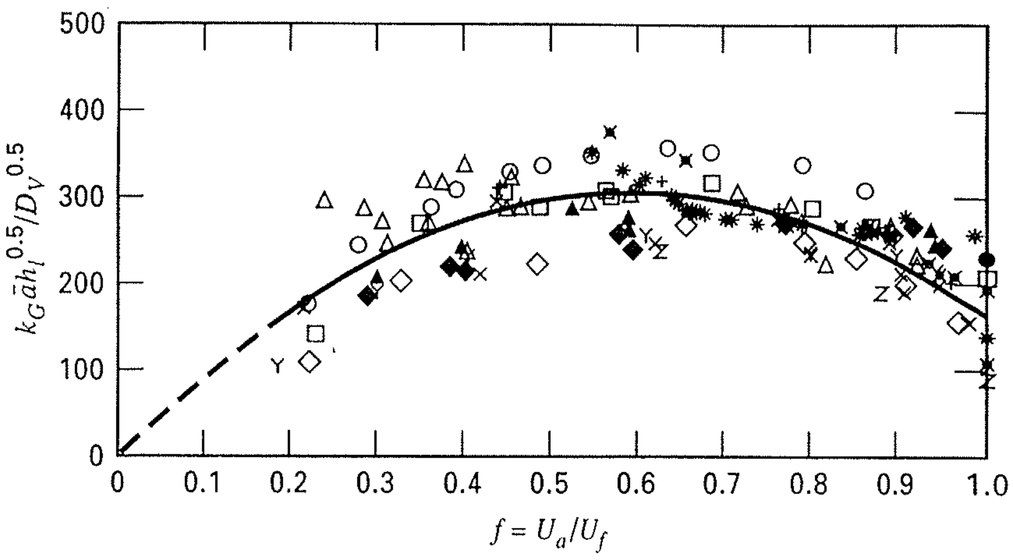

Figure 6.26 Comparison of experimental data to the correlation of Chan and Fair for gas-phase mass transfer.

[From H. Chan and J.R. Fair, *Ind. Eng. Chem. Process Des. Dev.*, **23,** 817 (1984) with permission.]

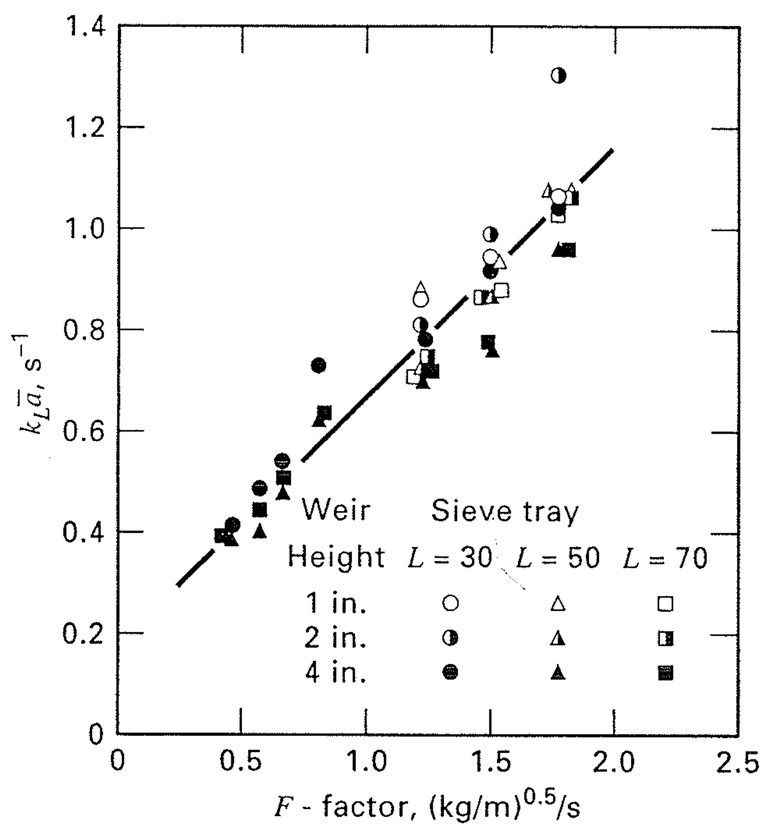

Figure 6.27 Effect of the F-factor on the liquid-phase volumetric mass-transfer coefficient for desorption of oxygen from water with air at 1 atm. and 25°C, where L = gal/(min)/(ft of average flow width).

However, the data bank did include data for tray spacings from 6 to 24 in.

EXAMPLE 6.7

Estimate the Murphree vapor-point efficiency for the absorber of Example 6.1, using results from Examples 6.5 and 6.6, for the tray of Example 6.6. In addition, determine the controlling resistance to mass transfer.

SOLUTION

Pertinent data for the two phases are as follows.

	Gas	**Liquid**
Molar flow rate, kmol/h	180.0	155.0
Molecular weight	44.0	18.6
Density, kg/m^3	1.92	986
Ethanol diffusivity, cm^2/s	7.86×10^{-2}	1.81×10^{-5}

Pertinent tray dimensions from Example 6.6 are $D_T = 1$ m, and $A = 0.785$ m^2; $A_a = 0.80$, $A = 0.628$ m^2 = 6,280 cm^2; $L_w = 28.7$ in. = 0.73 m.

From Example 6.6,

$$\phi_e = 0.28; \quad h_l = 0.70 \text{ in.} = 1.78 \text{ cm};$$
$$U_a = 5.99 \text{ ft/s} = 183 \text{ cm/s} = 1.83 \text{ m/s}$$

From Example 6.5,

$$U_f = 10.2 \text{ ft/s}; \quad f = U_a/U_f = 5.99/10.2 = 0.59$$
$$F = 1.83(1.92)^{0.5} = 2.54 \text{ (kg/m)}^{0.5}/\text{s}$$
$$q_L = \frac{(155.0)(18.6)}{986}\left(\frac{10^6}{3{,}600}\right) = 812 \text{ cm}^3/\text{s}$$

From (6-64),

$$\bar{t}_L = (1.78)(6{,}280)/812 = 13.8 \text{ s}$$

From (6-65),

$$\bar{t}_G = (1 - 0.28)(1.78)/[(0.28)(183)] = 0.025 \text{ s}$$

From (6-67),

$$k_L\bar{a} = 78.8(1.81 \times 10^{-5})^{0.5}(2.54 + 0.425) = 0.99 \text{ s}^{-1}$$

From (6-66),

$$k_G\bar{a} = 1{,}030(7.86 \times 10^{-2})^{0.5}[0.59 - 0.842(0.59)^2]/(1.78)^{0.5}$$
$$= 64.3 \text{ s}^{-1}$$

From (6-63),

$$N_L = (0.99)(13.8) = 13.7$$

From (6-62),

$$N_G = (64.3)(0.025) = 1.61$$

From Example 6.1, $K = 0.57$. Therefore, $KV/L = (0.57)(180)/155 = 0.662$.

From (6-61),

$$N_{OG} = \frac{1}{(1/1.61) + (0.662/13.7)} = \frac{1}{0.621 + 0.048} = 1.49$$

and the mass transfer of ethanol is seen to be controlled by the vapor-phase resistance. From (6-56), solving for E_{OV},

$$E_{OV} = 1 - \exp(-N_{OG}) = 1 - \exp(-1.49) = 0.77 = 77\%$$

Weeping, Entrainment, and Downcomer Backup

For a tray to operate at high efficiency, (1) weeping of liquid through the tray perforations must be small compared to flow over the outlet weir and into the downcomer, (2) entrainment of liquid by the gas must not be excessive, and (3) to prevent downcomer flooding, froth height in the downcomer must not approach tray spacing. The tray must operate in the stable region shown schematically in Figure 6.22. Weeping is associated with the lower limit of gas velocity, while entrainment flooding is associated with the upper limit.

Weeping occurs at low vapor velocities and/or high liquid rates when the clear liquid height on the tray exceeds the sum of the dry (no liquid flow) tray pressure drop, due to vapor flow, and the surface tension effect. Thus, to prevent weeping, it is necessary that

$$h_d + h_\sigma > h_l \tag{6-68}$$

everywhere on the active area of the tray. If weeping occurs uniformly over the tray active area or mainly near the downcomer, a ratio of weep rate to downcomer liquid rate as high as 0.1 may not cause an unacceptable decrease in tray efficiency. Methods for estimating weep rates are discussed by Kister [33].

The prediction of fractional liquid entrainment by the vapor, defined as $\psi = e/(L + e)$, can be made by the correlation of Fair [41], given in Figure 6.28. As shown, entrainment becomes excessive at high values of fraction of flooding, $f = U_a/U_f$, particularly for small values of the kinetic-energy ratio, F_{LV}. The effect of entrainment on the Murphree vapor efficiency can be estimated by the following relation derived by Colburn [42], where E_{MV} is the usual "dry" efficiency and $E_{MV,\text{wet}}$ is the "wet" efficiency:

$$\frac{E_{MV,\text{wet}}}{E_{MV}} = \frac{1}{1 + eE_{MV}/L} = \frac{1}{1 + E_{MV}[\psi/(1-\psi)]} \tag{6-69}$$

Equation (6-69) assumes that $\lambda = KV/L = 1$ and that the liquid is well mixed on the tray such that the composition of the entrained liquid is that of the liquid flowing to the tray below. For a given value of the entrainment ratio, ψ, the larger the value of E_{MV}, the greater is the effect of entrainment. For $E_{MV} = 1.0$ and $\psi = 0.10$, the "wet" efficiency is 0.90. An equation similar to (6-69) for the effect of weeping

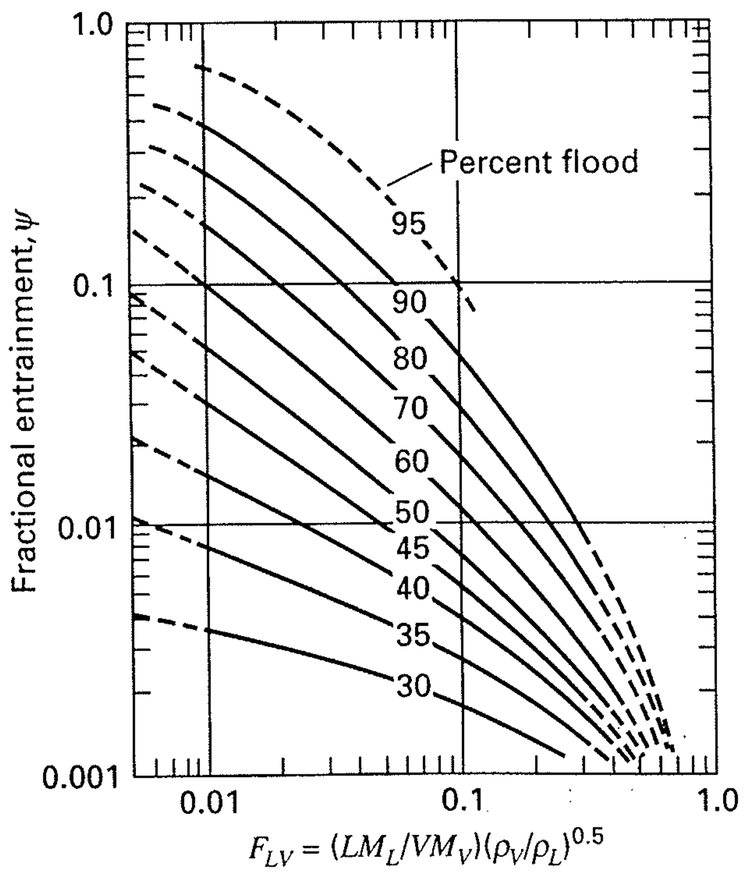

Figure 6.28 Correlation of Fair for fractional entrainment for sieve trays.

[Reproduced by permission from B.D. Smith, *Design of Equilibrium Stage Processes*, McGraw-Hill, New York (1963).]

is not available, because this effect depends greatly on the degree of liquid mixing on the tray and on the distribution of weeping over the active area of the tray. If weeping occurs only in the vicinity of the downcomer, no decrease in the value of E_{MV} is observed.

The height of clear liquid in the downcomer, h_{dc}, is always greater than the height of clear liquid on the tray because, by reference to Figure 6.3, the pressure difference across the froth in the downcomer is equal to the total pressure drop across the tray from which liquid enters the downcomer, plus the height of clear liquid on the tray below to which the liquid flows, and plus the head loss for liquid flow under the downcomer apron. Thus, the clear liquid head in the downcomer is

$$h_{dc} = h_t + h_l + h_{da} \tag{6-70}$$

where h_t is given by (6-49) and h_l by (6-51), and the hydraulic gradient is assumed to be negligible. The head loss for liquid flow under the downcomer, h_{da}, in inches of liquid can be estimated from an empirical orifice-type equation:

$$h_{da} = 0.03\left(\frac{q_L}{100\,A_{da}}\right)^2 \tag{6-71}$$

where q_L is the liquid flow in gpm and A_{da} is the area in ft^2 for liquid flow under the downcomer apron. If the height of the opening under the apron (typically 0.5 in. less than h_w) is h_a, then $A_{da} = L_w h_a$. The height of the froth in the downcomer is

$$h_{df} = h_{dc}/\phi_{df} \tag{6-72}$$

where the froth density, ϕ_{df}, can be taken conservatively as 0.5.

EXAMPLE 6.8

Using data from Examples 6.5, 6.6, and 6.7, estimate the entrainment rate, the froth height in the downcomer, and whether weeping occurs.

SOLUTION

Weeping criterion: From Example 6.6,

$$h_d = 1.56 \text{ in.} \quad h_\sigma = 0.36 \text{ in.} \quad h_l = 0.70 \text{ in.}$$

$$\text{From (6-68)}, 1.56 + 0.36 > 0.70$$

Therefore, if the liquid level is uniform across the active area, no weeping occurs.

Entrainment: From Example 6.5,

$$F_{LV} = 0.016 \quad \text{From Example 6.7, } f = 0.59$$

From Figure 6.28, $\psi = 0.06$. Therefore, for $L = 155$ from Example 6.7, the entrainment rate is $0.06(155) = 9.3$ kmol/h. Assuming that (6-69) is reasonably accurate for $\lambda = 0.662$ from Example 6.7, and that $E_{MV} = 0.78$, the effect of ψ on E_M, is given by

$$\frac{E_{MV,\text{wet}}}{E_{MV}} = \frac{1}{1 + 0.78(0.06/0.94)} = 0.95$$

or

$$E_{MV} = 0.95(0.78) = 0.74$$

Downcomer backup:

From Example 6.6, $h_t = 2.62$ in.
From Example 6.7, $L_w = 28.7$ in.
From Example 6.6, $h_w = 2.0$ in.
Assume that $h_a = 2.0 - 0.5 = 1.5$ in. Then

$$A_{da} = L_w h_a = 28.7(1.5) = 43.1 \text{ in.}^2 = 0.299 \text{ ft}^2$$

From Example 6.6, $q_L = 12.9$ gpm

$$\text{From (6-71)}, h_{da} = 0.03\left[\frac{12.9}{(100)(0.299)}\right]^2 = 0.006 \text{ in.}$$

From (6-70), $h_{dc} = 2.62 + 0.70 + 0.006 = 3.33$ in. of clear liquid backup

$$\text{From (6-72)}, h_{df} = \frac{3.33}{0.5} = 6.66 \text{ in. of froth in the downcomer}$$

Based on these results, neither weeping nor downcomer backup appear to be problems. An estimated 5% loss in tray efficiency occurs due to entrainment.

6.7 RATE-BASED METHOD FOR PACKED COLUMNS

Absorption and stripping are frequently conducted in packed columns, particularly when (1) the required column diameter is 2 ft or less; (2) the pressure drop must be low, as for a vacuum service; (3) corrosion considerations favor the use of ceramic or polymeric materials; and/or (4) low liquid holdup is desirable. Structured packing is often favored over random packing for revamps to overcome capacity limitations of trayed towers.

Packed columns are continuous, differential-contacting devices that do not have the physically distinguishable stages found in trayed towers. Thus, packed columns are best analyzed by mass-transfer considerations rather than by the equilibrium-stage concept described in earlier sections of this chapter for trayed towers. Nevertheless, in practice, packed-tower performance is often analyzed on the basis of equivalent equilibrium stages using a packed height equivalent to a theoretical (equilibrium) plate (stage), called the HETP or HETS and defined by the equation

$$\text{HETP} = \frac{\text{packed height}}{\text{number of equivalent equilibrium stages}} = \frac{l_T}{N_t} \tag{6-73}$$

The HETP concept, unfortunately, has no theoretical basis. Accordingly, although HETP values can be related to mass-transfer coefficients, such values are best obtained by back-calculation from (6-73) using experimental data from laboratory or commercial-size columns. To illustrate the application of the HETP concept, consider Example 6.1, which involves the recovery of ethyl alcohol from a CO_2-rich vapor by absorption with water. The required number of equilibrium stages is found to be just slightly more than 6, say, 6.1. Suppose that experience shows that if 1.5-in. metal Pall rings are used in a packed tower, an average HETP of

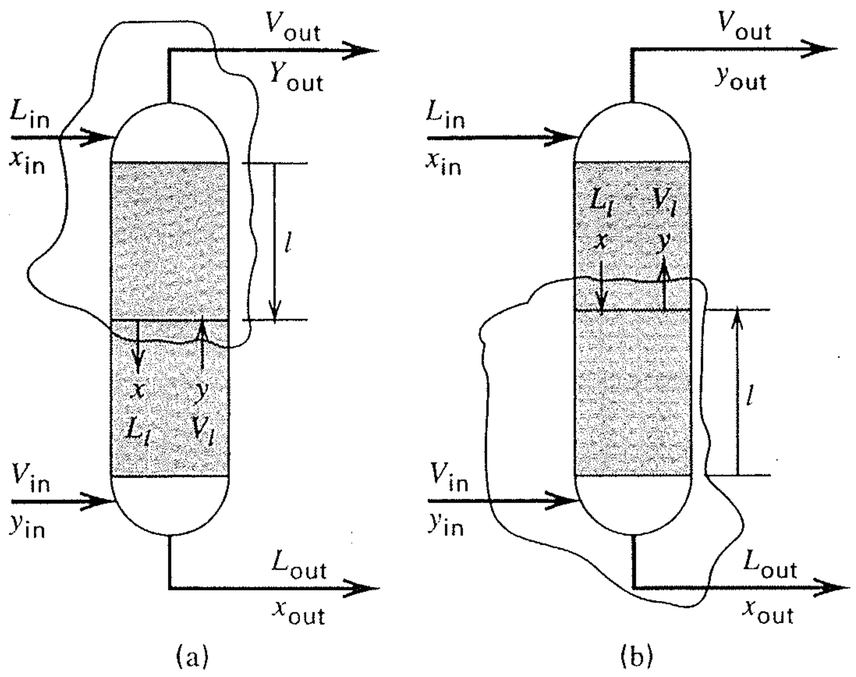

Figure 6.29 Packed columns with countercurrent flow: (a) absorber; (b) stripper.

2.25 ft can be achieved. From (6-73), the required packed height, l_T, is $l_T = (\text{HETP})N_t = 2.25(6.1) = 13.7$ ft. With metal Intalox IMTP #40 random packing, the HETP might be 2.0 ft, giving $l_T = 12.3$ ft. With Mellapak 250Y corrugated, sheet-metal structured packing, the HETP might be only 1.2 ft, giving $l_T = 7.3$ ft.

For packed columns, it is preferable to determine packed height from a more theoretically based method involving mass-transfer coefficients for the liquid and vapor phases. As with cascades of equilibrium stages, countercurrent flow of vapor and liquid is generally preferred over cocurrent flow. Consider the countercurrent-flow packed columns of packed height l_T, shown in Figure 6.29, which is analogous to Figure 6.8 for trayed towers. For packed absorbers and strippers, operating-line equations, that are analogous to those of Section 6.3 can be derived in terms of mole fractions and total molar flow rates. Thus, for the absorber in Figure 6.29a, a material balance around the upper envelope, for the solute, gives

$$x_{in}L_{in} + yV_l = xL_l + y_{out}V_{out} \tag{6-74}$$

or solving for y, assuming dilute solutions such that $V_l = V_{in} = V_{out} = V$ and $L_l = L_{in} = L_{out} = L$

$$y = x\left(\frac{L}{V}\right) + y_{out} - x_{in}\left(\frac{L}{V}\right) \tag{6-75}$$

Similarly for the stripper in Figure 6.29b,

$$y = x\left(\frac{L}{V}\right) + y_{in} - x_{out}\left(\frac{L}{V}\right) \tag{6-76}$$

In Equations (6-74) to (6-76), mole fractions y and x represent, respectively, bulk compositions of the gas and liquid streams in contact with each other at any elevation of the packed part of the column. For the case of absorption, with mass transfer of the solute from the gas stream to the liquid stream, the two-film theory, developed in Section 3.7, can be applied as illustrated in Figure 6.30. A concentration gradient exists in each film. At the interface between the two phases, physical equilibrium is assumed to exist. Thus, as with trayed towers, an operating line and an equilibrium line are of great importance in a packed column. For a given

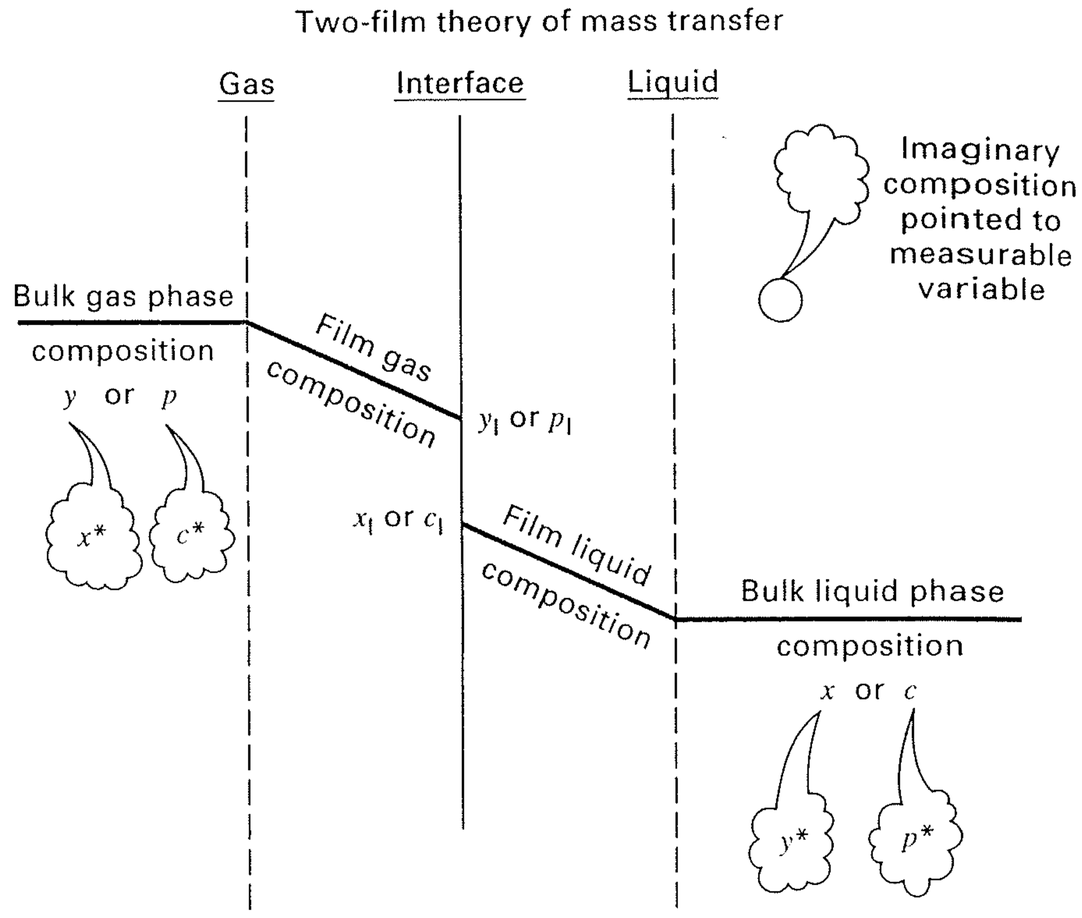

Figure 6.30 Interface properties in terms of bulk properties.

problem specification, the location of the two lines is independent of whether the tower is trayed or packed. Thus, the method for determining the minimum absorbent liquid or stripping vapor flow rates in a packed column is identical to the method for trayed towers, as presented in Section 6.3 and illustrated in Figure 6.9.

The rate of mass transfer for absorption or stripping in a packed column can be expressed in terms of mass-transfer coefficients for each phase. Coefficients, k, based on a unit area for mass transfer could be used, but the area for mass transfer in a packed bed is difficult to determine. Accordingly, as with mass transfer in the froth of a trayed tower, it is more common to use volumetric mass-transfer coefficients, ka, where the quantity a represents the area for mass transfer per unit volume of packed bed. Thus, ka is based on a unit volume of packed bed. At steady state in an absorber, in the absence of chemical reactions, and since species moles are conserved, the rate of solute mass transfer across the gas-phase film must equal the rate across the liquid-phase film. If the system is dilute with respect to the solute, unimolecular diffusion (UMD) may be approximated by the simpler equations for equimolar counterdiffusion (EMD) discussed in Chapter 3. The rate of mass transfer per unit volume of packed bed, r, may be written in terms of mole-fraction driving forces in each of the two phases or in terms of a partial-pressure driving force in the gas phase and a concentration driving force in the liquid phase, as indicated in Figure 6.30. Using the former, for absorption, with the subscript I to denote the interface:

$$r = k_y a(y - y_I) = k_x a(x_I - x) \tag{6-77}$$

The composition at the interface depends on the ratio, $k_x a/k_y a$, of the volumetric mass-transfer coefficients, because (6-77) can be rearranged to

$$\frac{y - y_I}{x - x_I} = -\frac{k_x a}{k_y a} \tag{6-78}$$

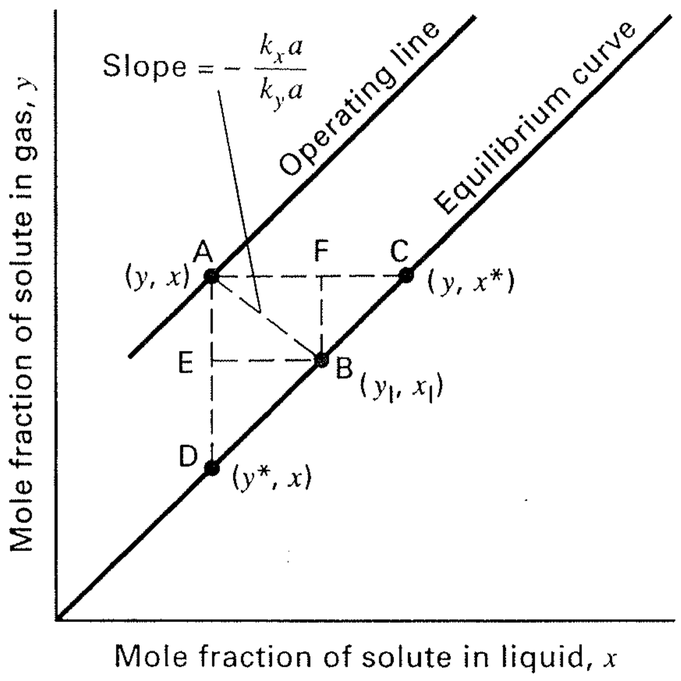

Figure 6.31 Interface composition in terms of the ratio of mass-transfer coefficients.

Thus, a straight line of slope $-k_x a/k_y a$ drawn from the operating line at point (y, x) intersects the equilibrium curve at (y_I, x_I). This result is shown graphically in Figure 6.31.

The slope $-k_x a/k_y a$ determines the relative resistances of the two phases to mass transfer. In Figure 6.31 the distance AE is the gas-phase driving force $(y - y_I)$, while AF is the liquid-phase driving force $(x_I - x)$. If the mass-transfer resistance in the gas phase is very low, y_I is approximately equal to y. Then, the resistance resides entirely in the liquid phase. This situation occurs in the absorption of a solute that is only slightly soluble in the liquid phase (i.e., a solute with a high K-value) and is referred to as a liquid-film resistance-controlling process. Alternatively, if the resistance in the liquid phase is very low, x_I is approximately equal to x. This situation occurs in the absorption of a solute that is very soluble in the liquid phase (i.e., a solute with a low K-value) and is referred to as a gas-film resistance-controlling process. It is important to know if one of the two resistances is controlling. If so, the rate of mass transfer can be increased by promoting turbulence in and/or increasing the dispersion of the controlling phase.

To avoid the need to determine the composition at the interface between the two phases, overall, volumetric mass-transfer coefficients can be defined in terms of overall driving forces for either the gas phase or the liquid phase. Thus, for mole-fraction driving forces,

$$r = K_y a(y - y^*) = K_x a(x^* - x) \tag{6-79}$$

where, as shown in Figure 6.31, y^* is the fictitious vapor mole fraction that is in equilibrium with the mole fraction, x, in the bulk liquid; and x^* is the fictitious liquid mole fraction that is in equilibrium with the mole fraction, y, in the bulk vapor. By combining (6-77) to (6-79), the overall coefficients can be expressed in terms of the separate coefficients for the two phases. Thus,

$$\frac{1}{K_y a} = \frac{1}{k_y a} + \frac{1}{k_x a}\left(\frac{y_I - y^*}{x_I - x}\right) \tag{6-80}$$

and

$$\frac{1}{K_x a} = \frac{1}{k_x a} + \frac{1}{k_y a}\left(\frac{x^* - x_I}{y - y_I}\right) \tag{6-81}$$

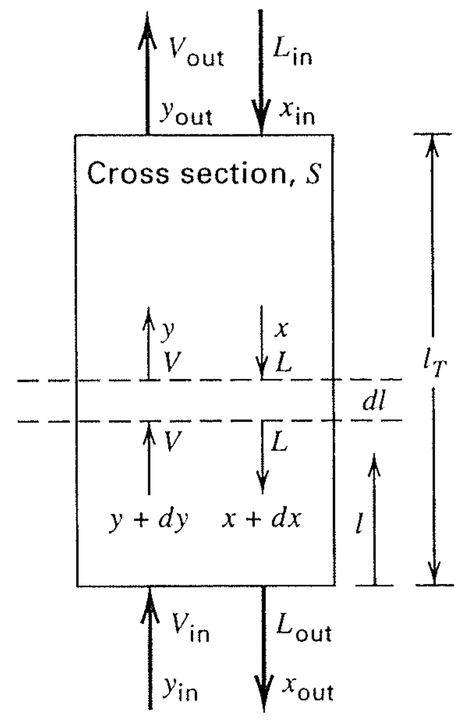

Figure 6.32 Differential contact in a countercurrent-flow, packed absorption column.

However, from Figure 6.31, for dilute solutions when the equilibrium curve is approximately a straight line through the origin,

$$\frac{y_I - y^*}{x_I - x} = \frac{\overline{ED}}{\overline{BE}} = K \tag{6-82}$$

and

$$\frac{x^* - x_I}{y - y_I} = \frac{\overline{CF}}{\overline{FB}} = \frac{1}{K} \tag{6-83}$$

where K is the K-value for the solute. Combining (6-80) with (6-82) and (6-81) with (6-83),

$$\frac{1}{K_y a} = \frac{1}{k_y a} + \frac{K}{k_x a} \tag{6-84}$$

and

$$\frac{1}{K_x a} = \frac{1}{k_x a} + \frac{1}{K k_y a} \tag{6-85}$$

Determination of the packed height of a column most commonly involves the overall gas-phase coefficient, $K_y a$, because the liquid usually has a strong affinity for the solute so that resistance to mass transfer is mostly in the gas. This is analogous to a trayed tower, where the tray efficiency from mass transfer considerations is commonly based on $K_{OG}a$ or N_{OG}. Consider the countercurrent-flow absorption column in Figure 6.32. For a dilute system, a differential material balance for a solute being absorbed over a differential height of packing dl, gives:

$$-V\,dy = K_y a(y - y^*)S\,dl \tag{6-86}$$

where S is the inside cross-sectional area of the tower. In integral form, with nearly constant terms placed outside the integral, (6-86) becomes

$$\frac{K_y a S}{V}\int_0^{l_T} dl = \frac{K_y a S l_T}{V} = \int_{y_{out}}^{y_{in}} \frac{dy}{y - y^*} \tag{6-87}$$

Solving for the packed height gives

$$l_T = \frac{V}{K_y a S}\int_{y_{out}}^{y_{in}} \frac{dy}{y - y^*} \tag{6-88}$$

Chilton and Colburn [43] suggested that the right-hand side of (6-88) be written as the product of two terms:

$$l_T = H_{OG} N_{OG} \tag{6-89}$$

where

$$H_{OG} = \frac{V}{K_y a S} \tag{6-90}$$

and

$$N_{OG} = \int_{y_{out}}^{y_{in}} \frac{dy}{y - y^*} \tag{6-91}$$

If (6-89) is compared to (6-73), it is seen that H_{OG} is analogous to HETP, as is N_{OG} to N_t.

The term H_{OG} is called the *overall height of a transfer unit* (HTU) based on the gas phase. Experimental data show that the HTU varies less with V than $K_y a$. The smaller the HTU, the more efficient is the contacting. The term N_{OG} is called the *overall number of transfer units* (NTU) based on the gas phase. It represents the overall change in solute mole fraction divided by the average mole-fraction driving force. The larger the NTU, the greater is the extent of contacting required.

Equation (6-91) was first integrated by Colburn [44]. By using the linear equilibrium condition $y^* = Kx$ to eliminate y^* and using the linear, solute material-balance operating line, (6-75), to eliminate x, the result is

$$\int_{y_{out}}^{y_{in}} \frac{dy}{y - y^*} = \int_{y_{out}}^{y_{in}} \frac{dy}{(1 - KV/L)y + y_{out}(KV/L) - Kx_{in}} \tag{6-92}$$

Letting $L/(KV) = A$, the absorption factor, and integrating (6-88), gives

$$N_{OG} = \frac{\ln\{[(A-1)/A][(y_{in} - Kx_{in})/(y_{out} - Kx_{in})] + (1/A)\}}{(A-1)/A} \tag{6-93}$$

By applying (6-93) and (6-90), the required packed height, l_T, can be determined from (6-89). However, (6-93) is very sensitive when $A < 0.9$.

The NTU (e.g., N_{OG}) and the HTU (e.g., H_{OG}) should not be confused with the number of equilibrium (theoretical) stages, N_t, and the HETP, respectively. However, when the operating and equilibrium lines are not only straight but also parallel, NTU = N_t and HTU = HETP. Otherwise, the NTU is greater than or less than N_t as shown in Figure 6.33 for the case of absorption. When the operating and equilibrium lines are straight but not parallel, then

$$\text{HETP} = H_{OG} \frac{\ln(1/A)}{(1-A)/A} \tag{6-94}$$

and

$$N_{OG} = N_t \frac{\ln(1/A)}{(1-A)/A} \tag{6-95}$$

Although the most common applications of the HTU and NTU are based on (6-89) to (6-91) and (6-93), a number of alternative groupings have been used, depending on the selected driving force for mass transfer and whether the overall basis is the gas phase, as above, or the liquid phase, where H_{OL} and N_{OL} apply. These groupings are summarized in Table 6.7. Included are driving forces based on partial pressures, p; mole ratios, X, Y; and concentrations, c; as well as mole fractions, x, y. Also included in Table 6.7 for later reference in the last section of this chapter are groupings for unimolecular diffusion (UMD) when solute concentration is not dilute. It is frequently necessary to convert a mass-transfer coefficient based on one type of driving force to another coefficient based on a different type of driving force. Table 3.15 gives the relationships among the different mass-transfer coefficients. The relationships include coefficients based on a concentration and mole-fraction driving force. In addition, a partial-pressure driving force is included for the gas phase.

EXAMPLE 6.9

Repeat Example 6.1 for absorption in a tower packed with 1.5-in. metal Pall rings. If $H_{OG} = 2.0$ ft, compute the required packed height.

SOLUTION

From Example 6.1, $V = 180$ kmol/h, $L = 151.5$ kmol/h, $y_{in} = 0.020$, $x_{in} = 0.0$, and $K = 0.57$. For 97% recovery of ethyl alcohol, by material balance,

$$y_{out} = \frac{(0.03)(0.02)(180)}{180 - (0.97)(0.02)(180)} = 0.000612$$

$$A = \frac{L}{KV} = \frac{151.5}{(0.57)(180)} = 1.477$$

$$\frac{y_{in}}{y_{out}} = \frac{0.020}{0.000612} = 32.68$$

From (6-93),

$$N_{OG} = \frac{\ln\{[(1.477-1)/1.477](32.68) + (1/1.477)\}}{(1.477-1)/1.477}$$

$$= 7.5 \text{ transfer units}$$

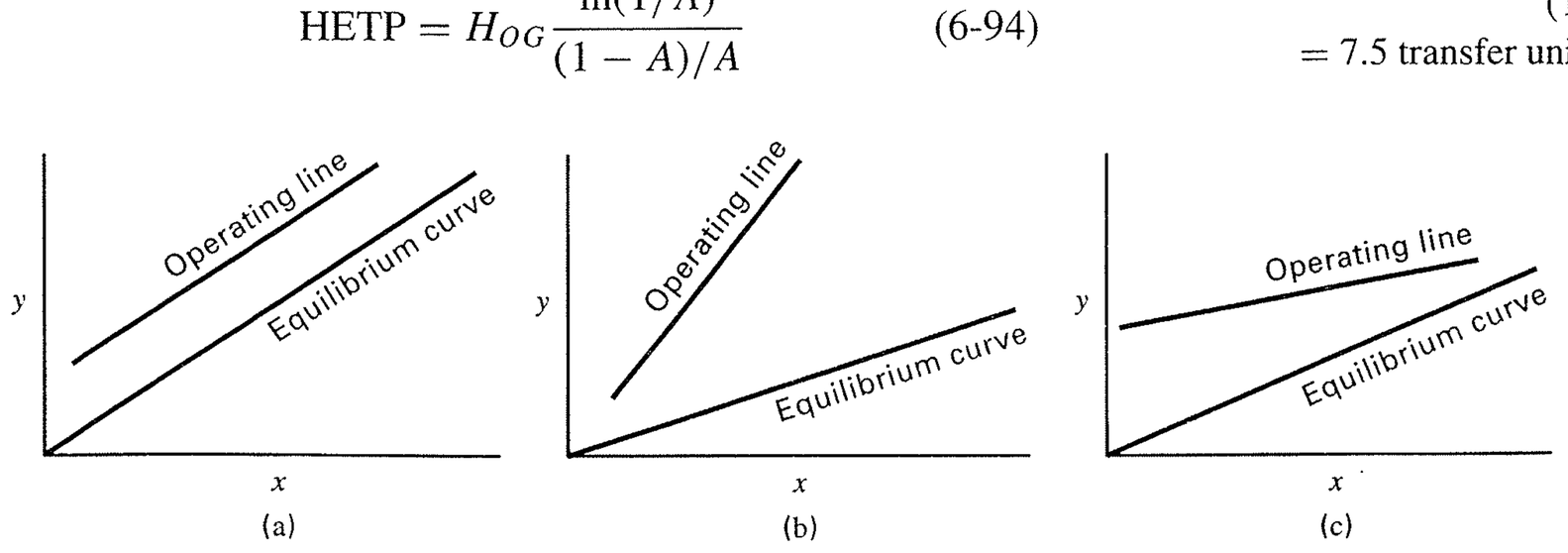

Figure 6.33 Relationship between the NTU and the number of theoretical stages N_t: (a) NTU = N_t; (b) NTU > N_t; (c) NTU < N_t.

Table 6.7 Alternative Mass-Transfer Coefficient Groupings

	Height of a Transfer Unit, HTU			Number of Transfer Units, NTU		
Driving Force	Symbol	EM Diffusion or Dilute UM Diffusion	UM Diffusion	Symbol	EM Diffusion[a] or Dilute UM Diffusion	UM Diffusion
1. $(y - y^*)$	H_{OG}	$\dfrac{V}{K_y aS}$	$\dfrac{V}{K'_y a(1-y)_{\text{LM}} S}$	N_{OG}	$\displaystyle\int \dfrac{dy}{(y-y^*)}$	$\displaystyle\int \dfrac{(1-y)_{\text{LM}}dy}{(1-y)(y-y^*)}$
2. $(p - p^*)$	H_{OG}	$\dfrac{V}{K_G aPS}$	$\dfrac{V}{K'_G a(1-y)_{\text{LM}} PS}$	N_{OG}	$\displaystyle\int \dfrac{dp}{(p-p^*)}$	$\displaystyle\int \dfrac{(P-p)_{\text{LM}}dp}{(P-p)(p-p^*)}$
3. $(Y - Y^*)$	H_{OG}	$\dfrac{V'}{K_Y aS}$	$\dfrac{V'}{K_Y aS}$	N_{OG}	$\displaystyle\int \dfrac{dY}{(Y-Y^*)}$	$\displaystyle\int \dfrac{dY}{(Y-Y^*)}$
4. $(y - y_{\text{I}})$	H_G	$\dfrac{V}{k_y aS}$	$\dfrac{V}{k'_y a(1-y)_{\text{LM}} S}$	N_G	$\displaystyle\int \dfrac{dy}{(y-y_{\text{I}})}$	$\displaystyle\int \dfrac{(1-y)_{\text{LM}}dy}{(1-y)(y-y_{\text{I}})}$
5. $(p - p_{\text{I}})$	H_G	$\dfrac{V}{k_p aPS}$	$\dfrac{V}{k'_p a(P-p)_{\text{LM}} S}$	N_G	$\displaystyle\int \dfrac{dp}{(p-p_{\text{I}})}$	$\displaystyle\int \dfrac{(P-p)_{\text{LM}}dp}{(P-p)(p-p_{\text{I}})}$
6. $(x^* - x)$	H_{OL}	$\dfrac{L}{K_x aS}$	$\dfrac{L}{K'_x a(1-x)_{\text{LM}} S}$	N_{OL}	$\displaystyle\int \dfrac{dx}{(x^*-x)}$	$\displaystyle\int \dfrac{(1-x)_{\text{LM}}dx}{(1-x)(x^*-x)}$
7. $(c^* - c)$	H_{OL}	$\dfrac{L}{K_L a(\rho_L/M_L)S}$	$\dfrac{L}{K'_L a(\rho_L/M_L - c)_{\text{LM}} S}$	N_{OL}	$\displaystyle\int \dfrac{dc}{(c^*-c)}$	$\displaystyle\int \dfrac{(\rho_L/M_L - c)_{\text{LM}}dx}{(\rho_L/M_L - c)(c^*-c)}$
8. $(X^* - X)$	H_{OL}	$\dfrac{L'}{K_X aS}$	$\dfrac{L'}{K_X aS}$	N_{OL}	$\displaystyle\int \dfrac{dX}{(X^*-X)}$	$\displaystyle\int \dfrac{dX}{(X^*-X)}$
9. $(x_{\text{I}} - x)$	H_L	$\dfrac{L}{k_x aS}$	$\dfrac{L}{k'_x a(1-x)_{\text{LM}} S}$	N_L	$\displaystyle\int \dfrac{dx}{(x_{\text{I}}-x)}$	$\displaystyle\int \dfrac{(1-x)_{\text{LM}}dx}{(1-x)(x_{\text{I}}-x)}$
10. $(c_{\text{I}} - c)$	H_L	$\dfrac{L}{k_L a(\rho_L/M_L)S}$	$\dfrac{L}{k'_L a(\rho_L/M_L - c)_{\text{LM}} S}$	N_L	$\displaystyle\int \dfrac{dc}{(c_{\text{I}}-c)}$	$\displaystyle\int \dfrac{(\rho_L/M_L - c)_{\text{LM}}dc}{(\rho_L/M_L - c)(c_{\text{I}}-c)}$

[a]The substitution $K_y = K'_y y_{\text{B}_{\text{LM}}}$ or its equivalent can be made.

The packed height, from (6-89), is

$$l_T = 2.0(7.5) = 15 \text{ ft}$$

Note that N_t for this example was determined in Example 6.1 to be about 6.1. The value of 7.5 for N_{OG} is greater than N_t because the slope of the operating line, L/G, is greater than the slope of the equilibrium line, K, so Figure 6.33b applies.

EXAMPLE 6.10

Experimental data have been obtained for air containing 1.6% by volume SO_2 being scrubbed with pure water in a packed column of 1.5 m^2 in cross-sectional area and 3.5 m in packed height. Entering gas and liquid flow rates are 0.062 and 2.2 kmol/s, respectively. If the outlet mole fraction of SO_2 in the gas is 0.004 and column temperature is near-ambient with $K_{SO_2} = 40$, calculate from the data:

(a) The N_{OG} for absorption of SO_2

(b) The H_{OG} in meters

(c) The volumetric, overall mass-transfer coefficient, $K_y a$ for SO_2 in kmol/m^3-s-(Δy).

SOLUTION

(a) Assume a straight operating line because the system is dilute in SO_2.

$$A = \frac{L}{KV} = \frac{2.2}{(40)(0.062)} = 0.89, \quad y_{\text{in}} = 0.016,$$
$$y_{\text{out}} = 0.004, \quad x_{\text{in}} = 0.0$$

From (6-93),

$$N_{OG} = \frac{\ln\{[(0.89-1)/0.89](0.016/0.004) + (1/0.89)\}}{(0.89-1)/0.89}$$
$$= 3.75$$

(b) $l_T = 3.5$ m. From (6-89), $H_{OG} = l_T/N_{OG} = 3.5/3.75 = 0.93$ m

(c) $V = 0.062$ kmol/s, $S = 1.5$ m^2.

From (6-90), $K_y a = V/H_{OG}S = 0.062/[(0.93)(1.5)] = 0.044$ kmol/m^3-s-(Δy)

EXAMPLE 6.11

A gaseous reactor effluent consisting of 2 mol% ethylene oxide in an inert gas is scrubbed with water at 30°C and 20 atm. The total gas feed rate is 2,500 lbmol/h, and the water rate entering the scrubber is 3,500 lbmol/h. The column, with a diameter of 4 ft, is packed in two 12-ft-high sections with 1.5-in. metal Pall rings. A liquid redistributor is located between the two packed sections. Under the operating conditions for the scrubber, the K-value for ethylene oxide is 0.85 and estimated values of $k_y a$ and $k_x a$ are 200 lbmol/h-ft^3-Δy and 165 lbmol/h-ft^3-Δx, respectively.

Calculate: (a) $K_y a$ and (b) H_{OG}.

SOLUTION

(a) From (6-84),

$$K_y a = \frac{1}{(1/k_y a) + (K/k_x a)} = \frac{1}{(1/200) + (0.85/165)}$$
$$= 98.5 \text{ lbmol/h-ft}^3\text{-}\Delta y$$

(b) $S = 3.14(4)^2/4 = 12.6 \text{ ft}^2$

From (6-90), $H_{OG} = V/K_y a S = 2{,}500/[(98.5)(12.6)] = 2.02$ ft.

Note that in this example, both gas-phase and liquid-phase resistances are important.

The value of H_{OG} can also be computed from values of H_G and H_L using equations in Table 6.7:

$$H_G = V/k_y a S = 2{,}500/[(200)(12.6)] = 1.0 \text{ ft}$$
$$H_L = L/k_x a S = 3{,}500/[(165)(12.6)] = 1.68 \text{ ft}$$

Substituting these two expressions and (6-90) into (6-84) gives the following relationship for H_{OG} in terms of H_G and H_L:

$$H_{OG} = H_G + H_L/A$$
$$A = L/KV = 3{,}500/[(0.85)(2{,}500)] = 1.65 \qquad (6\text{-}96)$$
$$H_{OG} = 1.0 + 1.68/1.65 = 2.02 \text{ ft}$$

6.8 PACKED-COLUMN EFFICIENCY, CAPACITY, AND PRESSURE DROP

Values of volumetric mass-transfer coefficients and corresponding HTUs depend on gas and/or liquid flow rates per unit inside cross-sectional area of the packed column. Therefore, column diameter must be estimated before determining required height of packing. The estimation of a suitable column diameter for a given system, packing, and operating conditions requires consideration of liquid holdup, flooding, and pressure drop.

Liquid Holdup

Typical experimental curves, taken from Billet [45] and shown also by Stichlmair, Bravo, and Fair [46], for specific pressure drop in meters of water head per meter of packed height, and specific liquid holdup in cubic meters per cubic meter of packed bed as a function of superficial gas velocity for different values of superficial water velocity are shown in Figures 6.34 and 6.35, respectively, for a 0.15-m-diameter column packed with 1-in. metal Bialecki rings to a height of 1.5 m and operated at 25°C and 1 bar. In Figure 6.34, the lowest curve corresponds to zero liquid flow, that is, the dry pressure drop. Over an almost 10-fold range of superficial air velocity (the velocity the air would have in the abscence of packing), the pressure drop for air flowing up through the packing is proportional to air velocity to the 1.86 power. As liquid flows down through the packing at an increasing rate, gas-phase pressure drop for a given gas velocity increases. However, below a certain limiting gas velocity, the curve for each liquid velocity is a straight line parallel to the dry-pressure-drop curve. In this region, the liquid holdup for each liquid velocity is constant, as shown in Figure 6.35. Thus, for a liquid velocity of 40 m/h, specific liquid holdup is 0.08 m^3/m^3 of packed bed until a superficial gas velocity of 1.0 m/h is reached. Instead of a packed-column void fraction, ϵ, of 0.94 for the gas to flow through (corresponding to zero liquid flow), the effective void fraction is reduced by

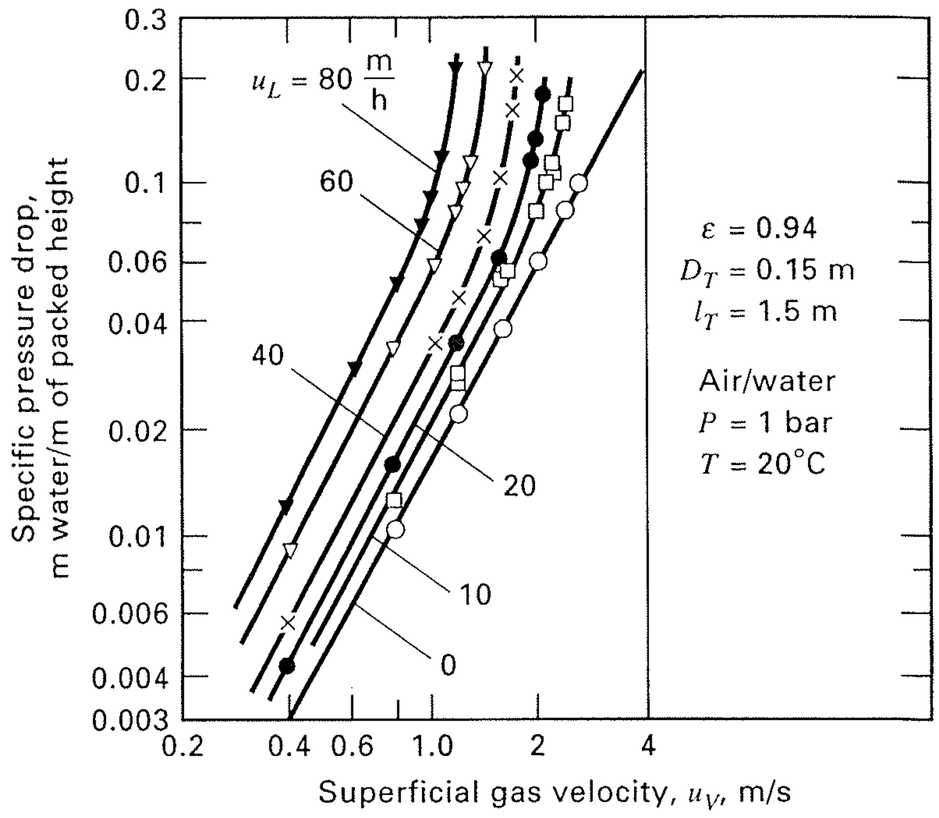

Figure 6.34 Specific pressure drop for dry and irrigated 25-mm metal Bialecki rings.

[From R. Billet, *Packed Column Analysis and Design,* Ruhr-University Bochum (1989) with permission.]

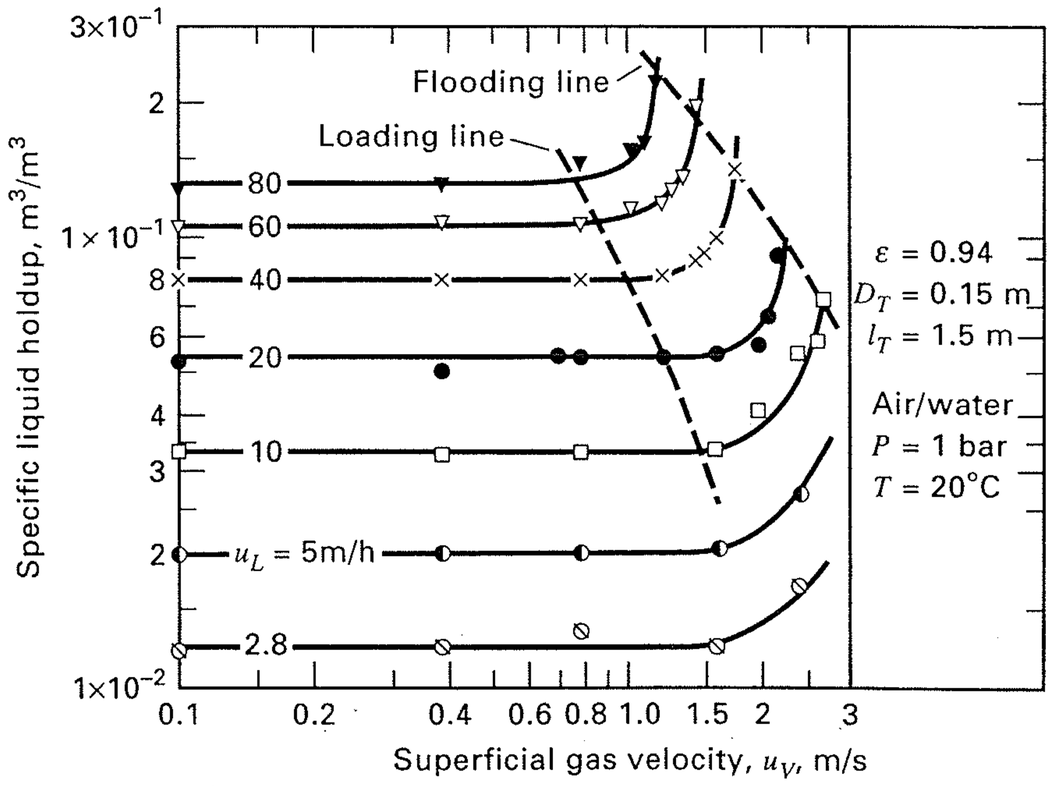

Figure 6.35 Specific liquid holdup for irrigated 25-mm metal Bialecki rings.

[From R. Billet, *Packed Column Analysis and Design,* Ruhr-University Bochum (1989) with permission.]

the liquid holdup to $0.94 - 0.08 = 0.86$, causing an increased pressure drop. For a given liquid velocity, the upper limit to the gas velocity for a constant liquid holdup is termed the *loading point.* Below this point, the gas phase is the continuous phase. Above this point, liquid begins to accumulate or load the bed, replacing gas holdup and causing a sharp increase in pressure drop. Finally, a gas velocity is reached at which the liquid surface is continuous across the top of the packing and the column is flooded. At the *flooding point,* the drag force of the counterflowing gas is sufficient to entrain the entire liquid. Approximate loci of both loading and flooding points are included in Figure 6.35.

The region between the loading point and the flooding point is the *loading region,* where significant liquid entrainment is observed, liquid holdup increases sharply, mass-transfer efficiency decreases, and column operation is unstable. Typically, according to Billet [45], the superficial gas velocity at the loading point is approximately 70% of that at the flooding point. Although a packed column can operate in the loading region, most packed columns are designed to operate at or below the loading point, in the *preloading region.*

The specific liquid holdup in the preloading region has been found, from extensive experiments by Billet and Schultes [47, 69] for a wide variety of random and structured packings and, for a number of gas–liquid systems, to depend on packing characteristics, and the viscosity, density, and superficial velocity of the liquid, u_L, according to the dimensionless expression

$$h_L = \left(12\frac{N_{\mathrm{Fr}_L}}{N_{\mathrm{Re}_L}}\right)^{1/3}\left(\frac{a_h}{a}\right)^{2/3} \tag{6-97}$$

where

$$N_{\mathrm{Re}_L} = \text{liquid Reynolds number} = \frac{\text{inertial force}}{\text{viscous force}} = \frac{u_L\rho_L}{a\mu_L} = \frac{u_L}{av_L} \tag{6-98}$$

where v_L is the kinematic viscosity.

$$N_{\mathrm{Fr}_L} = \text{liquid Froude number} = \frac{\text{inertial force}}{\text{gravitational force}} = \frac{u_L^2 a}{g} \tag{6-99}$$

and the ratio of specific hydraulic area of packing, a_h, to specific surface area of packing, a, is given by

$$a_h/a = C_h N_{\mathrm{Re}_L}^{0.15} N_{\mathrm{Fr}_L}^{0.1} \quad \text{for } N_{\mathrm{Re}_L} < 5 \tag{6-100}$$

$$a_h/a = 0.85\, C_h N_{\mathrm{Re}_L}^{0.25} N_{\mathrm{Fr}_L}^{0.1} \quad \text{for } N_{\mathrm{Re}_L} \geq 5 \tag{6-101}$$

Values of $a_h/a > 1$ are reasonable because of the creation of droplets and jet flow beside the rivulets that cover the packing surface [70].

Values of a and C_h are characteristic of the particular type and size of packing, as listed, together with packing void fraction, ϵ, and other packing constants in Table 6.8. Because the specific liquid holdup is constant in the preloading region, as seen in Figure 6.35, (6-97) does not involve gas-phase properties or gas velocity.

At low liquid velocities, liquid holdup can become so small that the packing is no longer completely wetted. When this occurs, packing efficiency decreases dramatically, particularly for aqueous systems of high surface tension. To ensure adequate wetting of packing, proven liquid distributors and redistributors should be used and superficial liquid velocities should exceed the following values:

Type of Packing Material	$u_{L_{\min}}$, m/s
Ceramic	0.00015
Oxidized or etched metal	0.0003
Bright metal	0.0009
Plastic	0.0012

EXAMPLE 6.12

An absorption column is to be designed using oil absorbent with a kinematic viscosity of three times that of water at 20°C. The superficial liquid velocity will be 0.01 m/s, which is safely above the minimum value for good wetting. The superficial gas velocity will be such that operation will be in the preloading region. Two packing materials are being considered: (1) randomly packed 50-mm metal Hiflow rings and (2) metal Montz B1-200 structured packing. Estimate the specific liquid holdup for each of these two packings.

SOLUTION

From Table 6.8,

Packing	a, m^2/m^3	ϵ	C_h
50-mm metal Hiflow rings	92.3	0.977	0.876
Montz metal B1-200	200.0	0.979	0.547

At 20°C for water, kinematic viscosity, $v = \mu/\rho = 1 \times 10^{-6}$ m^2/s. Therefore, for the oil, $\mu/\rho = 3 \times 10^{-6}$ m^2/s. From (6-98) and (6-99),

$$N_{\mathrm{Re}_L} = \frac{0.01}{3 \times 10^{-6} a} \qquad N_{\mathrm{Fr}_L} = \frac{(0.01)^2 a}{9.8}$$

Therefore,

Packing	N_{Re_L}	N_{Fr_L}
Hiflow	36.1	0.000942
Montz	16.67	0.00204

From (6-101), since $N_{\mathrm{Re}_L} > 5$, for the Hiflow packing, $a_h/a = (0.85)(0.876)(36.1)^{0.25}(0.000942)^{0.1} = 0.909$. For the Montz packing, $a_h/a = 0.85(0.547)(16.67)^{0.25}(0.00204)^{0.10} = 0.506$.

From (6-97), for the Hiflow packing,

$$h_L = \left[\frac{12(0.000942)}{36.1}\right]^{1/3}(0.909)^{2/3} = 0.0637 \text{ m}^3/\text{m}^3$$

For the Montz packing,

$$h_L = \left[\frac{12(0.0204)}{16.67}\right]^{1/3}(0.506)^{2/3} = 0.0722 \text{ m}^3/\text{m}^3$$

Note that for the Hiflow packing, the void fraction available for gas flow is reduced by the liquid flow from $\epsilon = 0.977$ (Table 6.8) to $0.977 - 0.064 = 0.913$ m^3/m^3. For the Montz packing, the reduction is from 0.979 to 0.907 m^3/m^3.

Table 6.8 Characteristics of Packings

Packing	Material	Size	F_P, ft²/ft³	a, m²/m³	ϵ, m³/m³	C_h	C_p	C_L	C_V	C_s	C_{Fl}
				Characteristics from Billet							
				Random Packings							
Berl saddles	Ceramic	25 mm	110	260.0	0.680	0.620		1.246	0.387		
Berl saddles	Ceramic	13 mm	240	545.0	0.650	0.833		1.364	0.232		
Bialecki rings	Metal	50 mm		121.0	0.966	0.798	0.719	1.721	0.302	2.916	1.896
Bialecki rings	Metal	35 mm		155.0	0.967	0.787	1.011	1.412	0.390	2.753	1.885
Bialecki rings	Metal	25 mm		210.0	0.956	0.692	0.891	1.461	0.331	2.521	1.856
DIN-PAK rings	Plastic	70 mm		110.7	0.938	0.991	0.378	1.527	0.326	2.970	1.912
DIN-PAK rings	Plastic	47 mm		131.2	0.923	1.173	0.514	1.690	0.354	2.929	1.991
Envi Pac rings	Plastic	80 mm, no. 3		60.0	0.955	0.641	0.358	1.603	0.257	2.846	1.522
Envi Pac rings	Plastic	60 mm, no. 2		98.4	0.961	0.794	0.338	1.522	0.296	2.987	1.864
Envi Pac rings	Plastic	32 mm, no. 1		138.9	0.936	1.039	0.549	1.517	0.459	2.944	2.012
Glitsch rings	Metal	30 PMK		180.5	0.975	0.930	0.851	1.920	0.450	2.694	1.900
Glitsch rings	Metal	30 P		164.0	0.959	0.851	1.056	1.577	0.398	2.564	1.760
Glitsch CMR rings	Metal	1.5″		174.9	0.974	0.935	0.632			2.697	1.841
Glitsch CMR rings	Metal	1.5″, T		188.0	0.972	0.870	0.627			2.790	1.870
Glitsch CMR rings	Metal	1.0″		232.5	0.971	1.040	0.641			2.703	1.996
Glitsch CMR rings	Metal	0.5″		356.0	0.952		0.882	2.038	0.495	2.644	2.178
Cascade minirings	Metal	30 PMK		180.2	0.975	0.930					
Cascade minirings	Metal	30 P		168.9	0.958	0.851					
Cascade minirings	Metal	1.5″ CMR, T		188.0	0.972	0.870					
Cascade minirings	Metal	1.5″ CMR	29	174.9	0.974	0.935					
Cascade minirings	Metal	1.0″ CMR	40	232.5	0.971	1.040					
Cascade minirings	Metal	0.5″ CMR		356.0	0.955	1.338					
Hackettes	Plastic	45 mm		139.5	0.928	0.643	0.399			2.832	1.966
Hiflow rings	Ceramic	75 mm	15	54.1	0.868		0.435				
Hiflow rings	Ceramic	50 mm	29	89.7	0.809		0.538	1.377	0.379	2.819	1.694
Hiflow rings	Ceramic	38 mm	37	111.8	0.788		0.621	1.659	0.464	2.840	1.930
Hiflow rings	Ceramic	20 mm, 6 stg.		265.8	0.776	0.958					
Hiflow rings	Ceramic	20 mm, 4 stg.		261.2	0.779	1.167	0.628	1.744	0.465		
Hiflow rings	Metal	50 mm	16	92.3	0.977	0.876	0.421	1.168	0.408	2.702	1.626
Hiflow rings	Metal	25 mm	42	202.9	0.962	0.799	0.689	1.641	0.402	2.918	2.177
Hiflow rings	Plastic	90 mm	9	69.7	0.968		0.276				
Hiflow rings	Plastic	50 mm, hydr.		118.4	0.925		0.311	1.553	0.369	2.894	1.871
Hiflow rings	Plastic	50 mm	20	117.1	0.924	1.038	0.327	1.487	0.345		

Hiflow rings	Plastic	25 mm		194.5	0.918		0.741	1.577	0.390	2.841	1.989
Hiflow rings, super	Plastic	50 mm, S		82.0	0.942		0.414	1.219	0.342	2.866	1.702
Hiflow saddles	Plastic	50 mm		86.4	0.938		0.454				
Intalox saddles	Ceramic	50 mm	40	114.6	0.761		0.747				
Intalox saddles	Plastic	50 mm	28	122.1	0.908		0.758				
NORPAC rings	Plastic	50 mm	14	86.8	0.947	0.651	0.350	1.080	0.322	2.959	1.786
NORPAC rings	Plastic	35 mm	21	141.8	0.944	0.587	0.371	0.756	0.425	3.179	2.242
NORPAC rings	Plastic	25 mm, type B		202.0	0.953	0.601	0.397	0.883	0.366	3.277	2.472
NORPAC rings	Plastic	25 mm, 10 stg.		197.9	0.920		0.383	0.976	0.410	2.865	2.083
NORPAC rings	Plastic	25 mm	31	180.0	0.927	0.601					
NORPAC rings	Plastic	22 mm		249.0	0.913		0.397				
NORPAC rings	Plastic	15 mm		311.4	0.918	0.343	0.365				
Pall rings	Ceramic	50 mm	43	155.2	0.754	1.066	0.233	1.278	0.333	3.793	3.024
Pall rings	Metal	50 mm	27	112.6	0.951	0.784	0.763	1.192	0.410	2.725	1.580
Pall rings	Metal	35 mm	40	139.4	0.965	0.644	0.967	1.012	0.341	2.629	1.679
Pall rings	Metal	25 mm	56	223.5	0.954	0.719	0.957	1.440	0.336	2.627	2.083
Pall rings	Metal	15 mm	70	368.4	0.933	0.590	0.990				
Pall rings	Plastic	50 mm	26	111.1	0.919	0.593	0.698	1.239	0.368	2.816	1.757
Pall rings	Plastic	35 mm	40	151.1	0.906	0.718	0.927	0.856	0.380	2.654	1.742
Pall rings	Plastic	25 mm	55	225.0	0.887	0.528	0.865	0.905	0.446	2.696	2.064
Raflux rings	Plastic	15 mm		307.9	0.894	0.491	0.595	1.913	0.370	2.825	2.400
Ralu flow	Plastic	1		165	0.940	0.640	0.485	1.486	0.360	3.612	2.401
Ralu flow	Plastic	2		100	0.945	0.640	0.350	1.270	0.320	3.412	2.174
Ralu rings	Plastic	50 mm, hydr.		94.3	0.939	0.439		1.481	0.341		
Ralu rings	Plastic	50 mm		95.2	0.983	0.640	0.468	1.520	0.303	2.843	1.812
Ralu rings	Plastic	38 mm		150	0.930	0.640	0.672	1.320	0.333	2.843	1.812
Ralu rings	Plastic	25 mm		190	0.940	0.719	0.800	1.320	0.333	2.841	1.989
Ralu rings	Metal	50 mm		105	0.975	0.784	0.763	1.192	0.345	2.725	1.580
Ralu rings	Metal	38 mm		135	0.965	0.644	1.003	1.277	0.341	2.629	1.679
Ralu rings	Metal	25 mm		215	0.960	0.714	0.957	1.440	0.336	2.627	2.083
Raschig rings	Carbon	25 mm		202.2	0.720	0.623		1.379	0.471		
Raschig rings	Ceramic	25 mm	179	190.0	0.680	0.577	1.329	1.361	0.412		
Raschig rings	Ceramic	15 mm	380	312.0	0.690	0.648		1.276	0.401		
Raschig rings	Ceramic	10 mm	1,000	440.0	0.650	0.791		1.303	0.272		
Raschig rings	Ceramic	6 mm	1,600	771.9	0.620	1.094		1.130			
Raschig rings	Metal	15 mm	170	378.4	0.917	0.455					
Raschig rings	Ceramic	25		190.0	0.680	0.577	1.329	1.361	0.412	2.454	1.899
Raschig Super-rings	Metal	0.3		315	0.960	0.750	0.760	1.500	0.450	3.560	2.340

(*Continued*)

Table 6.8 *(Continued)*

				Characteristics from Billet							
Packing	Material	Size	F_P, ft^2/ft^3	a, m^2/m^3	ϵ, m^3/m^3	C_h	C_p	C_L	C_V	C_s	C_{Fl}
Raschig Super-rings	Metal	0.5		250	0.975	0.620	0.780	1.450	0.430	3.350	2.200
Raschig Super-rings	Metal	1		160	0.980	0.750	0.500	1.290	0.440	3.491	2.200
Raschig Super-rings	Metal	2		97.6	0.985	0.720	0.464	1.323	0.400	3.326	2.096
Raschig Super-rings	Metal	3		80	0.982	0.620	0.430	0.850	0.300	3.260	2.100
Raschig Super-rings	Plastic	2		100	0.960	0.720	0.377	1.250	0.337	3.326	2.096
Tellerettes	Plastic	25 mm	40	190.0	0.930	0.588	0.538	0.899		2.913	2.132
Top-Pak rings	Aluminum	50 mm		105.5	0.956	0.881	0.604	1.326	0.389	2.528	1.579
VSP rings	Metal	50 mm, no. 2		104.6	0.980	1.135	0.773	1.222	0.420	2.806	1.689
VSP rings	Metal	25 mm, no. 1		199.6	0.975	1.369	0.782	1.376	0.405	2.755	1.970
Structured Packings											
Euroform	Plastic	PN-110		110.0	0.936	0.511	0.250	0.973	0.167	3.075	1.975
Gempak	Metal	A2 T-304		202.0	0.977	0.678	0.344			2.986	2.099
Impulse	Ceramic	100		91.4	0.838	1.900	0.417	1.317	0.327	2.664	1.655
Impulse	Metal	250		250.0	0.975	0.431	0.262	0.983	0.270	2.610	1.996
Koch-Sulzer	Metal	CY	70								
Koch-Sulzer	Metal	BX	21								
Mellapak	Plastic	250 Y	22	250.0	0.970	0.554	0.292			3.157	2.464
Montz	Metal	B1-100		100.0	0.987	0.626					
Montz	Metal	B1-200		200.0	0.979	0.547	0.355	0.971	0.390	3.116	2.339
Montz	Metal	B1-300	33	300.0	0.930	0.482	0.295	1.165	0.422	3.098	2.464
Montz	Plastic	C1-200		200.0	0.954		0.453	1.006	0.412		
Montz	Plastic	C2-200		200.0	0.900		0.481	0.739		2.653	1.973
Ralu Pak	Metal	YC-250		250.0	0.945	0.650	0.191	1.334	0.385	3.178	2.558

Column Diameter and Pressure Drop

Most packed columns consist of cylindrical vertical vessels. The column diameter is determined so as to safely avoid flooding and operate in the preloading region with a pressure drop of no greater than 1.5 in. of water head per foot of packed height (equivalent to 0.054 psi/ft of packing). In addition, for random packings, a nominal packing diameter not greater than one-eighth of the diameter of the column is selected; otherwise, poor distribution of liquid and vapor flow over the cross-sectional area of the column can occur, with liquid tending to migrate to the wall of the column.

Flooding data for packed columns with countercurrent flow of liquid and gas were first correlated successfully by Sherwood et al. [26], who used the same liquid-to-gas kinetic energy ratio, $F_{LV} = (LM_L/VM_V)(\rho_V/\rho_L)^{0.5}$, already discussed for the correlation of flooding and entrainment in trayed towers, as shown in Figures 6.24 and 6.28, respectively. The superficial gas velocity, u_V, was embedded in the dimensionless term $u_V^2 a/g\epsilon^3$, which was arrived at by considering the square of the actual gas velocity, u_V^2/ϵ^2, the hydraulic radius, $r_H = \epsilon/a$, which is the volume available for flow divided by the wetted surface area of the packing, and the gravitational acceleration, g, to give the dimensionless expression, $u_V^2 a/g\epsilon^3 = u_V^2 F_P/g$. The ratio, a/ϵ^3, is a function of the packing only, and is known as the packing factor, F_P. Values of a, ϵ, and F_P are included in Table 6.8. In some cases, F_P is a modified packing factor, treated as an empirical constant, backed out from experimental data so as to fit a generalized correlation. Additional factors were added by Sherwood et al. to account for liquid density and viscosity, and gas density.

In 1954, Leva [48] used experimental data on ring and saddle packings to extend the Sherwood et al. [26] flooding correlation to include lines of constant pressure drop, with the resulting chart becoming known as the generalized pressure-drop correlation (GPDC).

A modern version of the GPDC chart is that of Leva [49], as shown in Figure 6.36a. The abscissa is the same F_{LV} parameter, but the ordinate is given by

$$Y = \frac{u_V^2 F_P}{g}\left(\frac{\rho_V}{\rho_{H_2O_{(L)}}}\right) f\{\rho_L\} f\{u_L\} \qquad (6\text{-}102)$$

where the density of H_2O is taken as 62.4 lb/ft^3 with ρ_V in the same units. The functions $f\{\rho_L\}$ and $f\{\mu_L\}$ are corrections for liquid properties as given by Figures 6.36b and 6.36c, respectively.

For given fluid flow rates and properties, and a given packing material, the GPDC chart is used to compute $u_{V,f}$, the superficial gas velocity at flooding. Then a fraction of flooding, f, is selected (usually from 0.5 to 0.7), followed by calculation of the tower diameter from an equation similar to (6-44):

$$D_T = \left(\frac{4VM_V}{f u_{V,f}\pi\rho_V}\right)^{0.5} \qquad (6\text{-}103)$$

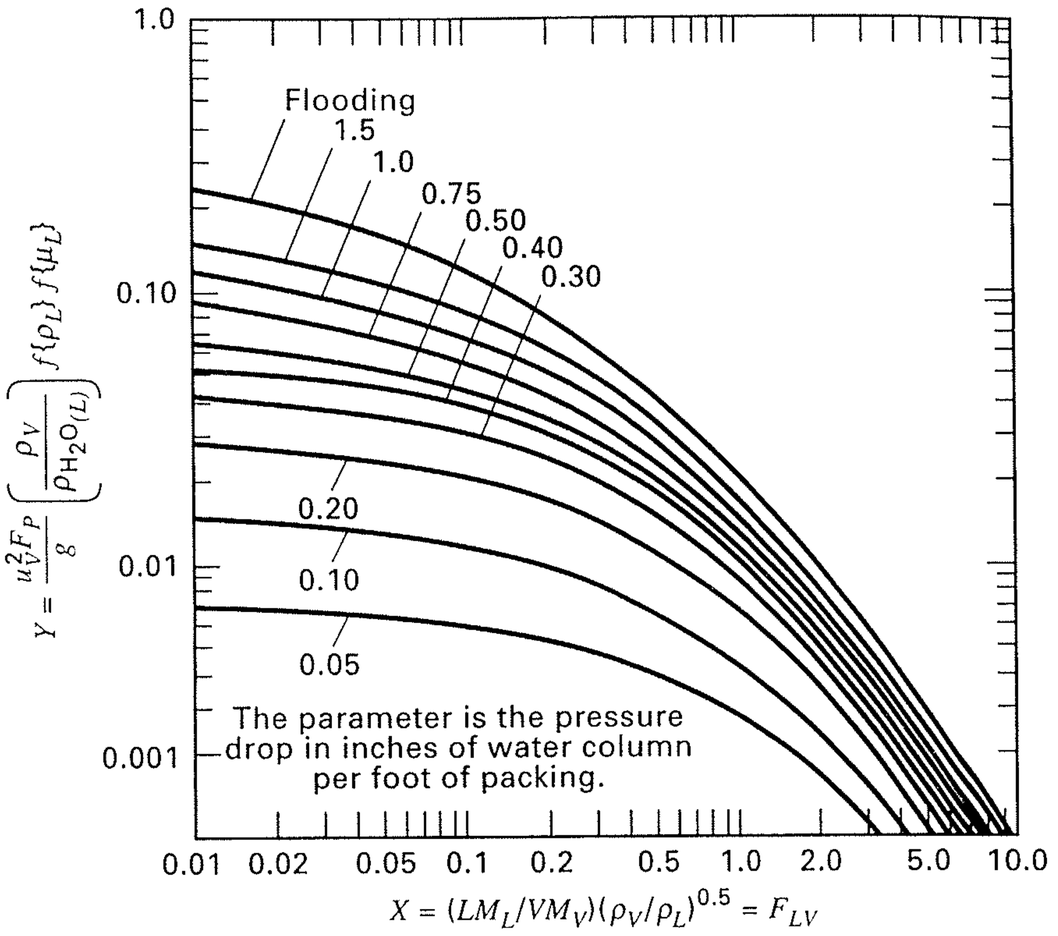

Figure 6.36 (a) Generalized pressure-drop correlation of Leva for packed columns. (b) Correction factor for liquid density. (c) Correction factor for liquid viscosity.
[From M. Leva, *Chem. Eng. Prog.*, **88** (1), 65–72 (1992) with permission.]

EXAMPLE 6.13

Air containing 5 mol% NH_3 at a total flow rate of 40 lbmol/h enters a packed column operating at 20°C and 1 atm, where 90% of the ammonia is scrubbed by a countercurrent flow of 3,000 lb/h of water. Use the GPDC chart of Figure 6.36 to estimate the superficial, gas-flooding velocity, the column inside diameter for

operation at 70% of flooding, and the pressure drop per foot of packing for two packing materials:

(a) One-inch ceramic Raschig rings ($F_P = 179$ ft^2/ft^3)

(b) One-inch metal IMTP packing ($F_P = 41$ ft^2/ft^3)

SOLUTION

Because the superficial gas velocity is highest at the bottom of the column, calculations are made for conditions there.

Inlet gas:

$$M_V = 0.95(29) + 0.05(17) = 28.4, \quad V = 40 \text{ lbmol/h}$$
$$\rho_V = PM_V/RT = (1)(28.4)/[(0.730)(293)(1.8)]$$
$$= 0.0738 \text{ lb/ft}^3$$

Exiting liquid:

Ammonia absorbed = 0.90(0.05)(40)(17) = 30.6 lb/h or 1.8 lbmol/h

Water rate (neglecting any stripping by the gas) = 3,000 lb/h or 166.7 lbmol/h

Mole fraction of ammonia = 1.8/(166.7 + 1.8) = 0.0107

$$M_L = 0.0107(17) + (0.9893)(18) = 17.9,$$
$$L = 1.8 + 166.7 = 168.5 \text{ lbmol/h}$$

Take: $\rho_L = 62.4$ lb/ft^3 and $\mu_L = 1.0$ cP

Now,

$$X = F_{LV}(\text{abscissa in Figure 6.36a})$$
$$= \frac{(168.5)(17.9)}{(40)(28.4)}\left(\frac{0.0738}{62.4}\right)^{0.5} = 0.092$$

From Figure 6.36a, $Y = 0.125$ at flooding.

From Figure 6.36b, $f\{\rho_L\} = 1.14$.

From Figure 6.36c, $f\{\mu_L\} = 1.0$.

From (6-102),

$$u_V^2 = 0.125\left(\frac{g}{F_P}\right)\frac{62.4}{(0.0738)(1.14)(1.0)} = 92.7\, g/F_P\,.$$

Using $g = 32.2$ ft/s^2,

Packing Material	F_P, ft^2/ft^3	u_o, ft/s
Raschig rings	179	4.1
IMTP packing	41	8.5

For $f = 0.70$, using (6-103),

Packing Material	$fu_{V,f}$, ft/s	D_T, in.
Raschig rings	2.87	16.5
IMTP packing	5.95	11.5

From Figure 6.36a, for $F_{LV} = 0.092$ and $Y = 0.70^2(0.125) = 0.0613$ at 70% of flooding, the pressure drop is 0.88 in. of water head per foot of packed height for both packings.

Based on these results, the IMTP packing has a much greater capacity than the Raschig rings, since the required column cross-sectional area is reduced by about 50%.

Experimental flooding-point data for a variety of packing materials are in reasonable agreement with the upper curve of the GPDC chart of Figure 6.36. Unfortunately, such good agreement is not always the case for pressure drop, particularly for operation at superficial vapor velocities above 50% of flooding, where pressure drop is greater than 0.5 in. of water head per foot of packed height. Reasons for the difficulty of achieving a simple generalization of pressure drop measurements are discussed in detail by Kister [33]. As an example of the possible magnitude of the disparity, the predicted pressure drop of 0.88 in. of water per foot in Example 6.13 for operation with IMTP packing at 70% of flooding is in poor agreement with the value of 0.63 in. of water head per foot determined from data supplied by the packing manufacturer.

If Figure 6.36a is crossplotted as pressure drop versus Y for constant values of F_{LV}, it is found that a pressure drop of from 2.5 to 3 in. of water head per foot is predicted at the flooding condition for all packings. However, studies by Kister and Gill [33, 50] for both random and structured packings show that the pressure drop at flooding is strongly dependent on the packing factor, F_P, by the empirical expression

$$\Delta P_{\text{flood}} = 0.115 F_P^{0.7} \tag{6-104}$$

where ΔP_{flood} has units of inches of water head per foot of packed height and F_P has units of ft^2/ft^3. As seen in Table 6.8, the range of F_P is from about 10 to 100. Thus, (6-103) predicts pressure drops at flooding from as low as 0.6 to as high as 3 in. of water head per foot of packed height. Kister and Gill also give an interpolation procedure for estimating pressure drop, which utilizes experimental data in conjunction with a GPDC-type plot.

Theoretically based models for predicting pressure drop in packed beds with countercurrent gas–liquid flows have been presented by Stichlmair et al. [46], who use a particle model, and Billet and Schultes [51, 69], who use a channel model. Both models extend well-accepted equations for dry-bed pressure drop to account for the effect of liquid holdup. Billet and Schultes [69] include a semitheoretical model for predicting the superficial vapor velocity at the loading point, $u_{V,l}$, which provides an alternative, perhaps more accurate, method for estimating column diameter. Their model, which is based on a liquid velocity of zero at the phase boundary at the loading point, gives

$$u_{V,l} = \left(\frac{g}{\Psi_l}\right)^{1/2}\left[\frac{\epsilon}{a^{1/6}} - a^{1/2}\xi_l^{1/3}\right]\xi_l^{1/6}\left(\frac{\rho_L}{\rho_V}\right)^{1/2} \tag{6-105}$$

where $u_{V,l}$ is in m/s,

g = gravitational acceleration = 9.807 m/s^2

$$\Psi_l = \frac{g}{C^2}\left[F_{LV}\left(\frac{\mu_L}{\mu_V}\right)^{0.4}\right]^{-2n_s} \tag{6-106}$$

ϵ and a are obtained from Table 6.8,

F_{LV} = kinetic energy ratio of Figures 6.24 and 6.36a,

$$\xi_l = \left(12\frac{\mu_L}{g\rho_L}u_{L,l}\right) \tag{6-107}$$

μ_L and μ_V are in kg/m-s

ρ_L and ρ_V are in kg/m^3

$u_{L,l}$ = superficial liquid velocity at loading point

$$= u_{V,l}\frac{\rho_V L M_L}{\rho_L V M_V} \text{ in m/s}$$

The values for n_s and C depend on the value of the kinetic energy ratio as follows:

If $F_{LV} \leq 0.4$, the liquid trickles downward over the packing as a disperse phase and $n_s = -0.326$, while $C = C_s$ from Table 6.8.

If $F_{LV} > 0.4$, the column holdup reaches such a large value that the empty spaces within the bed close up and the liquid flows downward as a continuous phase while the gas rises in the form of bubbles, with $n_s = -0.723$ and

$$C = 0.695\left(\frac{\mu_L}{\mu_V}\right)^{0.1588} C_s \quad \text{(from Table 6.8)} \qquad (6\text{-}108)$$

Billet and Schultes [69] also present a model for predicting the superficial vapor velocity at the flooding point, $u_{V,f}$, that involves the flooding constant, C_{Fl}, in Table 6.8, but a suitable expression is

$$u_{V,f} = \frac{u_{V,l}}{0.7} \qquad (6\text{-}109)$$

When a gas flows through a packed column under conditions of no liquid flow, a correlation for the pressure drop can be obtained in a manner similar to that for flow through an empty, straight pipe, by plotting a modified friction factor against a modified Reynolds number as shown in Figure 6.37 from the widely used study by Ergun [52]. In this plot, in which D_P is an effective packing material diameter, it can be seen that at low, superficial gas velocities (modified $N_{\text{Re}} < 10$), typical of laminar flow, the pressure drop per unit height is proportional to the superficial vapor velocity, u_V. At high gas velocities, typical of turbulent flow, the pressure drop per unit height approaches a dependency of the square of the gas velocity. Most packed columns used for separations operate in the turbulent region (modified $N_{\text{Re}} > 1{,}000$). Thus, dry pressure-drop data shown in Figure 6.34 for Bialecki rings show an exponential dependency on gas velocity of about 1.86. Also, as shown in Figure 6.34, when liquid flows countercurrent to the gas in the preloading region, this same dependency continues, but at a higher pressure drop because the volume for gas flow decreases due to liquid holdup.

Based on extensive experimental studies using more than 50 different packing materials, including structured packings, Billet and Schultes [51, 69] developed a correlation for dry-gas pressure drop, ΔP_o, similar in form to that of Figure 6.37. Their dimensionally consistent correlating equation is

$$\frac{\Delta P_o}{l_T} = \Psi_o \frac{a}{\epsilon^3}\frac{u_V^2 \rho_V}{2}\frac{1}{K_W} \qquad (6\text{-}110)$$

where

l_T = height of packing

K_W = a wall factor

K_W can be important for columns with an inadequate ratio of effective packing diameter to inside column diameter, and is given by

$$\frac{1}{K_W} = 1 + \frac{2}{3}\left(\frac{1}{1-\epsilon}\right)\frac{D_P}{D_T} \qquad (6\text{-}111)$$

where the effective packing diameter, D_P, is determined from

$$D_P = 6\left(\frac{1-\epsilon}{a}\right) \qquad (6\text{-}112)$$

The dry-packing resistance coefficient (a modified friction factor), Ψ_o, is given by the empirical expression

$$\Psi_o = C_p\left(\frac{64}{N_{\text{Re}_V}} + \frac{1.8}{N_{\text{Re}_V}^{0.08}}\right) \qquad (6\text{-}113)$$

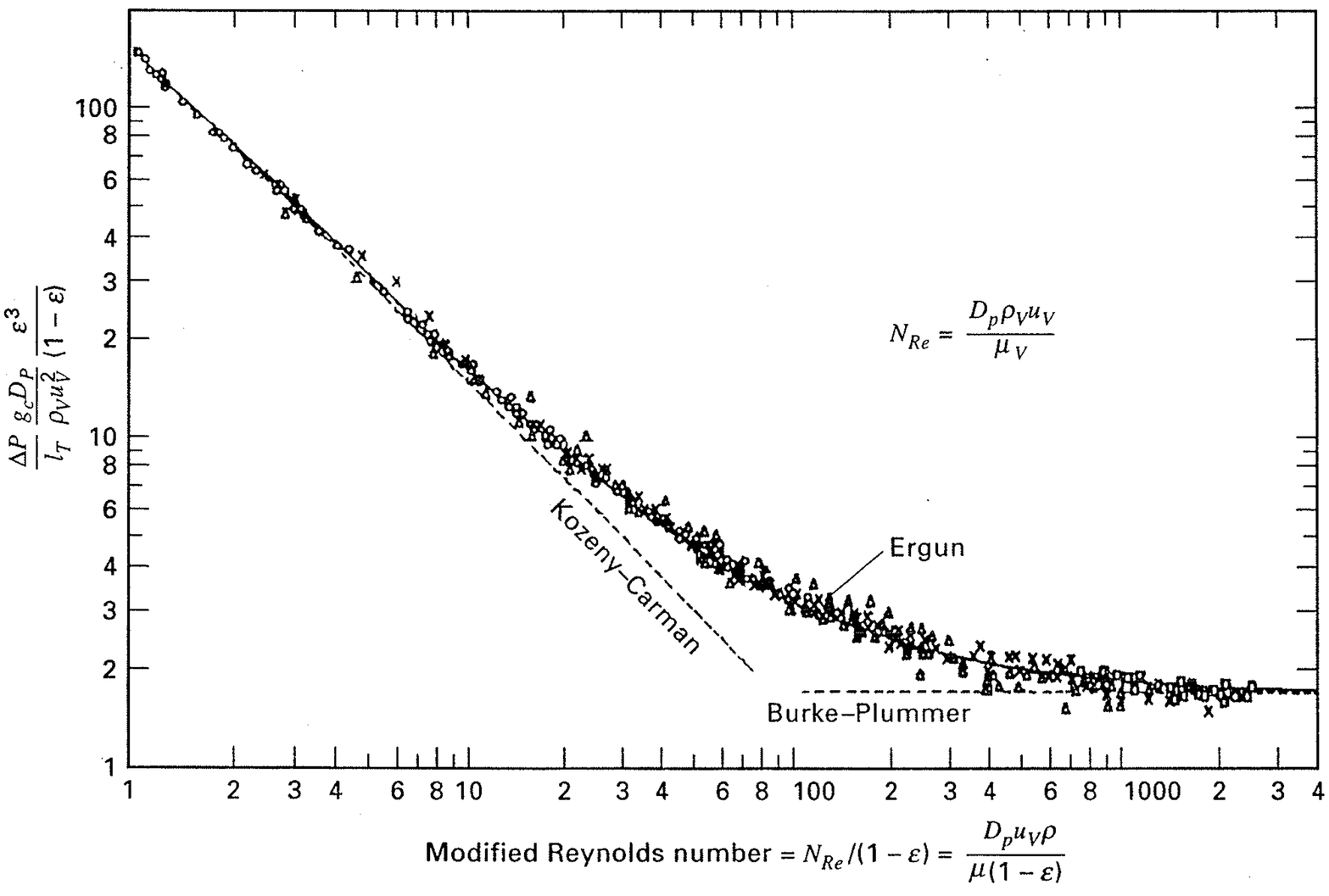

Figure 6.37 Ergun correlation for dry-bed pressure drop.
[From S. Ergun, *Chem. Eng. Prog.* **48** (2), 89–94 (1952) with permission.]

where

$$N_{\mathrm{Re}_V} = \frac{u_V D_P \rho_V}{(1-\epsilon)\mu_V} K_W \qquad (6\text{-}114)$$

and C_p is a packing constant, determined from experimental data, and tabulated for a number of packings in Table 6.8. In (6-113), the laminar-flow region is characterized by the term $64/N_{\mathrm{Re}_V}$, while the next term characterizes the more common turbulent-flow regime.

When a packed tower is irrigated with a downward-flowing liquid, the cross-sectional area for gas flow is reduced by the liquid holdup and the surface structure exposed to the gas is changed as a result of the coating of the packing with a liquid film. The pressure drop now becomes dependent on the holdup and a two-phase flow resistance, and was found by Billet and Schultes [69] to depend on the liquid-flow Froude number as follows for flow rates up to the loading point:

$$\frac{\Delta P}{\Delta P_o} = \left(\frac{\epsilon}{\epsilon - h_L}\right)^{3/2} \exp\left[\frac{13300}{a^{3/2}}\left(N_{\mathrm{Fr}_L}\right)^{1/2}\right] \qquad (6\text{-}115)$$

where

h_L is given by (6-97) and is in m^2/m^3,

ϵ and a are given in Table 6.8, where a in (6-115) must be in m^2/m^3, and

N_{Fr_L} is given by (6-99).

EXAMPLE 6.14

A column packed with 25-mm metal Bialecki rings is to be designed for the following vapor and liquid conditions:

	Vapor	Liquid
Mass flow rate, kg/h	515	1,361
Density, kg/m^3	1.182	1,000
Viscosity, kg/m-s	1.78×10^{-5}	1.00×10^{-3}
Molecular weight	28.4	18.02
Surface tension, kg/s^2		2.401×10^{-2}

Using the equations of Billet and Schultes, determine the vapor and liquid superficial velocities at the loading and flooding points, the specific liquid holdup at the loading point, the specific pressure drop at the loading point, and the column diameter for operation at the loading point.

SOLUTION

From Table 6.8, the following constants apply to the Bialecki rings:

$a = 210\ m^2/m^3$

$\epsilon = 0.956$

$C_h = 0.692$

$C_p = 0.891$

$C_s = 2.521$

First, compute the superficial vapor velocity at the loading point. From the abscissa label of Figure 6.36a,

$$F_{LV} = \frac{1{,}361}{515}\left(\frac{1.182}{1{,}000}\right)^{1/2} = 0.0908$$

Because $F_{LV} < 0.4$, $n_s = -0.326$ and C in (6-106) $= C_s = 2.521$.

From (6-106),

$$\Psi_l = \frac{9.807}{2.521^2}\left[0.0908\left(\frac{0.001}{0.0000178}\right)^{0.4}\right]^{-2(-0.326)} = 0.923$$

$$u_{L,l} = u_{V,l}\frac{\rho_V L M_L}{\rho_L V M_V} = u_{V,l}\frac{(1.182)(1{,}361)}{(1{,}000)(515)} = 0.00312\, u_{V,l}$$

From (6-107),

$$\xi_l = \left(12\frac{(0.001)}{(9.807)(1{,}000)}(0.00312)\, u_{V,l}\right) = 3.82 \times 10^{-9} u_{V,l}$$

From (6-105),

$$u_{V,l} = \left(\frac{9.807}{0.923}\right)^{1/2}\left[\frac{0.956}{210^{1/6}} - 210^{1/2}\left(3.82 \times 10^{-9}\, u_{V,l}\right)^{1/3}\right] \times \left(3.82 \times 10^{-9}\, u_{V,l}\right)^{1/6}\left(\frac{1{,}000}{1.182}\right)^{1/2}$$

$$= 3.26\left[0.392 - 0.0227\, u_{V,l}^{1/3}\right] 1.15\, u_{V,l}^{1/6}$$

$$= \left(1.47 - 0.0851\, u_{V,l}^{1/3}\right) u_{V,l}^{1/6}$$

Solving this nonlinear equation in $u_{V,l}$ gives $u_{V,l}$ = superficial vapor velocity at the loading point = 1.46 m/s.

The corresponding superficial liquid velocity $= u_{L,l}$ $= 0.00312\, u_{V,l} = 0.00312(1.46) = 0.00457$ m/s.

The superficial vapor flooding velocity $= u_{V,f} = \dfrac{u_{V,l}}{0.7} = \dfrac{1.46}{0.7} =$ 2.09 m/s.

The corresponding superficial liquid velocity $=$

$$u_{L,f} = \frac{0.00457}{0.7} = 0.00653 \text{ m/s.}$$

Next, compute the specific liquid holdup at the loading point.

From (6-98) and (6-99),

$$N_{\mathrm{Re}_L} = \frac{(0.00457)(1{,}000)}{(210)(0.001)} = 21.8$$

and

$$N_{\mathrm{Fr}_L} = \frac{(0.00457)^2(210)}{9.807} = 0.000447$$

Because $N_{\mathrm{Re}_L} > 5$, (6-101) applies:

$$a_h/a = 0.85(0.692)(21.8)^{0.25}(0.000447)^{0.1} = 0.588$$

From (6-97), the specific liquid holdup at the loading point is

$$h_L = \left(12\frac{0.000447}{21.8}\right)^{1/3} 0.588^{2/3} = 0.0440\ m^3/m^3$$

Before computing the specific pressure drop at the loading point, we must compute the column diameter for operation at the loading point.

Applying (6-103),

$$D_T = \left[\frac{4(515/3600)}{(1.46)(3.14)(1.182)}\right]^{1/2} = 0.325 \text{ m}$$

From (6-112),

$$D_P = 6\left(\frac{1-0.956}{210}\right) = 0.00126 \text{ m}$$

From (6-111),

$$\frac{1}{K_W} = 1 + \frac{2}{3}\left(\frac{1}{1-0.956}\right)\frac{0.00126}{0.325} = 1.059 \text{ and } K_W = 0.944$$

From (6-114),

$$N_{\mathrm{Re}_V} = \frac{(1.46)(0.00126)(1.182)}{(1-0.956)(0.0000178)}(0.944) = 2{,}621$$

From (6-113),

$$\Psi_o = 0.891\left(\frac{64}{2{,}621} + \frac{1.8}{2{,}621^{0.08}}\right) = 0.876$$

From (6-110), the specific dry-gas pressure drop is

$$\frac{\Delta P_o}{l_T} = 0.876\frac{(210)(1.46)^2(1.182)}{(0.956)^3(2)}(1.059)$$
$$= 281 \text{ kg/m}^2\text{-s}^2 = \text{Pa/m}$$

From (6-115), the specific pressure drop at the loading point is

$$\frac{\Delta P}{l_T} = 281\left(\frac{0.956}{0.956 - 0.0440}\right)^{3/2}\exp\left[\frac{13300}{210^{3/2}}(0.000447)^{1/2}\right]$$
$$= 331 \text{ kg/m}^2\text{-s}^2$$

or 0.406 in. of water/ft

Mass-Transfer Efficiency

The mass-transfer efficiency of a packed column is incorporated in the HETP or the more theoretically based HTUs and volumetric mass-transfer coefficients. Although the HETP concept lacks a sound theoretical basis, its simplicity, coupled with the relative ease with which equilibrium-stage calculations can be made with computer-aided simulation programs, has made it a widely used method for estimating packing height. In the preloading region and where good distribution of vapor and liquid is initiated and maintained, values of the HETP depend mainly on packing type and size, liquid viscosity, and surface tension. For rough estimates the following relations, taken from Kister [33], can be used.

1. Pall rings and similar high-efficiency random packings with low-viscosity liquids:

$$\text{HETP, ft} = 1.5D_P, \text{ in.} \qquad (6\text{-}116)$$

2. Structured packings at low-to-moderate pressure with low-viscosity liquids:

$$\text{HETP, ft} = 100/a, \text{ ft}^2/\text{ft}^3 + 4/12 \qquad (6\text{-}117)$$

3. Absorption with viscous liquid:

$$\text{HETP} = 5 \text{ to } 6 \text{ ft}$$

4. Vacuum service:

$$\text{HETP, ft} = 1.5D_P, \text{ in.} + 0.5 \qquad (6\text{-}118)$$

5. High-pressure service (> 200 psia):

   HETP for structured packings may be greater than predicted by (6-117)

6. Small-diameter columns, $D_T < 2$ ft:

$$\text{HETP, ft} = D_T, \text{ ft, but not less than 1 ft}$$

In general, lower values of HETP are achieved with smaller-size random packings, particularly in small-diameter columns, and with structured packings, particularly those with large values of a, the packing surface area per packed volume. The experimental data of Figure 6.38 for no. 2 (2-in.-diameter) Nutter rings from Kunesh [53] show that in the preloading region, the HETP is relatively independent of the vapor-flow F-factor:

$$F = u_V(\rho_V)^{0.5} \qquad (6\text{-}119)$$

provided that the ratio L/V is maintained constant as the superficial gas velocity, u_V, is increased. Beyond the loading point, and as the flooding point is approached, the HETP can increase dramatically like the pressure drop and liquid holdup.

Experimental mass-transfer data for packed columns are usually correlated in terms of volumetric mass-transfer coefficients and/or HTUs, rather than in terms of HETPs. The data are obtained from experiments in which either the liquid-phase or the gas-phase mass-transfer resistance is negligible, so that the other resistance can be studied and correlated independently. For applications where both resistances may be important, the two resistances are added together according to the two-film theory of Whitman [54], as discussed in Chapter 3, to obtain the overall resistance. This theory assumes the absence of any mass-transfer resistance at the interface between the gas and liquid phases. Thus, the two phases are in equilibrium at the interface.

The two-film theory defines an overall coefficient in terms of the individual volumetric mass-transfer coefficients discussed in Section 6.7. Most commonly, reference is made to the overall gas-phase resistance, (6-84),

$$\frac{1}{K_y a} = \frac{1}{k_y a} + \frac{K}{k_x a}$$

for mass-transfer rates expressed in terms of mole-fraction driving forces by (6-77),

$$r = k_y a(y - y_\text{I}) = k_x a(x_\text{I} - x) = K_y a(y - y^*)$$

where K is the vapor–liquid equilibrium ratio.

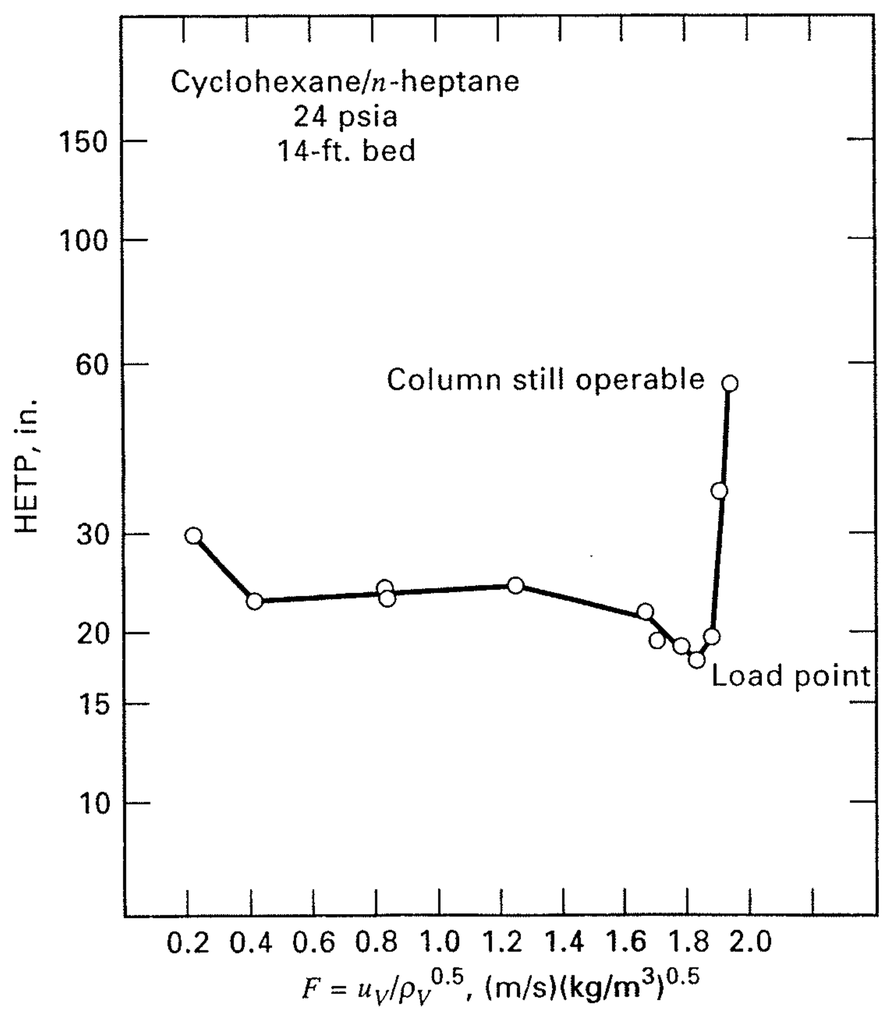

Figure 6.38 Effect of F-factor on HETP.

Alternatively, as summarized in Table 6.7, mass-transfer rates can be expressed in terms of liquid-phase concentrations and gas-phase partial pressure

$$r = k_p a(p - p_I) = k_L a(c_I - c) = K_G a(p - p^*) \quad (6\text{-}120)$$

If we define a Henry's-law constant at the equilibrium interface between the two phases by

$$p_I = H' c_I \quad (6\text{-}121)$$

and let

$$p^* = H' c \quad (6\text{-}122)$$

then

$$\frac{1}{K_G a} = \frac{1}{k_p a} + \frac{H'}{k_L a} \quad (6\text{-}123)$$

Alternatively, expressions can be derived for $K_x a$ and $K_L a$.

It should be noted that the units of various mass transfer coefficients differ:

	SI Units	American Engineering Units
r	mol/m^3-s	lbmol/ft^3-h
$k_y a$, $k_x a$, $K_x a$, $K_y a$	mol/m^3-s	lbmol/ft^3-h
$k_p a$, $K_G a$	mol/m^3-s-kPa	lbmol/ft^3-h-atm
$k_L a$, $k_G a$, $k_c a$	s^{-1}	h^{-1}
k_L, k_G, k_c	m/s	ft/h

Instead of using mass-transfer coefficients directly for column design, the transfer-unit concept of Chilton and Colburn [43,44] is often employed because HTUs: (1) have only one dimension (length), (2) generally vary with column conditions less than mass-transfer coefficients, and (3) are related to an easily understood geometrical quantity, namely, height per theoretical stage. Definitions of individual and overall HTUs are included in Table 6.7 for the dilute case. By substituting these definitions into (6-84),

$$H_{OG} = H_G + (KV/L)H_L \quad (6\text{-}124)$$

Alternatively, an expression can be derived for H_{OL}. In the absorption or stripping of very insoluble gases, the solute K-value or Henry's law constant, H' in (6-112), is very large, making the last terms in (6-84), (6-123), and (6-124) large such that the resistance of the gas phase is negligible and the rate of mass transfer is controlled by the liquid phase. Such data can then be used to study the effect of the variables on the volumetric, liquid-phase mass-transfer coefficient and HTU. Typical data are shown in Figure 6.39 for three different-size Berl-saddle packings for the stripping of oxygen from water by air, in a 20-in.-I.D. column operated at near-ambient temperature and pressure in the preloading region, as reported in an early study by Sherwood and Holloway [55]. The effect of liquid velocity on $k_L a$ is seen to be quite pronounced, with $k_L a$ increasing at about the 0.75 power of the liquid mass velocity. Gas velocity was observed to have no effect on $k_L a$ in the preloading region. Also included in Figure 6.39 are the data plotted in terms of H_L, where

$$H_L = \frac{M_L L}{\rho_L k_L a S} \quad (6\text{-}125)$$

As seen, H_L does not depend as strongly as $k_L a$ on liquid mass velocity, $M_L L/S$.

Another system for which the rate of mass transfer is controlled by the liquid phase is CO_2–air–H_2O, where CO_2 can be either absorbed or stripped. Measurements on this system for a variety of modern metal, ceramic, and plastic packings are reported by Billet [45]. Data on the effect of liquid loading on $k_L a$ in the preloading region for two different-size ceramic Hiflow ring packings are shown in Figure 6.40. The effect of gas velocity on $k_L a$ in terms of the F-factor at a constant liquid rate is shown in Figure 6.41 for the same system, but with 50-mm plastic Pall rings and Hiflow rings. Up to an F-factor value of about 1.8 m$^{-1/2}$-s^{-1}-kg$^{1/2}$, which is in the preloading region, no effect of gas velocity is

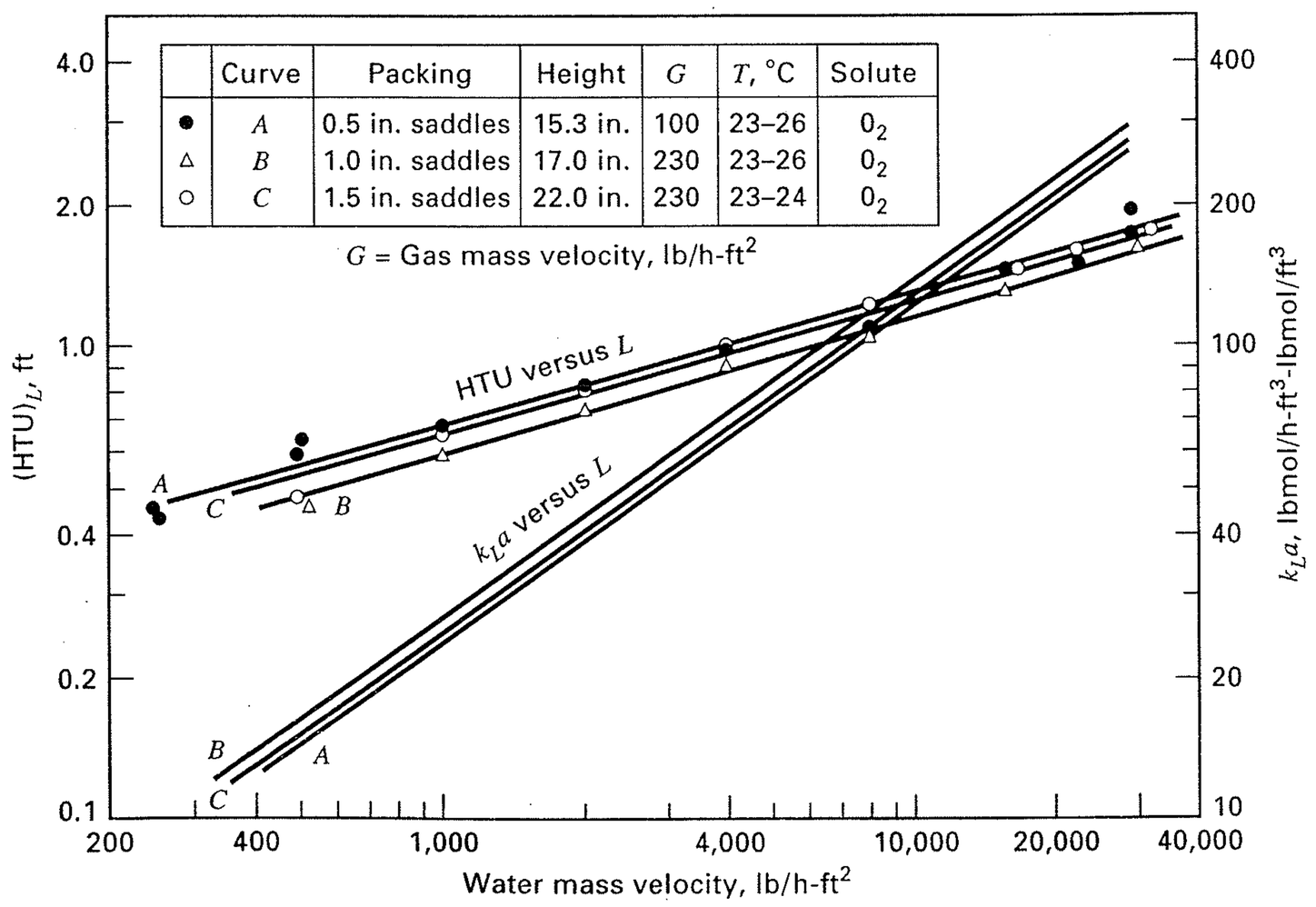

Figure 6.39 Effect of liquid rate on liquid-phase mass transfer of O_2.
[From T.K. Sherwood and F.A.L. Holloway, *Trans. AIChE.*, **36,** 39–70 (1940) with permission.]

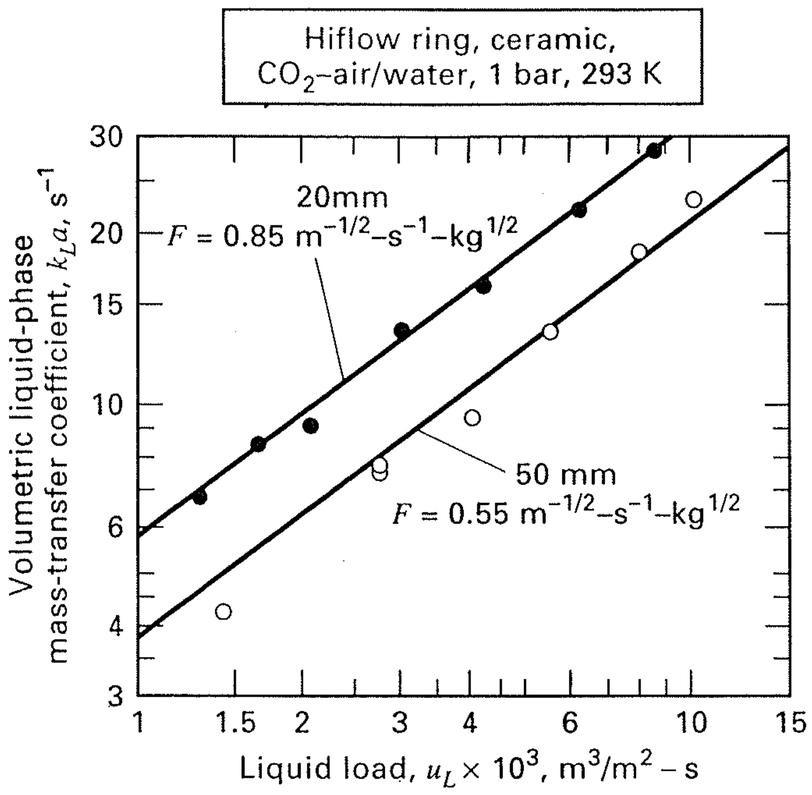

Figure 6.40 Effect of liquid load on liquid-phase mass transfer of CO_2.

[From R. Billet, *Packed Column Analysis and Design*, Ruhr-University Bochum (1989) with permission.]

observed. Above the loading limit, k_La increases with increasing gas velocity because of increased liquid holdup, which increases interfacial surface area for mass transfer. Although it is not illustrated in Figures 6.39 to 6.41, another major factor that influences the rate of mass transfer in the liquid phase is the solute molecular diffusivity in the solvent. For a given packing, experimental data on different systems in the preloading region can usually be correlated satisfactorily by the following empirical expression, which includes only the liquid velocity and liquid diffusivity:

$$k_La = C_1 D_L^{1/2} u_L^n \qquad (6\text{-}126)$$

where n has been observed by different investigators to vary from about 0.6 to 0.95, with 0.75 being a typical value. The exponent on the diffusivity is consistent with the penetration theory discussed in Chapter 3.

A convenient system for studying gas-phase mass transfer is NH_3–air–H_2O. The high solubility of NH_3 in H_2O corresponds to a relatively low K-value. Accordingly, the last terms in (6-84), (6-123), and (6-124) may be negligible so that the gas-phase resistance controls the rate of mass transfer. The small effect of the liquid-phase resistance can be backed out using a correlation such as (6-126). The typical effect of superficial vapor velocity, expressed in terms of the F-factor of (6-119), on the volumetric, gas-phase mass-transfer coefficient in the preloading region is shown in Figure 6.42 for two different plastic packings at the same liquid velocity. The coefficients are proportional to about the 0.75 power of F. Figure 6.43 shows that the liquid velocity also affects the gas-phase mass-transfer coefficient, probably because as the liquid rate is increased, the holdup increases and more interfacial surface is created.

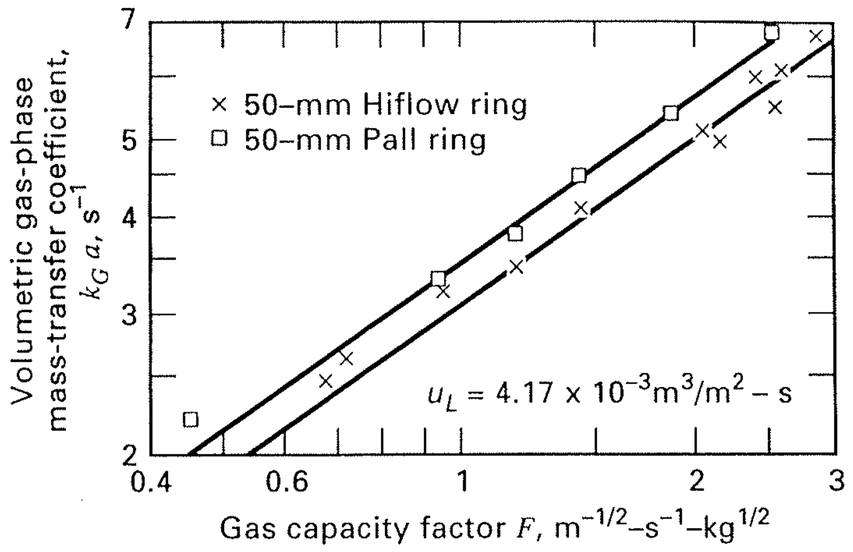

Figure 6.42 Effect of gas rate on gas-phase mass transfer of NH_3.

[From R. Billet, *Packed Column Analysis and Design*, Ruhr-University Bochum (1989) with permission.]

The volumetric, gas-phase mass-transfer coefficients, k_Ga, plotted in Figures 6.42 and 6.43, are based on gas-phase molar concentrations. Thus, they have the same units as k_La. For a given packing, experimental data on k_pa or k_Ga for different systems in the preloading region can usually be correlated satisfactorily with empirical correlations of the form

$$k_pa = C_2 D_G^{0.67} F^{m'} u_L^{n'} \qquad (6\text{-}127)$$

where D_G is the gas diffusivity of the solute and m' and n' have been observed by different investigators to vary from 0.65 to 0.85 and from 0.25 to 0.5, respectively, a typical value for m' being 0.8.

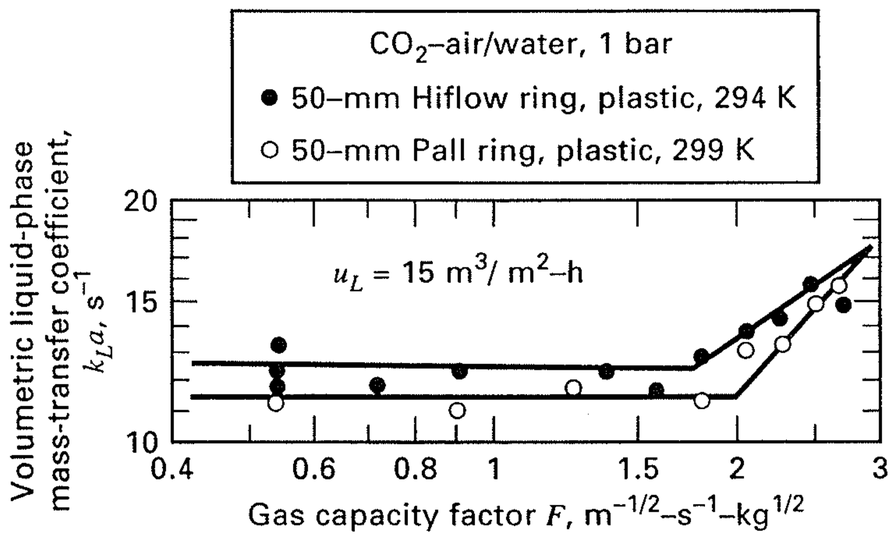

Figure 6.41 Effect of gas rate on liquid-phase mass transfer of CO_2.

[From R. Billet, *Packed Column Analysis and Design*, Ruhr-University Bochum (1989) with permission.]

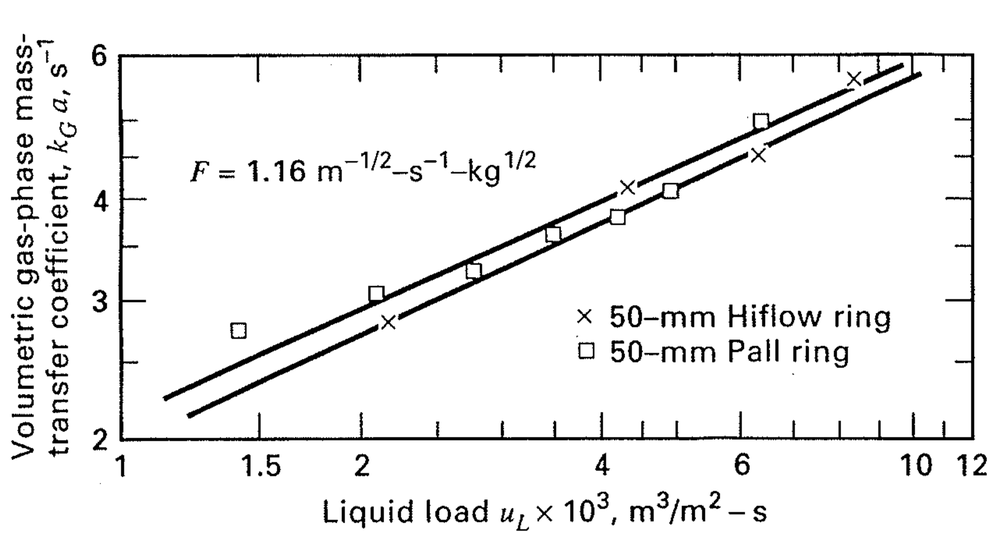

Figure 6.43 Effect of liquid rate on gas-phase mass transfer of NH_3.

[From R. Billet, *Packed Column Analysis and Design*, Ruhr-University Bochum (1989) with permission.]

Table 6.9 Generalized Correlations for Mass Transfer in Packed Columns

Investigator	Year	Ref. No.	Type of Correlations	Packings
Shulman et al.	1955	64	k_p, k_L, a	Raschig rings, Berl saddles
Cornell et al.	1960	56, 57	H_G, H_L	Raschig rings, Berl saddles
Onda et al.	1968	65	k_p, k_L, a	Raschig rings, Berl saddles
Bolles and Fair	1979, 1982	58, 59	H_G, H_L	Raschig rings, Berl saddles, Pall rings
Bravo and Fair	1982	60	a	Raschig rings, Berl saddles, Pall rings
Bravo et al.	1985	61	k_G, k_L	Sulzer
Fair and Bravo	1987	62	k_G, k_L, a	Sulzer, Gempak, Mellapak, Montz, Ralu Pak
Fair and Bravo	1991	63	k_G, k_L, a	Flexipac, Gempak, Intalox 2T, Montz, Mellapak, Sulzer
Billet and Schultes	1991	67	k_Ga, k_La	14 random packings and 4 structured packings
Billet and Schultes	1999	69	k_Ga, k_La	19 random packings and 6 structured packings

The development of separate generalized correlations for gas- and liquid-phase mass-transfer coefficients and/or HTUs, which began with the study of Sherwood and Holloway [55] on the liquid phase, has led to a significant number of empirical and semitheoretical equations, most of which are based on the application of the two-film theory by Fair and coworkers [56–63] and others [64, 65]. In some cases, values of k_G and k_L are correlated separately from a; in others, the combinations k_Ga and k_La are used. Important features of some of these correlations are summarized in Table 6.9. The development of such correlations from experimental data is difficult because, as shown by Billet [66] in a comprehensive study with metal Pall rings, values of the mass-transfer coefficients are significantly affected by the technique used to pack the column and the number of liquid feed-distribution points per unit of column cross section, when this number is less than 10 points/ft^2. When 25 points/ft^2 are used and $D_T/D_P > 10$, column diameter has little, if any, effect on mass-transfer coefficients for packed heights up to 20 ft.

In an extensive investigation, Billet and Schultes [67] measured and correlated volumetric mass-transfer coefficients and HTUs for 31 different binary and ternary chemical systems with 67 different types and sizes of packings in columns of diameter ranging from 2.4 in. to 4.6 ft. Additional data are reported by Billet and Schultes [69], particularly for Hiflow rings and Raschig Super-rings. The systems include some for which mass-transfer resistance resides mainly in the liquid phase and others for which resistance in the gas phase is predominant. They assume uniform distribution of gas and liquid over the cross-sectional area of the column and apply the two-film theory of mass transfer discussed in Chapter 3. For the liquid-phase resistance, they assume that the liquid flows in a thin film through the irregular channels of the packing, with continual remixing of the liquid at points of contact with the packing such that Higbie's penetration theory of diffusion [68], as developed in Chapter 3, can be applied. Thus, for the diffusing component, in terms of concentration units, the volumetric mass-transfer coefficient is defined by

$$r = (k_L a_{Ph})(c_{L_I} - c_L) \tag{6-128}$$

From the penetration theory of Higbie, (3-194),

$$k_L = 2(D_L/\pi t_L)^{0.5} \tag{6-129}$$

where t_L = time of exposure of the liquid film before remixing. Billet and Schultes assume that this time is governed by a length of travel equal to the hydraulic diameter of the packing:

$$t_L = h_L d_H / u_L \tag{6-130}$$

where d_H, the hydraulic diameter, is equal to $4r_H$ or $4\epsilon/a$. Thus, in terms of the height of a liquid transfer unit, (6-129) and (6-130) give

$$H_L = \frac{u_L}{k_L a_{Ph}} = \frac{\sqrt{\pi}}{2}\left(\frac{4h_L\epsilon}{D_L a u_L}\right)^{1/2}\frac{u_L}{a_{Ph}} \tag{6-131}$$

Equation (6-131) was modified to include an empirical constant, C_L, which is back-calculated for each packing to fit the experimental data. The final predictive equation given by Billet and Schultes is

$$H_L = \frac{1}{C_L}\left(\frac{1}{12}\right)^{1/6}\left(\frac{4h_L\epsilon}{D_L a u_L}\right)^{1/2}\frac{u_L}{a}\left(\frac{a}{a_{Ph}}\right) \tag{6-132}$$

where values of C_L are included in Table 6.8.

A similar development was made by Billet and Schultes for the gas-phase resistance, except that the time of exposure of the gas between periods of mixing was determined empirically, to give

$$H_G = \frac{1}{C_V}(\epsilon - h_L)^{1/2}\left(\frac{4\epsilon}{a^4}\right)^{1/2}(N_{\mathrm{Re}_V})^{-3/4}(N_{\mathrm{Sc}_V})^{-1/3}\left(\frac{u_V a}{D_G a_{Ph}}\right) \tag{6-133}$$

where C_V is included in Table 6.8 and

$$N_{\mathrm{Re}_V} = \frac{u_V \rho_V}{a\mu_V} \tag{6-134}$$

$$N_{\mathrm{Sc}_V} = \frac{\mu_V}{\rho_V D_V} \tag{6-135}$$

Equations (6-132) and (6-133) contain an area ratio, a_{Ph}/a, which is the ratio of the phase interface area to the packing surface area, which from Billet and Schultes [69] is not the same as the hydraulic area ratio, a_h/a, given by (6-100) and

(6-101). Instead, they give the following correlation:

$$\frac{a_{Ph}}{a} = 1.5(ad_h)^{-1/2}(N_{\mathrm{Re}_L,h})^{-0.2}(N_{\mathrm{We}_L,h})^{0.75}(N_{\mathrm{Fr}_L,h})^{-0.45} \tag{6-136}$$

where

$$d_h = \text{packing hydraulic diameter} = 4\frac{\epsilon}{a} \tag{6-137}$$

and the following liquid-phase dimensionless groups use the packing hydraulic diameter as the characteristic length:

$$\text{Reynolds number} = N_{\mathrm{Re}_L,h} = \frac{u_L d_h \rho_L}{\mu_L} \tag{6-138}$$

$$\text{Weber number} = N_{\mathrm{We}_L,h} = \frac{u_L^2 \rho_L d_h}{\sigma} \tag{6-139}$$

$$\text{Froude number} = N_{\mathrm{Fr}_L,h} = \frac{u_L^2}{g d_h} \tag{6-140}$$

Following the estimation of H_L and H_G from (6-132) and (6-133), respectively, the overall HTU value can be determined from (6-124), followed by the determination of packed height from

$$l_T = H_{OG} N_{OG} \tag{6-141}$$

where the determination of N_{OG} is discussed in Section 6.7.

EXAMPLE 6.15

For the absorption of ethyl alcohol from CO_2 with water, as considered in Example 6.1, a 2.5-ft-I.D. tower, packed with 1.5-in. metal Pall-like rings, is to be used. It is estimated that the tower will operate in the preloading region with a pressure drop of approximately 1.5 in. of water head per foot of packed height. From Example 6.9, the required number of overall transfer units based on the gas phase is 7.5. Estimate H_G, H_L, H_{OG}, HETP, and the required packed height in feet using the following estimates of flow conditions and physical properties at the bottom of the packing:

	Vapor	**Liquid**
Flow rate, lb/h	17,480	6,140
Molecular weight	44.05	18.7
Density, lb/ft^3	0.121	61.5
Viscosity, cP	0.0145	0.63
Surface tension, dynes/cm	—	101
Diffusivity of ethanol, m^2/s	7.75×10^{-6}	1.82×10^{-9}
Kinematic viscosity, m^2/s	0.75×10^{-5}	0.64×10^{-6}

SOLUTION

Cross-sectional area of tower $= (3.14)(2.5)^2/4 = 4.91$ ft^2.
Volumetric liquid flow rate $= 6{,}140/61.5 = 99.8$ ft^3/h.
u_L = superficial liquid velocity $= 99.8/[(4.91)(3{,}600)] = 0.0056$ ft/s or 0.0017 m/s.
From Section 6.8, $u_L > u_{L,\min}$, but the velocity is on the low side.
u_V = superficial gas velocity $= 17{,}480/[(0.121)(4.91)(3{,}600)] = 8.17$ ft/s $= 2.49$ m/s.
Let the packing characteristics for the 1.5-inch metal Pall-like rings be as follows (somewhat different from values for Pall rings in Table 6.8):

$$a = 149.6 \text{ m}^2/\text{m}^3, \quad \epsilon = 0.952$$
$$C_h = \text{approximately } 0.7, \quad C_L = 1.227, \quad C_V = 0.341$$

Estimation of specific liquid holdup, h_L:

From (6-98),

$$N_{\mathrm{Re}_L} = \frac{0.0017}{(0.64 \times 10^{-6})(149.6)} = 17.8.$$

From (6-99),

$$N_{\mathrm{Fr}_L} = \frac{(0.0017)^2(149.6)}{9.8} = 4.41 \times 10^{-5}$$

From (6-101),

$$\frac{a_h}{a} = 0.85(0.7)(17.8)^{0.25}(4.41 \times 10^{-5})^{0.10} = 0.045$$
$$a_h = 0.045(149.6) = 6.73 \text{ m}^2/\text{m}^3$$

From (6-97),

$$h_L = \left[\frac{12(4.41 \times 10^{-5})}{17.8}\right]^{1/3}(0.045)^{2/3} = 0.0128 \text{ m}^3/\text{m}^3$$

Estimation of H_L:

First compute a_{Ph}, the ratio of phase interface area to packing surface area.

From (6-137),

$$d_h = 4\frac{0.952}{149.6} = 0.0255 \text{ m}$$

From (6-138),

$$N_{\mathrm{Re}_L,h} = \frac{(0.0017)(0.0255)}{(0.64 \times 10^{-6})} = 67.7$$

From (6-139),

$$N_{\mathrm{We}_L,h} = \frac{(0.0017)^2[(61.5)(16.02)](0.0255)}{[(101)(0.001)]} = 0.000719$$

From (6-140),

$$N_{\mathrm{Fr}_L,h} = \frac{(0.0017)^2}{(9.807)(0.0255)} = 1.156 \times 10^{-5}$$

From (6-136),

$$\frac{a_{Ph}}{a} = 1.5(149.6)^{-1/2}(0.0255)^{-1/2}(67.7)^{-0.2} \times (0.000719)^{0.75}(1.156 \times 10^{-5})^{-0.45} = 0.242$$

Estimation of H_L:

From (6-132), using consistent SI units:

$$H_L = \frac{1}{1.227}\left(\frac{1}{12}\right)^{1/6}\left[\frac{(4)(0.0128)(0.952)}{(1.82 \times 10^{-9})(149.6)(0.0017)}\right]^{1/2} \times \left(\frac{0.0017}{149.6}\right)\left(\frac{1}{0.242}\right) = 0.26 \text{ m} = 0.85 \text{ ft}$$

Estimation of H_G:

From (6-134),

$$N_{\mathrm{Re}_V} = 2.49/[(149.6)(0.75 \times 10^{-5})] = 2{,}220$$

From (6-135),

$$N_{\mathrm{Sc}_V} = 0.75 \times 10^{-5}/7.75 \times 10^{-6} = 0.968$$

From (6-133), using consistent SI units,

$$H_G = \frac{1}{0.341}(0.952 - 0.0128)^{1/2}\left[\frac{(4)(0.952)}{(149.6)^4}\right]^{1/2} \times (2220)^{-3/4}(0.968)^{-1/3}\left[\frac{(2.49)}{7.75 \times 10^{-6}(0.242)}\right]$$
$$= 1.03 \text{ m} \quad \text{or} \quad 3.37 \text{ ft}$$

Estimation of H_{OG}:

From Example 6.1, the K-value for ethyl alcohol = 0.57,

$$V = 17{,}480/44.05 = 397 \text{ lbmol/h},$$
$$L = 6{,}140/18.7 = 328 \text{ lbmol/h},$$

and $$1/A = KV/L = (0.57)(397)/328 = 0.69$$

From (6-124),

$$H_{OG} = 3.37 + 0.69(0.85) = 3.96 \text{ ft}$$

The mass-transfer resistance in the gas phase is much larger than that in the liquid phase.

Estimation of Packed Height:

From (6-141),

$$l_T = 3.96(7.5) = 29.7 \text{ ft}$$

Estimation of HETP:

From (6-94), for straight operating and equilibrium lines, with $A = 1/0.69 = 1.45$,

$$\text{HETP} = 3.96\left[\frac{\ln(0.69)}{(1 - 1.45)/1.45}\right] = 4.73 \text{ ft}$$

6.9 CONCENTRATED SOLUTIONS IN PACKED COLUMNS

When the solute concentration in the gas and/or liquid is concentrated so that the operating line and/or equilibrium line are noticeably curved, then the procedure given in Section 6.7 for determining N_{OG} and l_T cannot be used because (6-91) cannot be analytically integrated to give (6-93). Instead, alternative methods can be employed or the computer-aided methods discussed in Chapters 10 and 11 can be applied.

For concentrated solutions, the two columns in Table 6.7 labeled UM (unimolecular) diffusion apply. To obtain these columns from the two columns labeled EM (equimolar) diffusion, we let

$$L' = L(1 - x) \quad \text{and} \quad V' = V(1 - y)$$

where L' and V' are the constant flow rates of the inert (solvent) liquid and (carrier) gas, respectively on a solute-free basis. Then

$$d(Vy) = V'd\left(\frac{y}{1 - y}\right) = V'\frac{dy}{(1 - y)^2} = V\frac{dy}{(1 - y)} \tag{6-141}$$

$$d(Lx) = L'd\left(\frac{x}{1 - x}\right) = L'\frac{dx}{(1 - x)^2} = L\frac{dx}{(1 - x)} \tag{6-142}$$

Equation (6-88) now becomes

$$l_T = \int_{y_2}^{y_1}\left(\frac{V}{K'_y aS}\right)\frac{dy}{(1 - y)(y - y^*)} = \frac{V}{K'_y\, aS}\int_{y_2}^{y_1}\frac{dy}{(1 - y)(y - y^*)} \tag{6-143}$$

where 1 refers to inlet and 2 refers to outlet conditions. Based on the liquid phase,

$$l_T = \int_{x_1}^{x_2}\left(\frac{L}{K'_x\, aS}\right)\frac{dx}{(1 - x)(x^* - x)} = \frac{L}{K'_x aS}\int_{x_1}^{x_2}\frac{dx}{(1 - x)(x^* - x)} \tag{6-144}$$

where the overall mass-transfer coefficients are primed to signify UM diffusion.

If the numerators and denominators of (6-143) and (6-144) are multiplied by $(1 - y)_{\text{LM}}$ and $(1 - x)_{\text{LM}}$, respectively, where $(1 - y)_{\text{LM}}$ is the log mean of $(1 - y)$ and $(1 - y^*)$, and $(1 - x)_{\text{LM}}$ is the log mean of $(1 - x)$ and $(1 - x^*)$, we obtain the expressions in rows 1 and 6 of columns 4 and 7 in Table 6.7:

$$l_T = \int_{y_2}^{y_1}\left[\frac{V}{K'_y a(1 - y)_{\text{LM}}S}\right]\frac{(1 - y)_{\text{LM}}\, dy}{(1 - y)(y - y^*)} = \frac{V}{K'_y a(1 - y)_{\text{LM}}S}\int_{y_2}^{y_1}\frac{(1 - y)_{\text{LM}}\, dy}{(1 - y)(y - y^*)} \tag{6-145}$$

$$l_T = \int_{x_1}^{x_2}\left[\frac{L}{K'_x a(1 - x)_{\text{LM}}S}\right]\frac{(1 - x)_{\text{LM}}\, dx}{(1 - x)(x^* - x)} = \frac{L}{K'_x a(1 - x)_{\text{LM}}S}\int_{x_1}^{x_2}\frac{(1 - x)_{\text{LM}}\, dx}{(1 - x)(x^* - x)} \tag{6-146}$$

In these equations $K'_y(1 - y)_{\text{LM}}$ is equal to the concentration-independent K_y, and $K'_x(1 - x)_{\text{LM}}$ is equal to the concentration-independent K_x. If there is appreciable absorption, vapor flow rate V decreases from the bottom to the top of the absorber. However, the values of Ka are also a function of flow rate, such that the ratio V/Ka is approximately constant and HTU groupings, $[L/K'_x a(1 - x)_{\text{LM}}S]$ and $[V/K'_y a(1 - y)_{\text{LM}}S]$, can often be taken out of the integral sign without incurring errors larger than those inherent in experimental measurements of Ka. Usually, average values of V, L, and $(1 - y)_{\text{LM}}$ are used.

Another approach is to leave all of the terms in (6-145) or (6-146) under the integral sign and evaluate l_T by a stepwise or graphical integration. In either case, to obtain the terms $(y - y^*)$ or $(x^* - x)$, the equilibrium and operating lines must be established. The equilibrium curve is determined from appropriate thermodynamic data or correlations. To establish the operating line, which will not be straight if the solutions are concentrated, the appropriate material-balance equations must be developed. With reference to Figure 6.29, an overall balance around the upper part of the absorber gives

$$V + L_{\text{in}} = V_{\text{out}} + L \tag{6-147}$$

Similarly a balance around the upper part of the absorber for the component being absorbed, assuming a pure-liquid absorbent, gives:

$$Vy = V_{out}y_{out} + Lx \tag{6-148}$$

An absorbent balance around the upper part of the absorber is:

$$L_{in} = L(1 - x) \tag{6-149}$$

Combining (6-147) to (6-149) to eliminate V and L gives

$$y = \frac{V_{out}y_{out} + [L_{in}x/(1 - x)]}{V_{out} + [L_{in}x/(1 - x)]} \tag{6-150}$$

Equation (6-150) allows the y–x operating line to be calculated from a knowledge of terminal conditions only.

A simpler approach to the problem of concentrated gas or liquid mixtures is to linearize the operating line by expressing all concentrations in mole ratios, and the gas and liquid flows on a solute-free basis, that is, $V' = (1 - y)V$, $L' = (1 - x)L$. Then, in place of (6-145) and (6-146), we have

$$l_T = \int_{Y_2}^{Y_1} \left(\frac{V'}{K_Y aS}\right) \frac{dY}{(Y - Y^*)} = \frac{V'}{K_Y aS} \int_{Y_2}^{Y_1} \frac{dY}{(Y - Y^*)} \tag{6-151}$$

$$l_T = \int_{X_1}^{X_2} \left(\frac{L'}{K_X aS}\right) \frac{dX}{(X^* - X)} = \frac{L'}{K_X aS} \int_{X_1}^{X_2} \frac{dX}{(X^* - X)} \tag{6-152}$$

This set of equations is listed in rows 3 and 8 of Table 6.7.

EXAMPLE 6.16

To remove 95% of the ammonia from an air stream containing 40% ammonia by volume, 488 lbmol/h of an absorbent per 100 lbmol/h of entering gas are to be used, which is greater than the minimum requirement.

Equilibrium data are given in Figure 6.44. Pressure is 1 atm and temperature is assumed constant at 298 K. Calculate the number of transfer units by:

(a) Equation (6-145) using a curved operating line determined from (6-150)

(b) Equation (6-151) using mole ratios.

SOLUTION

(a) Take as a basis $L_{in} = 488$ lbmol/h. Then $V_{out} = 100 - (40)(0.95) = 62$ lbmol/h, and $y_{out} = (0.05)(40)/62 = 0.0323$. From (6-150), it is possible to construct the curved operating line of Figure 6.44. For example, if $x = 0.04$,

$$y = \frac{(62)(0.0323) + [(488)(0.04)/(1 - 0.04)]}{62 + [(488)(0.04)/(1 - 0.04)]} = 0.27$$

It is now possible to calculate the following values of y, y^*, $(1 - y)_{LM} = [(1 - y) - (1 - y^*)]/\ln[(1 - y)/(1 - y^*)]$, and $(1 - y)_{LM}/[(1 - y)(y - y^*)]$ for use in (6-145). For example, in Figure 6.44, for $x = 0.044$, y (on the operating line) = 0.30, and y^*

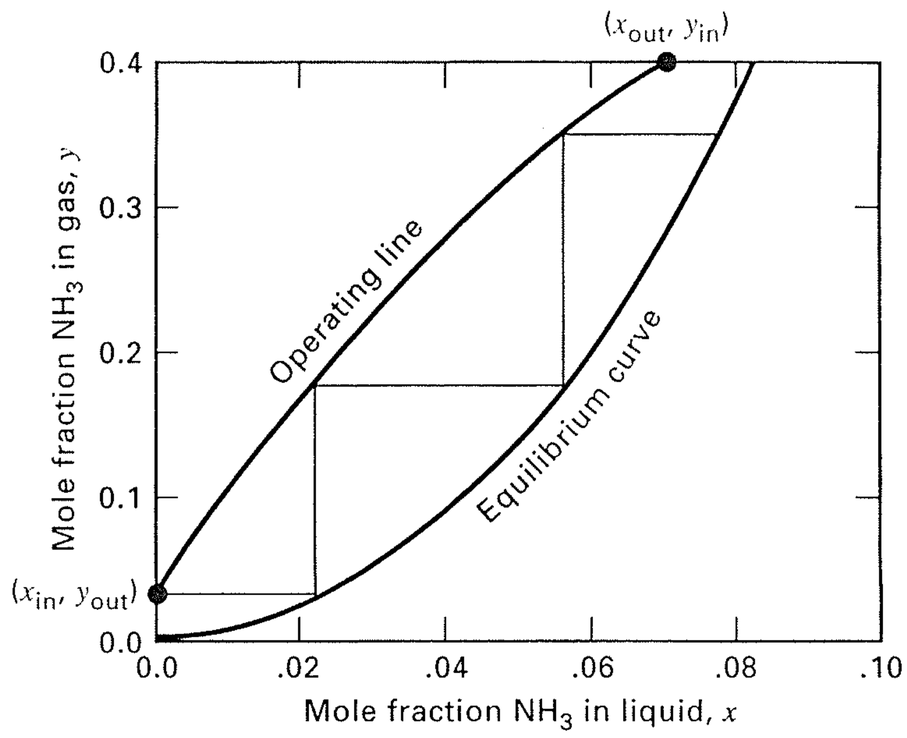

Figure 6.44 Determination of the number of theoretical stages for Example 6.15.

(on the equilibrium curve) = 0.12, from which the other four quantities in the following table follow.

y	y^*	$(y - y^*)$	$(1 - y)$	$(1 - y)_{LM}$	$\frac{(1 - y)_{LM}}{(1 - y)(y - y^*)}$
0.03	0.002	0.028	0.97	0.99	36.47
0.05	0.005	0.045	0.95	0.97	22.68
0.10	0.01	0.09	0.90	0.94	11.60
0.15	0.025	0.125	0.85	0.91	8.56
0.20	0.04	0.16	0.80	0.89	6.95
0.25	0.08	0.17	0.75	0.85	6.66
0.30	0.12	0.18	0.70	0.82	6.51
0.35	0.17	0.18	0.65	0.73	6.24
0.40	0.26	0.14	0.60	0.67	7.97

Note that since $(1 - y) \approx (1 - y)_{LM}$, these two terms frequently cancel out of the NTU equations, particularly when y is small.

Figure 6.45 is a plot of $(1 - y)_{LM}/[(1 - y)(y - y^*)]$ versus y to determine N_{OG}. The integral on the right-hand side of (6-145), between $y = 0.4$ and $y = 0.0322$, is $3.44 = N_{OG}$. This is approximately 1 more than the number of equilibrium stages of 2.6, as seen in the steps of Figure 6.44.

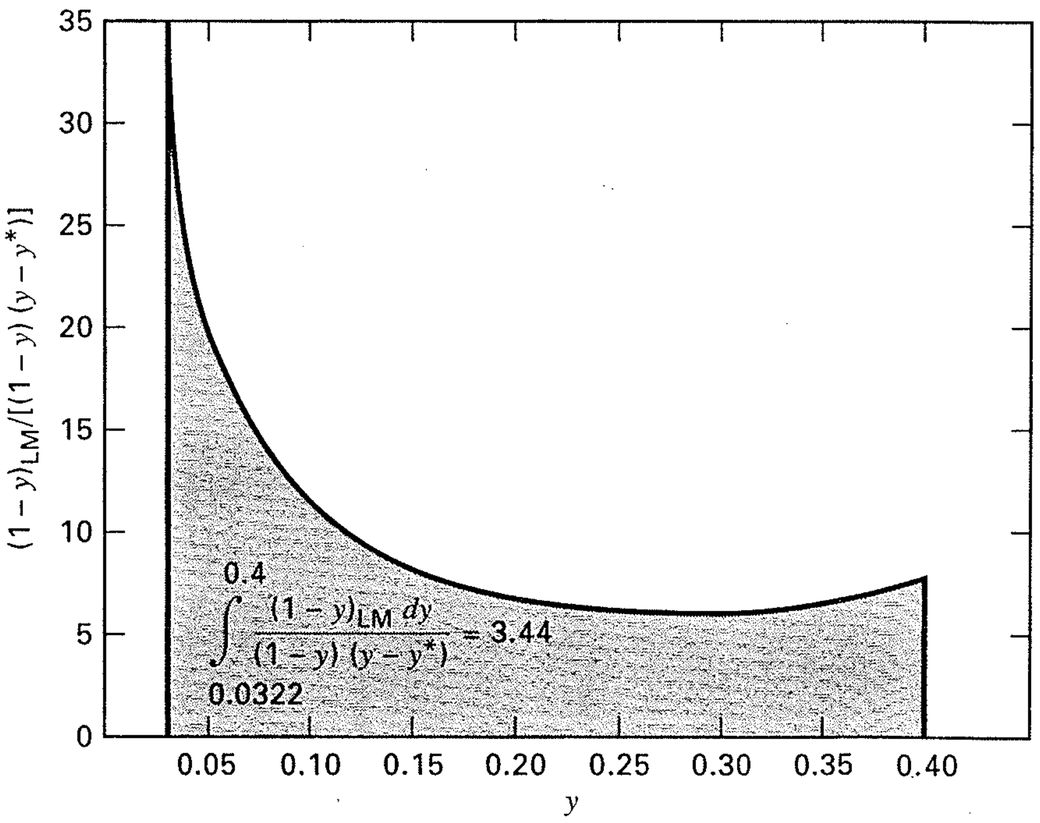

Figure 6.45 Determination of the number of transfer units for Examples 6.15.

(b) It is a simple matter to obtain the following values for $Y = y/(1-y)$, $Y^* = y^*/(1-y^*)$, $(Y - Y^*)$, and $(Y - Y^*)^{-1}$.

y	Y	y^*	Y^*	$(Y - Y^*)^{-1}$
0.03	0.031	0.002	0.002	34.48
0.05	0.053	0.005	0.005	20.83
0.1	0.111	0.01	0.010	9.9
0.15	0.176	0.025	0.026	6.66
0.20	0.250	0.04	0.042	4.8
0.25	0.333	0.08	0.087	4.06
0.30	0.43	0.12	0.136	3.40
0.35	0.54	0.17	0.205	2.98
0.40	0.67	0.26	0.310	2.78

Graphical integration of the right-hand-side integral of (6-151) is carried out by determining the area under the curve of Y versus $(Y - Y^*)^{-1}$ between $Y = 0.67$ and $Y = 0.033$. The result is $N_{OG} = 3.46$. Alternatively, the numerical integration can be performed on a computer with a spreadsheet.

It must be pointed out that for concentrated solutions, the assumption of constant temperature may not be valid and can result in a large error. If an overall energy balance indicates a temperature change that alters the equilibrium curve significantly, it is best to use a computer-aided method that includes the energy balance. Such methods are presented in Chapter 10.

SUMMARY

1. A liquid can be used to selectively absorb one or more components from a gas mixture. A gas can be used to selectively desorb or strip one or more components from a liquid mixture.

2. The fraction of a component that can be absorbed or stripped in a countercurrent cascade depends on the number of equilibrium stages and the absorption factor, $A = L/(KV)$, or the stripping factor, $S = KV/L$, respectively.

3. Absorption and stripping are most commonly conducted in trayed towers equipped with sieve or valve trays, or in towers packed with random or structured packings.

4. Absorbers are most effectively operated at high pressure and low temperature. The reverse is true for stripping. However, high costs of gas compression, refrigeration, and vacuum often preclude operation at the most thermodynamically favorable conditions.

5. For a given gas flow rate and composition, a desired degree of absorption of one or more components, a choice of absorbent, and an operating temperature and pressure, there is a minimum absorbent flow rate, given by (6-9) to (6-11), that corresponds to the use of an infinite number of equilibrium stages. For the use of a finite and reasonable number of stages, an absorbent rate of 1.5 times the minimum is typical. A similar criterion, (6-12), holds for a stripper.

6. The number of equilibrium stages required for a selected absorbent or stripping agent flow rate for the absorption or stripping of a dilute solution can be determined from the equilibrium line, (6-1), and an operating line, (6-3) or (6-5), using graphical, algebraic, or numerical methods. Graphical methods, such as Figure 6.11, offer considerable visual insight into stage-by-stage changes in compositions of the gas and liquid streams.

7. Rough estimates of overall stage efficiency, defined by (6-21), can be made with the correlations of Drickamer and Bradford (6-22), O'Connell (6-23), and Figure 6.15. More accurate and reliable procedures involve the use of a small Oldershaw column or semitheoretical equations, e.g., of Chan and Fair, based on mass-transfer considerations, to determine a Murphree vapor-point efficiency, (6-30), from which a Murphree vapor tray efficiency can be estimated from (6-31) to (6-34), which can then be related to the overall efficiency using (6-37).

8. Tray diameter can be determined from (6-44) based on entrainment flooding considerations using Figure 6.24. Tray vapor pressure drop, the weeping constraint, entrainment, and downcomer backup can be estimated from (6-49), (6-68), (6-69), and (6-70), respectively.

9. Packed-column height can be estimated using the HETP, (6-73), or HTU/NTU, (6-89), concepts, with the latter having a more fundamental theoretical basis in the two-film theory of mass transfer. For straight equilibrium and operating lines, HETP is related to the HTU by (6-94), and the number of equilibrium stages is related to the NTU by (6-95).

10. Below a so-called loading point, in a preloading region, the liquid holdup in a packed column is independent of the vapor velocity. The loading point is typically about 70% of the flooding point, and most packed columns are designed to operate in the preloading region at from 50% to 70% of flooding. From the GPDC chart of Figure 6.36, the flooding point can be estimated, from which the column diameter can be determined with (6-102). The loading point can be estimated from (6-105).

11. One significant advantage of a packed column is its relatively low pressure drop per unit of packed height, as compared to a trayed tower. Packed-column pressure drop can be roughly estimated from Figure 6.36 or more accurately from (6-106) or (6-115).

12. Numerous rules of thumb are available for estimating the HETP of packed columns. However, the preferred approach is to estimate H_{OG} from separate semitheoretical mass-transfer correlations for the liquid and gas phases, such as those of (6-132) and (6-133) based on the extensive experimental work of Billet and Schultes.

13. Determination of theoretical stages for concentrated solutions involves numerical integration because of curved equilibrium and/or operating lines.

REFERENCES

1. WASHBURN, E.W., Ed.-in-Chief, *International Critical Tables,* McGraw-Hill, New York, Vol. **III,** p. 255 (1928).

2. LOCKETT, M., *Distillation Tray Fundamentals,* Cambridge University Press, Cambridge, UK, p. 13 (1986).

3. OKONIEWSKI, B.A., *Chem. Eng. Prog.,* **88** (2), 89–93 (1992).

4. SAX, N.I., *Dangerous Properties of Industrial Materials,* 4th ed., Van Nostrand Reinhold, New York, pp. 440–441 (1975).

5. LEWIS, W.K., *Ind. Eng. Chem.*, **14,** 492–497 (1922).

6. DRICKAMER, H.G., and J.R. BRADFORD, *Trans. AIChE,* **39,** 319–360 (1943).

7. JACKSON, R.M., and T.K. SHERWOOD, *Trans. AIChE,* **37,** 959–978 (1941).

8. O'CONNELL, H.E., *Trans. AIChE,* **42,** 741–755 (1946).

9. WALTER, J.F., and T.K. SHERWOOD, *Ind. Eng. Chem.,* **33,** 493–501 (1941).

10. EDMISTER, W.C., *The Petroleum Engineer,* C45–C54 (Jan. 1949).

11. LOCKHART, F.J., and C.W. LEGGETT, in K.A. KOBE and J.J. MCKETTA, Jr., Ed., *Advances in Petroleum Chemistry and Refining,* Vol. 1, Interscience, New York, Vol. **1,** pp. 323–326 (1958).

12. HOLLAND, C.D., *Multicomponent Distillation,* Prentice-Hall, Englewood Cliffs, NJ (1963).

13. MURPHREE, E.V., *Ind. Eng. Chem.,* **17,** 747 (1925).

14. HAUSEN, H., *Chem. Ing. Tech.,* **25,** 595 (1953).

15. STANDART, G., *Chem Eng. Sci.,* **20,** 611 (1965).

16. LEWIS, W.K., *Ind. Eng. Chem.,* **28,** 399 (1936).

17. GERSTER, J.A., A.B. HILL, N.H. HOCHGRAF, and D.G. ROBINSON, "Tray Efficiencies in Distillation Columns," Final Report from the University of Delaware, American Institute of Chemical Engineers, New York (1958).

18. *Bubble-Tray Design Manual,* AIChE, New York (1958).

19. GILBERT, T.J., *Chem. Eng. Sci.,* **10,** 243 (1959).

20. BARKER, P.E., and M.F. SELF, *Chem. Eng. Sci.,* **17,** 541 (1962).

21. BENNETT, D.L., and H.J. GRIMM, *AIChE J.,* **37,** 589 (1991).

22. OLDERSHAW, C.F., *Ind. Eng. Chem. Anal. Ed.,* **13,** 265 (1941).

23. FAIR, J.R., H.R. NULL, and W.L. BOLLES, *Ind. Eng. Chem. Process Des. Dev.,* **22,** 53–58 (1983).

24. SOUDERS, M., and G.G. BROWN, *Ind. Eng. Chem.,* **26,** 98–103 (1934).

25. FAIR, J.R., *Petro/Chem. Eng.,* **33,** 211–218 (Sept. 1961).

26. SHERWOOD, T.K., G.H. SHIPLEY, and F.A.L. HOLLOWAY, *Ind. Eng. Chem.,* **30,** 765–769 (1938).

27. *Glitsch Ballast Tray, Bulletin No. 159,* Fritz W. Glitsch and Sons, Dallas, TX (from FRI report of Sept. 3, 1958).

28. *Glitsch V-1 Ballast Tray, Bulletin No. 160,* Fritz W. Glitsch and Sons, Dallas, TX (from FRI report of Sept. 25, 1959).

29. OLIVER, E.D., *Diffusional Separation Processes. Theory, Design, and Evaluation,* John Wiley and Sons, New York, pp. 320–321 (1966).

30. BENNETT, D.L., R. AGRAWAL, and P.J. COOK, *AIChE J.,* **29,** 434–442 (1983).

31. SMITH, B.D., *Design of Equilibrium Stage Processes,* McGraw-Hill, New York (1963).

32. KLEIN, G.F., *Chem. Eng.,* **89** (9), 81–85 (1982).

33. KISTER, H.Z., *Distillation Design,* McGraw-Hill, New York (1992).

34. LOCKETT, M.J., *Distillation Tray Fundamentals,* Cambridge University Press, Cambridge, UK, p. 146 (1986).

35. American Institute of Chemical Engineers (AIChE), *Bubble-Tray Design Manual*, AIChE, New York, (1958).

36. CHAN, H., and J.R. FAIR, *Ind. Eng. Chem. Process Des. Dev.,* **23,** 814–819 (1984).

37. CHAN, H., and J.R. FAIR, *Ind. Eng. Chem. Process Des. Dev.,* **23,** 820–827 (1984).

38. SCHEFFE, R.D., and R.H. WEILAND, *Ind. Eng. Chem. Res.,* **26,** 228–236 (1987).

39. FOSS, A.S., and J.A. GERSTER, *Chem. Eng. Prog.,* **52,** 28-J to 34-J (Jan. 1956).

40. GERSTER, J.A., A.B. HILL, N.N. HOCHGRAF, and D.G. ROBINSON, "Tray Efficiencies in Distillation Columns," Final Report from University of Delaware, American Institute of Chemical Engineers (AIChE), New York (1958).

41. FAIR, J.R., *Petro./Chem. Eng.,* **33** (10), 45 (1961).

42. COLBURN, A.P., *Ind. Eng. Chem.,* **28,** 526 (1936).

43. CHILTON, T.H., and A.P. COLBURN, *Ind. Eng. Chem.*, **27,** 255–260, 904 (1935).

44. COLBURN, A.P., *Trans. AIChE*, **35,** 211–236, 587–591 (1939).

45. BILLET, R., *Packed Column Analysis and Design,* Ruhr-University Bochum (1989).

46. STICHLMAIR, J., J.L. BRAVO, and J.R. FAIR, *Gas Separation and Purification,* **3,** 19–28 (1989).

47. BILLET, R., and M. SCHULTES, *Packed Towers in Processing and Environmental Technology,* translated by J.W. Fullarton, VCH Publishers, New York (1995).

48. LEVA, M., *Chem. Eng. Prog. Symp. Ser.,* **50** (10), 51 (1954).

49. LEVA, M., *Chem. Eng. Prog.,* **88** (1), 65–72 (1992).

50. KISTER, H.Z., and D.R. GILL, *Chem. Eng. Prog.,* **87** (2), 32–42 (1991).

51. BILLET, R., and M. SCHULTES, *Chem. Eng. Technol.,* **14,** 89–95 (1991).

52. ERGUN, S., *Chem. Eng. Prog.,* **48** (2), 89–94 (1952).

53. KUNESH, J.G., *Can. J. Chem. Eng.,* **65,** 907–913 (1987).

54. WHITMAN, W.G., *Chem. and Met. Eng.,* **29,** 146–148 (1923).

55. SHERWOOD, T.K., and F.A.L. HOLLOWAY, *Trans. AIChE.,* **36,** 39–70 (1940).

56. CORNELL, D., W.G. KNAPP, and J.R. FAIR, *Chem. Eng. Prog.,* **56** (7) 68–74 (1960).

57. CORNELL, D., W.G. KNAPP, and J.R. FAIR, *Chem. Eng. Prog.,* **56** (8), 48–53 (1960).

58. BOLLES, W.L., and J.R. FAIR, *Inst. Chem. Eng. Symp. Ser.,* **56,** 3/35 (1979).

59. BOLLES, W.L., and J.R. FAIR, *Chem. Eng.,* **89** (14), 109–116 (1982).

60. BRAVO, J.L., and J.R. FAIR, *Ind. Eng. Chem. Process Des. Devel.,* **21,** 162–170 (1982).

61. BRAVO, J.L., J.A. ROCHA, and J.R. FAIR, *Hydrocarbon Processing,* **64** (1), 56–60 (1985).

62. FAIR, J.R., and J.L. BRAVO, *I. Chem. E. Symp. Ser.,* **104,** A183–A201 (1987).

63. FAIR, J.R., and J.L. BRAVO, *Chem. Eng. Prob.,* **86** (1), 19–29 (1990).

64. SHULMAN, H.L., C.F. ULLRICH, A.Z. PROULX, and J.O. ZIMMERMAN, *AIChE J.,* **1,** 253–258 (1955).

65. ONDA, K., H. TAKEUCHI, and Y.J. OKUMOTO, *J. Chem. Eng. Jpn.,* **1,** 56–62 (1968).

66. BILLET, R., *Chem. Eng. Prog.,* **63** (9), 53–65 (1967).

67. BILLET, R., and M. SCHULTES, *Beitrage zur Verfahrens-Und Umwelttechnik,* Ruhr-Universitat Bochum, pp. 88–106 (1991).

68. HIGBIE, R., *Trans. AIChE,* **31,** 365–389 (1935).

69. BILLET, R., and M. SCHULTES, *Chem. Eng. Res. Des., Trans. IChemE,* **77**A, 498–504 (1999).

70. M. SCHULTES, Private Communication (2004).

71. SLOLEY, A.W., *Chem. Eng. Prog.,* **95** (1), 23–35 (1999).

72. STUPIN, W.J., and H.Z. KISTER, *Trans. IChemE.,* **81**A, 136–146 (2003).

EXERCISES

Section 6.1

6.1 In any absorption operation, the absorbent is stripped to some extent depending on the K-value of the absorbent. In any stripping operation, the stripping agent is absorbed to some extent depending on its K-value. In Figure 6.1, it is seen that both absorption and stripping occur. Which occurs to the greatest extent in terms of kilomoles per hour? Should the operation be called an absorber or a stripper? Why?

6.2 Prior to 1950, only two types of commercial random packings were in common use: Raschig rings and Berl saddles. Starting in the 1950s, a wide variety of commercial random packings began to appear. What advantages do these newer packings have? By what advances in packing design and fabrication techniques were these advantages achieved? Why were structured packings introduced?

6.3 Bubble-cap trays were widely used in the design of trayed towers prior to the 1960s. Today sieve and valve trays are favored. However, bubble-cap trays are still occasionally specified, especially for operations that require very high turndown ratios or appreciable liquid residence time. What characteristics of bubble-cap trays make it possible for them to operate satisfactorily at low vapor and liquid rates?

Section 6.2

6.4 In Example 6.3, a lean oil of 250 MW is used as the absorbent. Consideration is being given to the selection of a new absorbent. Available streams are:

	Rate, gpm	Density, lb/gal	MW
C_5s	115	5.24	72
Light oil	36	6.0	130
Medium oil	215	6.2	180

Which stream would you choose? Why? Which streams, if any, are unacceptable?

6.5 Volatile organic compounds (VOCs) can be removed from water effluents by stripping in packed towers. Possible stripping agents are steam and air. Alternatively, the VOCs can be removed by carbon adsorption. The U.S. Environmental Protection Agency (EPA) has identified air stripping as the best available technology from an economic standpoint. What are the advantages and disadvantages of air compared to steam?

6.6 Prove by equations why, in general, absorbers should be operated at high pressure and low temperature, while strippers should be operated at low pressure and high temperature. Also prove, by equations, why a tradeoff exists between number of stages and flow rate of the separating agent.

Section 6.3

6.7 The exit gas from an alcohol fermenter consists of an air–CO_2 mixture containing 10 mol% CO_2 that is to be absorbed in a 5.0-N solution of triethanolamine, containing 0.04 mol of carbon dioxide per mole of amine solution. If the column operates isothermally at 25°C, if the exit liquid contains 78.4% of the CO_2 in the feed gas to the absorber, and if absorption is carried out in a six-theoretical-plate column, calculate:

(a) Moles of amine solution required per mole of feed gas.

(b) Exit gas composition.

Equilibrium Data

Y	0.003	0.008	0.015	0.023	0.032	0.043
X	0.01	0.02	0.03	0.04	0.05	0.06
Y	0.055	0.068	0.083	0.099	0.12	
X	0.07	0.08	0.09	0.10	0.11	

Y = moles CO_2/mole air; X = moles CO_2/mole amine solution

6.8 Ninety-five percent of the acetone vapor in an 85 vol% air stream is to be absorbed by countercurrent contact with pure water in a valve-tray column with an expected overall tray efficiency of 50%. The column will operate essentially at 20°C and 101 kPa pressure. Equilibrium data for acetone–water at these conditions are:

Mole percent acetone in water	3.30	7.20	11.7	17.1
Acetone partial pressure in air, torr	30.00	62.80	85.4	103.0

Calculate:

(a) The minimum value of L'/V', the ratio of moles of water per mole of air.

(b) The number of equilibrium stages required using a value of L'/V' of 1.25 times the minimum.

(c) The concentration of acetone in the exit water.

From Table 5.2 for N connected equilibrium stages, there are $2N + 2C + 5$ degrees of freedom. Specified in this problem are

Stage pressures (101 kPa)	N
Stage temperatures (20°C)	N
Feed stream composition	C-1
Water stream composition	C-1
Feed stream T, P	2
Water stream, T, P	2
Acetone recovery	1
L/V	1
	$2N + 2C + 4$

The remaining specification is the feed flow rate, which can be taken on a basis of 100 kmol/h.

6.9 A solvent-recovery plant consists of a plate-column absorber and a plate-column stripper. Ninety percent of the benzene (B) in the gas stream is recovered in the absorption column. Concentration of benzene in the inlet gas is 0.06 mol B/mol B-free gas. The oil entering the top of the absorber contains 0.01 mol B/mol pure oil. In the leaving liquid, $X = 0.19$ mol B/mol pure oil. Operating temperature is 77°F (25°C).

Open, superheated steam is used to strip benzene out of the benzene-rich oil at 110°C. Concentration of benzene in the oil = 0.19 and 0.01 (mole ratios) at inlet and outlet, respectively. Oil (pure)-to-steam (benzene-free) flow rate ratio = 2.0. Vapors are condensed, separated, and removed.

MW oil = 200 MW benzene = 78 MW gas = 32

Equilibrium Data at Column Pressures

X in Oil	Y in Gas, 25°C	Y in Steam, 110°C
0	0	0
0.04	0.011	0.1
0.08	0.0215	0.21
0.12	0.032	0.33
0.16	0.042	0.47
0.20	0.0515	0.62
0.24	0.060	0.795
0.28	0.068	1.05

Calculate:

(a) The molar flow rate ratio of B-free oil to B-free gas in the absorber; (b) The number of theoretical plates in the absorber; and (c) The minimum steam flow rate required to remove the benzene from 1 mol of oil under given terminal conditions, assuming an infinite-plates column.

6.10 A straw oil used to absorb benzene from coke-oven gas is to be steam-stripped in a sieve-plate column at atmospheric pressure to recover the dissolved benzene. Equilibrium conditions at the operating temperature are approximated by Henry's law such that, when the oil phase contains 10 mol% C_6H_6, the C_6H_6 partial pressure above the oil is 5.07 kPa. The oil may be considered non-volatile. The oil enters containing 8 mol% benzene, 75% of which is to be recovered. The steam leaving contains 3 mol% C_6H_6. (a) How many theoretical stages are required? (b) How many moles of steam are required per 100 mol of oil–benzene mixture? (c) If 85% of the benzene is to be recovered with the same oil and steam rates, how many theoretical stages are required?

Section 6.4

6.11 Groundwater at a flow rate of 1,500 gpm, containing three volatile organic compounds (VOCs), is to be stripped in a trayed tower with air to produce drinking water that will meet EPA standards. Relevant data are given below. Determine the maximum air flow rate in scfm (60F, 1 atm) and the number of equilibrium stages required if an air flow rate of twice the minimum is used and the tower operates at 25°C and 1 atm. Also determine the composition in parts per million for each VOC in the resulting drinking water.

Component	K-value	Concentration, ppm: Ground water	Concentration, ppm: Max. for Drinking water
1,2-Dichloroethane (DCA)	60	85	0.005
Trichloroethylene (TCE)	650	120	0.005
1,1,1-Trichloroethane (TCA)	275	145	0.200

Note: ppm = parts per million by weight.

6.12 Sulfur dioxide and butadienes (B3 and B2) are to be stripped with nitrogen from the liquid stream as shown in Figure 6.46 so that

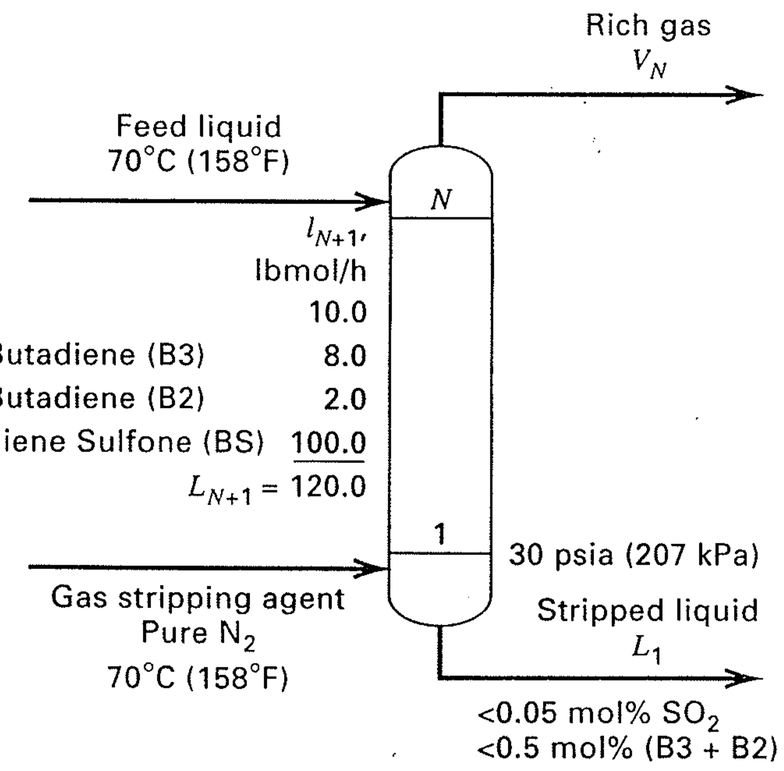

Figure 6.46 Data for Exercise 6.12.

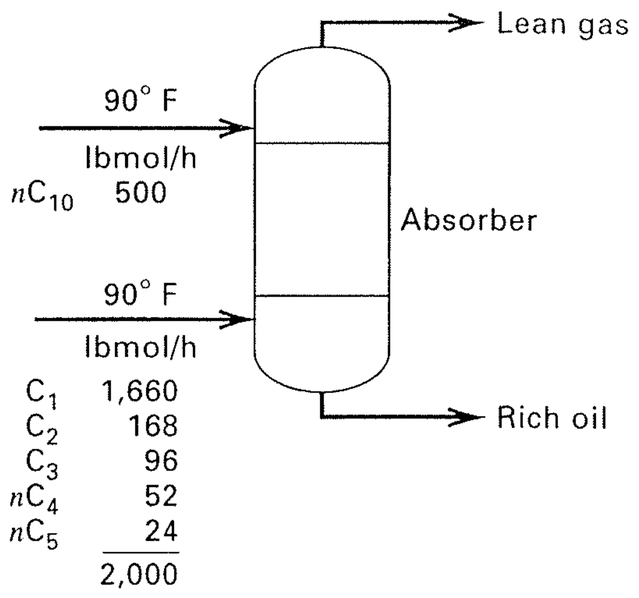

Figure 6.47 Data for Exercise 6.13.

butadiene sulfone (BS) product will contain less than 0.05 mol% SO_2 and less than 0.5 mol% butadienes. Estimate the flow rate of nitrogen, N_2, and the number of equilibrium stages required. At 70°C, *K*-values for SO_2, B2, B3, and BS are, respectively, 6.95, 3.01, 4.53, and 0.016.

6.13 Determine by the Kremser method the separation that can be achieved for the absorption operation indicated in Figure 6.47 for the following combinations of conditions: (a) Six equilibrium stages and 75 psia operating pressure, (b) Three equilibrium stages and 150 psia operating pressure, (c) Six equilibrium stages and 150 psia operating pressure. At 90°F and 75 psia, the *K*-value of $nC_{10} = 0.0011$.

6.14 One thousand kilomoles per hour of rich gas at 70°F with 25% C_1, 15% C_2, 25% C_3, 20% nC_4, and 15% nC_5 by moles is to be absorbed by 500 kmol/h of nC_{10} at 90°F in an absorber operating at 4 atm. Calculate by the Kremser method the percent absorption of each component for 4, 10, and 30 theoretical stages. What do you conclude from the results? (Note: The *K*-value of nC_{10} at 80°F and 4 atm is 0.0014.)

Section 6.5

6.15 Using the performance data of Example 6.3, back-calculate the overall stage efficiency for propane and compare the result with estimates from the Drickamer–Bradford and O'Connell correlations.

6.16 Several hydrogenation processes are being considered that will require hydrogen of 95% purity. A refinery stream of 800,000 scfm (at 32°F, 1 atm), currently being used for fuel and containing 72.5% H_2, 25% CH_4, and 2.5% C_2H_6 is available. To convert this gas to the required purity, oil absorption, activated charcoal adsorption, and membrane separation are being considered. For oil absorption, an available *n*-octane stream can be used as the absorbent. Because the 95% H_2 must be delivered to a hydrogenation process at not less than 375 psia, it is proposed to operate the absorber at 400 psia and 100°F. If at least 80% of the hydrogen fed to the absorber is to leave in the exit gas, determine:

(a) The minimum absorbent rate in gallons per minute.

(b) The actual absorbent rate if 1.5 times the minimum amount is used.

(c) The number of theoretical stages.

(d) The stage efficiency for each of the three species in the feed gas, using the O'Connell correlation.

(e) The number of trays actually required.

(f) The composition of the exit gas, taking into account the stripping of octane.

(g) If the octane lost to the exit gas is not recovered, estimate the annual cost of this lost oil if the process operates 7,900 h/year and the octane is valued at $1.00/gal.

6.17 The absorption operation of Examples 6.1 and 6.4 is being scaled up by a factor of 15, such that a column with an 11.5-ft diameter will be needed. In addition, because of the low efficiency of 30% for the original operation, a new tray design has been developed and tested in an Oldershaw-type column. The resulting Murphree vapor-point efficiency, E_{OV}, for the new tray design for the system of interest is estimated to be 55%. Estimate E_{MV} and E_o. (To estimate the length of the liquid flow path, Z_L, use Figure 6.16. Also, assume that $u/D_E = 6\ \text{ft}^{-1}$.)

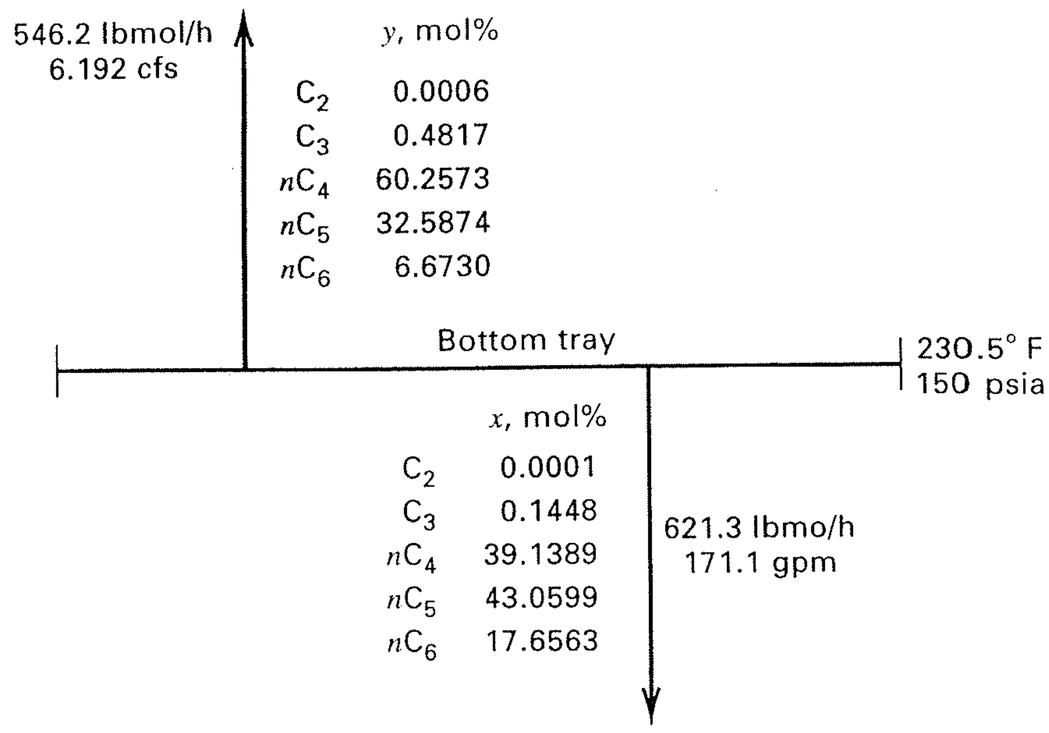

Figure 6.48 Data for Exercise 6.18.

Section 6.6

6.18 Conditions at the bottom tray of a reboiled stripper are as shown in Figure 6.48. If valve trays are used with a 24-in. tray spacing, estimate the required column diameter for operation at 80% of flooding.

6.19 Determine the flooding velocity and column diameter for the following conditions at the top tray of a hydrocarbon absorber equipped with valve trays:

Pressure	400 psia
Temperature	128°F
Vapor rate	530 lbmol/h
Vapor MW	26.6
Vapor density	1.924 lb/ft^3
Liquid rate	889 lbmol/h
Liquid MW	109
Liquid density	41.1 lb/ft^3
Liquid surface tension	18.4 dynes/cm
Foaming factor	0.75
Tray spacing	24 in.
Fraction flooding	0.85
Valve trays	

6.20 For Exercise 6.16, if a flow rate of 40,000 gpm of octane is used to carry out the absorption in a sieve-tray column using 24-in. tray spacing, a weir height of 2.5 in., and holes of $\frac{1}{4}$-in. diameter, determine for a foaming factor of 0.80 and a fraction flooding of 0.70:

(a) The column diameter based on conditions near the bottom of the column.

(b) The vapor pressure drop per tray.

(c) Whether weeping will occur.

(d) The entrainment rate.

(e) The fractional decrease in E_{MV} due to entrainment.

(f) The froth height in the downcomer.

6.21 Repeat the calculations of Examples 6.5, 6.6, and 6.7 for a column diameter corresponding to 40% of flooding.

6.22 For the acetone absorber of Figure 6.1, assuming the use of sieve trays with a 10% hole area and $\frac{3}{16}$-in. holes with an 18-in. tray spacing, estimate:

(a) The column diameter for a foaming factor of 0.85 and a fraction of flooding of 0.75.

(b) The vapor pressure drop per tray.

(c) The number of transfer units, N_G and N_L, from (6-62) and (6-63), respectively.

(d) N_{OG} from (6-61).

(e) The controlling resistance to mass transfer.

(f) E_{OV} from (6-56).

From your results, determine if 30 actual trays are adequate.

6.23 Design a VOC stripper for the flow conditions and separation of Example 6.2 except that the wastewater and air flow rates are twice as high. To develop the design, determine:

(a) The number of equilibrium stages required.

(b) The column diameter for sieve trays.

(c) The vapor pressure drop per tray.

(d) Murphree vapor-point efficiencies using the Chan and Fair method.

(e) The number of trays actually required.

Section 6.7

6.24 Air containing 1.6 vol% sulfur dioxide is scrubbed with pure water in a packed column of 1.5-m^2 cross-sectional area and 3.5-m height packed with no. 2 plastic Super Intalox saddles, at a pressure of 1 atm. Total gas flow rate is 0.062 kmol/s, the liquid flow rate is 2.2 kmol/s, and the outlet gas SO_2 concentration is $y = 0.004$. At the column temperature, the equilibrium relationship is given by $y^* = 40x$.

(a) What is L/L_{min}?

(b) Calculate N_{OG} and compare your answer to that for the number of theoretical stages required.

(c) Determine H_{OG} and the HETP from the operating data.

(d) Calculate K_Ga from the data, based on a partial-pressure driving force as in item 2 of Table 6.7.

6.25 An SO_2–air mixture is being scrubbed with water in a countercurrent-flow packed tower operating at 20°C and 1 atm. Solute-free water enters the top of the tower at a constant rate of 1,000 lb/h and is well distributed over the packing. The liquor leaving contains 0.6 lb SO_2/100 lb of solute-free water. The partial pressure of SO_2 in the spent gas leaving the top of the tower is 23 torr. The mole ratio of water to air is 25. The necessary equilibrium data are given below.

(a) What percent of the SO_2 in the entering gases is absorbed in the tower?

(b) In operating the tower it was found that the rate coefficients k_p and k_L remained substantially constant throughout the tower at the following values:

$$k_L = 1.3 \text{ ft/h}$$

$$k_p = 0.195 \text{ lbmol/h-ft}^2\text{-atm}$$

At a point in the tower where the liquid concentration is 0.001 lbmol SO_2 per lbmol of water, what is the liquid concentration at the gas–liquid interface in lbmol/ft^3? Assume that the solution has the same density as H_2O.

Solubility of SO_2 in H_2O at 20°C

lb SO_2 / 100 lb H_2O	Partial Pressure of SO_2 in Air, torr
0.02	0.5
0.05	1.2
0.10	3.2
0.15	5.8
0.20	8.5
0.30	14.1
0.50	26.0
0.70	39.0
1.0	59

6.26 A wastewater stream of 600 gpm, containing 10 ppm (by weight) of benzene, is to be stripped with air in a packed column operating at 25°C and 2 atm to produce water containing 0.005 ppm of benzene. The packing is 2-in. Flexirings made of polypropylene. The vapor pressure of benzene at 25°C is 95.2 torr. The solubility of benzene in water at 25°C is 0.180 g/100 g. An expert in VOC stripping with air has suggested use of 1,000 scfm of air (60°F, 1 atm), at which condition one should achieve for the mass transfer of benzene:

$$k_L a = 0.067 \text{ s}^{-1} \quad \text{and} \quad k_G a = 0.80 \text{ s}^{-1}$$

Determine:

(a) The minimum air stripping rate in scfm. Is it less than the rate suggested by the expert? If not, use 1.4 times your minimum value.

(b) The stripping factor based on the air rate suggested by the expert.

(c) The number of transfer units, N_{OG}, required.

(d) The overall mass-transfer coefficient, $K_G a$, in units of mol/m^3-s-kPa and s^{-1}. Which phase controls mass transfer?

(e) The volume of packing in cubic meters.

Section 6.8

6.27 Germanium tetrachloride ($GeCl_4$) and silicon tetrachloride ($SiCl_4$) are used in the production of optical fibers. Both chlorides are oxidized at high temperature and converted to glasslike particles. However, the $GeCl_4$ oxidation is quite incomplete and it is necessary to scrub the unreacted $GeCl_4$ from its air carrier in a packed column operating at 25°C and 1 atm with a dilute caustic solution. At these conditions, the dissolved $GeCl_4$ has no vapor pressure and mass transfer is controlled by the gas phase. Thus, the equilibrium curve is a straight line of zero slope. Why? The entering gas is 23,850 kg/day of air containing 288 kg/day of $GeCl_4$. The air also contains 540 kg/day of Cl_2, which, when dissolved, also will have no vapor pressure. The two liquid-phase reactions are

$$GeCl_4 + 5OH^- \rightarrow HGeO_3^- + 4Cl^- + 2H_2O$$

$$Cl_2 + 2OH^- \rightarrow ClO^- + Cl^- + H_2O$$

It is desired to absorb 99% of both $GeCl_4$ and Cl_2 in an existing 2-ft-diameter column that is packed to a height of 10 ft with $\frac{1}{2}$-in. ceramic Raschig rings. The liquid rate should be set so that the column operates at 75% of flooding. For the packing: $\epsilon = 0.63$, $F_P = 580 \text{ ft}^{-1}$, and $D_P = 0.01774$ m.

Gas-phase mass-transfer coefficients for $GeCl_4$ and Cl_2 can be estimated from the following empirical equations developed from experimental studies, where μ, ρ, and D_i are gas-phase properties:

$$K_y a = k_y a$$

$$\frac{k_y}{(V/S)} = 1.195 \left[\frac{D_p V'}{\mu(1-\epsilon_o)} \right]^{-0.36} (N_{Sc})^{-2/3}$$

$$\epsilon_o = \epsilon - h_L$$

$$h_L = 0.03591(L')^{0.331}$$

$$a = \frac{14.69(808\ V'/\rho^{1/2})^n}{(L')^{0.111}}$$

$$n = 0.01114L' + 0.148$$

where

S = column cross sectional area, m^2

k_y = kmol/m^2-s

V = molar gas rate, kmol/s

D_p = equivalent packing diameter, m

μ = gas viscosity, kg/m-s

ρ = gas density, kg/m^3

N_{Sc} = Schmidt number = $\mu/\rho D_i$

D_i = molecular diffusivity of component i in the gas, m^2/s

a = interfacial area for mass transfer, m^2/m^3 of packing

L' = liquid mass velocity, kg/m^2-s

V' = gas mass velocity, kg/m^2-s

For the two diffusing species, take

$$D_{GeCl_4} = 0.000006 \text{ m}^2/\text{s}$$

$$D_{Cl_2} = 0.000013 \text{ m}^2/\text{s}$$

Determine:

(a) The dilute caustic flow rate in kilograms per second.

(b) The required packed height in feet based on the controlling species ($GeCl_4$ or Cl_2). Is the 10 ft of packing adequate?

(c) The percent absorption of $GeCl_4$ and Cl_2 based on the available 10 ft of packing. If the 10 ft of packing is not sufficient, select an alternative packing that is adequate.

6.28 For the VOC stripping task of Exercise 6.26, the expert has suggested that we use a tower diameter of 0.80 m for which we can expect a pressure drop of 500 N/m^2-m of packed height (0.612 in. H_2O/ft). Verify the information from the expert by estimating:

(a) The fraction of flooding using the GPDC chart of Figure 6.36 with $F_P = 24 \text{ ft}^2/\text{ft}^3$.

(b) The pressure drop at flooding.

(c) The pressure drop at the operating conditions of Exercise 6.26 using the GPDC chart.

(d) The pressure drop at operating conditions using the correlation of Billet and Schultes by assuming that 2-in. plastic Flexiring packing has the same characteristics as 2-in. plastic Pall rings.

6.29 For the VOC stripping task of Exercise 6.26, the expert suggested certain mass-transfer coefficients. Check this information by estimating the coefficients from the correlations of Billet and Schultes by assuming that 2-in. plastic Flexiring packing has the same characteristics as 2-in. plastic Pall rings.

6.30 A 2 mol% NH_3-in-air mixture at 68°F and 1 atm is to be scrubbed with water in a tower packed with 1.5-in. ceramic Berl saddles. The inlet water mass velocity will be 2400 lb/h-ft^2, and the inlet gas mass velocity 240 lb/h-ft^2. Assume that the tower temperature remains constant at 68°F, at which the gas solubility relationship follows Henry's law, $p = Hx$, where p is the partial pressure of ammonia over the solution, x is the mole fraction of ammonia in the liquid, and H is the Henry's law constant, equal to 2.7 atm/mole fraction.

(a) Calculate the required packed height for absorption of 90% of the NH_3.

(b) Calculate the minimum water mass velocity in lb/h-ft^2 for absorbing 98% of the NH_3.

(c) The use of 1.5-in. ceramic Hiflow rings rather than the Berl saddles has been suggested. What changes would this cause in K_Ga, pressure drop, maximum liquid rate, K_La, column height, column diameter, H_{OG}, and N_{OG}?

6.31 You are to design a packed column to absorb CO_2 from air into fresh, dilute-caustic solution. The entering air contains 3 mol% CO_2, and a 97% recovery of CO_2 is desired. The gas flow rate is 5,000 ft^3/min at 60°F, 1 atm. It may be assumed that in the range of operation, the equilibrium curve is $Y^* = 1.75X$, where Y and X are mole ratios of CO_2 to carrier gas and liquid, respectively. A column diameter of 30 in. with 2-in. Intalox saddle packing can be assumed for the initial design estimates. Assume the caustic solution has the properties of water. Calculate:

(a) The minimum caustic solution-to-air molar flow rate ratio.

(b) The maximum possible concentration of CO_2 in the caustic solution.

(c) The number of theoretical stages at $L/V = 1.4$ times minimum.

(d) The caustic solution rate.

(e) The pressure drop per foot of column height. What does this result suggest?

(f) The overall number of gas transfer units, N_{OG}.

(g) The height of packing, using a K_Ga of 2.5 lbmol/h-ft^3-atm.

Section 6.9

6.32 At a point in an ammonia absorber using water as the absorbent and operating at 101.3 kPa and 20°C, the bulk gas phase contains 10 vol% NH_3. At the interface, the partial pressure of NH_3 is 2.26 kPa. The concentration of the ammonia in the body of the liquid is 1 wt%. The rate of ammonia absorption at this point is 0.05 kmol/h-m^2.

(a) Given this information and the equilibrium curve in Figure 6.49, calculate X, Y, Y_I, X_I, X^*, Y^*, K_Y, K_X, k_Y, and k_X.

(b) What percent of the mass-transfer resistance is in each phase?

(c) Verify for these data that $1/K_Y = 1/k_Y + H'/k_X$.

6.33 One thousand cubic feet per hour of a 10 mol% NH_3 in air mixture is required to produce nitrogen oxides. This mixture is to be obtained by desorbing an aqueous 20 wt% NH_3 solution with air at 20°C. The spent solution should not contain more than 1 wt% NH_3.

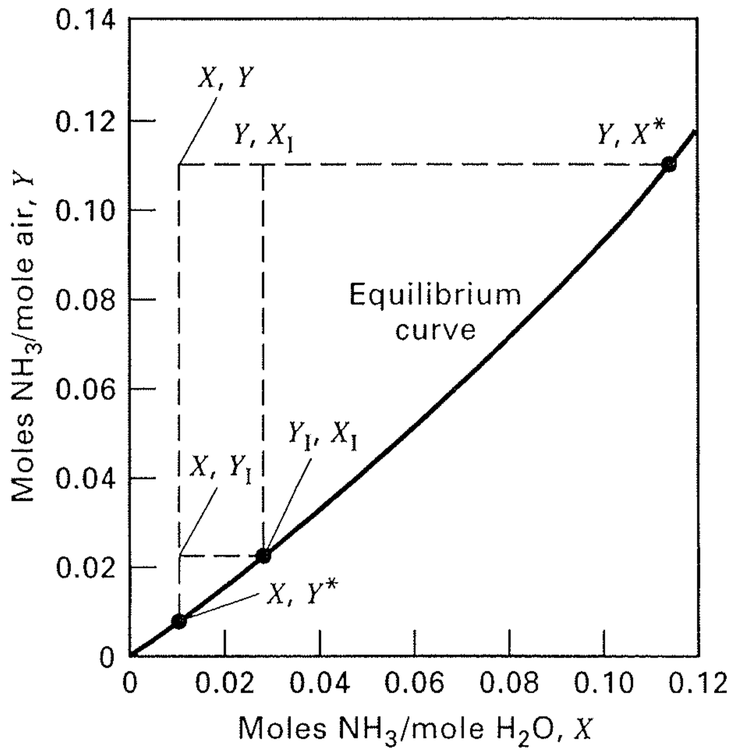

Figure 6.49 Data for Exercise 6.32.

Calculate the volume of packing required for the desorption column. Vapor–liquid equilibrium data for Exercise 6.32 can be used and $K_Ga = 4$ lbmol/h-ft^3-atm partial pressure.

6.34 Ammonia, present at a partial pressure of 12 torr in an air stream saturated with water vapor at 68°F and 1 atm, must be removed to the extent of 99.6% by water absorption at the same temperature and pressure. Two thousand pounds of dry air per hour are to be handled.

(a) Calculate the minimum amount of water necessary using the equilibrium data for Exercise 6.32 in Figure 6.49.

(b) Assuming an operation at 2 times the minimum water flow and at one-half the flooding gas velocity, compute the dimensions of a column packed with 38-mm ceramic Berl Saddles.

(c) Repeat part (b) for 50-mm Pall rings.

(d) Which of the two packings would you recommend?

6.35 Exit gas from a chlorinator consists of a mixture of 20 mol% chlorine in air. This concentration is to be reduced to 1% chlorine by water absorption in a packed column to operate isothermally at 20°C and atmospheric pressure. Using the following equilibrium x–y data, calculate for 100 kmol/h of feed gas:

(a) The minimum water rate in kilograms per hour.

(b) N_{OG} for twice the minimum water rate.

Data for x–y at 20°C (in chlorine mole fractions):

x	0.0001	0.00015	0.0002	0.00025	0.0003
y	0.006	0.012	0.024	0.04	0.06

6.36 Calculate the diameter and height for the column of Example 6.15 if the tower is packed with 1.5-in. metal Pall rings. Assume that the absorbing solution has the properties of water and use conditions at the bottom of the tower, where flow rates are highest.

6.37 You are asked to design a packed column to recover acetone from air continuously, by absorption with water at 60°F. The air contains 3 mol% acetone, and a 97% recovery is desired. The gas flow rate is 50 ft^3/min at 60°F, 1 atm. The maximum-allowable gas superficial velocity in the column is 2.4 ft/s. It may be assumed that in the range of operation, $Y^* = 1.75X$, where Y and X are mole ratios for acetone.

Calculate:

(a) The minimum water-to-air molar flow rate ratio.

(b) The maximum acetone concentration possible in the aqueous solution.

(c) The number of theoretical stages for a flow rate ratio of 1.4 times the minimum.

(d) The corresponding number of overall gas transfer units.

(e) The height of packing, assuming $K_Ya = 12.0$ lbmol/h-ft^3-molar ratio difference.

(f) The height of packing as a function of the molar flow rate ratio, assuming that V and HTU remain constant.

6.38 Determine the diameter and packed height of a countercurrently operated packed tower required to recover 99% of the ammonia from a gas mixture that contains 6 mol% NH_3 in air. The tower, packed with 1-in. metal Pall rings, must handle 2,000 ft^3/min of gas as measured at 68°F and 1 atm. The entering water-absorbent rate will be twice the theoretical minimum, and the gas velocity will be such that it is 50% of the flooding velocity. Assume isothermal operation at 68°F and 1 atm. Equilibrium data are given in Figure 6.49.

6.39 A tower, packed with Montz B1-200 metal structured packing, is to be designed to absorb SO_2 from air by scrubbing with water. The entering gas, at an SO_2-free flow rate of 6.90 lbmol/h-ft^2 of bed cross section, contains 80 mol% air and 20 mol% SO_2. Water enters at a flow rate of 364 lbmol/h-ft^2 of bed cross section. The exiting gas is to contain only 0.5 mol% SO_2. Assume that neither air nor water will be transferred between phases and that the tower operates at 2 atm and 30°C. Equilibrium data in mole fractions for SO_2 solubility in water at 30°C and 2 atm (*Perry's Chemical Engineers' Handbook,* 4th ed., Table 14.31, p. 14-6) have been fitted by a least-squares method to the equation

$$y = 12.697x + 3148.0x^2 - 4.724 \times 10^5 x^3 + 3.001 \times 10^7 x^4 - 6.524 \times 10^8 x^5$$

(a) Derive the following molar material balance operating line for SO_2 mole fractions:

$$x = 0.0189\left(\frac{y}{1-y}\right) - 0.00010$$

(b) Write a computer program or use a spreadsheet program to calculate the number of required transfer units based on the overall gas-phase resistance.